Summer 8-2020

Development of a Microarray Biosensor for Real-Time and Continuous Measurement of Neurochemicals

Md Imran Hossain

DEVELOPMENT OF A MICROARRAY BIOSENSOR FOR REAL-TIME AND CONTINUOUS MEASUREMENT OF NEUROCHEMICALS

by

Md Imran Hossain, MS

A Dissertation Presented in Partial Fulfillment
of the Requirements of the Degree
Doctor of Philosophy

COLLEGE OF ENGINEERING AND SCIENCE
LOUISIANA TECH UNIVERSITY

August 2020

ABSTRACT

Continuous simultaneous measurement of glutamate (GLU), an excitatory neurochemical, and γ-aminobutyric acid (GABA), an inhibitory neurochemical, constitutes one of the major challenges in neuroscientific research. Maintaining appropriate levels of GLU and GABA is important for normal brain functions. Abnormal levels of GLU and GABA are responsible for various brain dysfunctions, like epilepsy and traumatic brain injury. GLU and GABA being non-electroactive are challenging to detect in real-time. To date, GABA is detected mainly via microdialysis with a high-performance liquid chromatography (HPLC) system that employs electrochemical (EC) and spectroscopic methodologies. However, these systems are bulky and unsuitable for real-time continuous monitoring. As opposed to microdialysis, biosensors are easy to miniaturize and are highly suitable for *in-vivo* studies. Unfortunately, this method requires a rather cumbersome process that relies on externally applied pre-reactors and reagents. Here, we report the design and implementation of a GABA microarray probe that operates on a newly conceived principle. It consists of two microbiosensors, one for GLU and one for GABA detection, modified with glutamate oxidase and GABASE enzymes, respectively. The detection of GABA by this probe is based upon the *in-situ* generation of α-ketoglutarate from the GLU oxidation that takes place at both microbiosensor sites. By simultaneously measuring and subtracting the H_2O_2 oxidation currents of GLU microbiosensor from GABA microbiosensor, GABA and GLU can be

detected continuously in real-time *in vitro* and *ex vivo*. This mechanism happens without the addition of any externally applied reagents. We optimized our novel approach in commercially available ceramic-based probes. The GABA probe was successfully tested in an adult rat brain slice preparation. However, those electrodes are geometrically limited (we cannot have a sentinel site at the same spatial level as GLU and GABA sites). Keeping theseissues in mind, we have developed a microwire array sensor that is not only capable of simultaneous measurement of GLU and GABA, but is also able to track signal resulting from interferents (e.g. Ascorbic Acid, AA). The unique geometry enables these microwire probes to measure GLU, GABA and interferents in the same spatial level. A Simple fabrication procedure and easy integration with the existing amperometric systems allow us to use them in cell culture, brain tissue, and *in vivo* recordings as an inexpensive alternative to our planar electrodes. We demonstrated the effectiveness of the probes in rat brain tissue. We were able to get. Additionally, we determined the excitation/inhibition (E/I) ratios for different stimulations which have clinical relevance. Our results about this E/I balance can help refine electrical stimulation parameter for different clinical purposes (e.g. deep brain stimulation). Finally, we successfully tested our probe in awake-free behaving rats. In summary, our results suggest that microwire probes have the potential to become a powerful tool for measuring GLU and GABA in various *ex-vivo* and *in-vivo* disease models, such as epilepsy.

APPROVAL FOR SCHOLARLY DISSEMINATION

The author grants to the Prescott Memorial Library of Louisiana Tech University the right to reproduce, by appropriate methods, upon request, any or all portions of this Dissertation. It is understood that "proper request" consists of the agreement, on the part of the requesting party, that said reproduction is for his personal use and that subsequent reproduction will not occur without written approval of the author of this Dissertation. Further, any portions of the Dissertation used in books, papers, and other works must be appropriately referenced to this Dissertation.

Finally, the author of this Dissertation reserves the right to publish freely, in the literature, at any time, any or all portions of this Thesis.

Author _____

Date _____

DEDICATION

I dedicate this dissertation to my parents Montaz Hossain and Tohura Hossain, to my wife Farah, who inspired me throughout my PhD dissertation and to my siblings Munna and Tamanna.

TABLE OF CONTENTS

LIST OF FIGURES

LIST OF TABLES

ACKNOWLEDGMENTS

I would like to express my sincere gratitude to my advisor and mentor, Dr. Prabhu Umashanker Arumugam, who has supported me immensely and nurtured my research endeavors throughout my doctoral research. My sincere appreciation to the committee members: Dr. Shabnam Siddiqui, Dr. Teresa A. Murray, Dr. Levi Good and Dr. Leland Weiss. I would also like to thank Dr. Teresa Murray and Dr. Shabnam Siddiqui for giving me guidance in experiments and help along the way. I want to thank my former lab members, Dr. Gaurab Dutta and Dr. Chao Tan for their mentorship and guidance. I thank Dr. Haocheng Yin and Mr. Chenggong Gong for their constant cooperation in the lab experiments. I thank Dr. Phillip Doughty and Kayla Ponder for their help in the tissue and live rat experiments. Finally, I thank Mr. Davis Bailey, Ms. Debbie Wood, and Mr. Phillip Chapman in IfM for their assistance.

CHAPTER 1

INTRODUCTION

1.1 Problem Statement

The brain is the most complex organ in the human body. It has hundreds of billions of neurons and they are connected through an intricate network of synapses. Because of the central role it plays in vital electrophysical functions, the brain has been at the center of research for over a century. Yet the inherent multifaceted nature of the brain's physiology and the complex nature of the brain pathology addressed further research needs in this field. The brain interconnects various organs with electrical pulses, neurochemical transportation, stimulation receptors etc. If these connections are disturbed in any way, various neurological disorders occur. Diseases like Alzheimer's disease, Parkinson's disease, and epilepsy are direct consequences of neurochemical imbalance in the brain [1].

The detection of various neurochemicals with sufficient resolution, sensitivity and selectivity is essential for understanding the complex interplay of neurons and chemicals. Although various methods are available for the detection of these neurochemicals, often times they are limited by spatio-temporal resolutions, introduction of external reagents etc. Therefore, a self-sufficient sensor that can continuously detect neurochemicals with

high spatio-temporal resolution without the addition of any external reagents is a highly desirable tool to strengthen current investigation efforts. In this work we add to the existing body work [2]–[4] on the development of multiplexed neural probes for real-time sensing of neurochemicals.

1.2 Research Motivation

Glutamate (GLU) is the main excitatory neuron of the brain and γ-aminobutyric acid (GABA) is the main inhibitory neuron of the brain. This seemingly opposite characteristic of these neurochemical maintains a healthy balance in the brain. The imbalance of these neurochemicals results in abnormal signaling. This is an underlying signature of brain dynamical disorders such as epilepsy, Parkinson's disease and Alzheimer's disease, traumatic brain injury, and drug addiction [2], [5]–[8]. This critical research need to monitor the long-term spatio-temporal dynamics of GLU and GABA in the brain served as the main motivational factor of our research.

The current gold standard for neurochemical detection is based on microdialysis. However, microdialysis sampling takes in the range of minutes whereas vesicular event happens in the seconds range. Additionally, microdialysis needs to be integrated with microfluidic set up [9], chromatography which requires an additional bulky setup. Other spectroscopic or optical methods are limited by low temporal resolution and unavailability of reporter molecule (e.g. fluorescence dye). In recent decades electrochemical sensors have risen as a strong contender for real-time, continuous detection of neurochemicals [3], [10]. GLU and GABA being non-electroactive are challenging to detect directly on the sensor surface. Therefore, researchers generally use an enzyme modified surface for GLU or GABA detection [11], [12]. Still, several

limitations of these sensors remain. Surface fouling and the need to add an external reagent for sensing GABA limit *in-vivo* real time application [11], [13]. A sensor that does is self-contained (does not need external reagent) and usable long-term without fouling is a desirable tool for investigators worldwide. Additionally, microarray using different platforms (e.g., wires) needs to be investigated to find an inexpensive and more versatile alternative to present methods.

1.3 Research Objectives

The main objective of this dissertation is to develop a robust microsensor that can simultaneously detect GLU and GABA in real-time. We added to existing literature of GLU-GABA microsensor with various surface modifications[14]. To overcome the limitations of commercially available electrodes, we also fabricated an in-house custom-made probe using microwires that can offer the same functionalities at a lower cost. Overall, we want to accomplish the following three objectives.

1) Development and optimization of commercial (8-TRK) probe for simultaneous measurement of GLU and GABA: We will modify the commercially available 8-TRK (Cenmet, Lexington, KY, USA) for high sensitivity, high selectivity, lower limit of detection (LOD) and longer linear range without addition of any external reagents. We calibrate GABA in presence of both α-ketoglutarate and glutamate solution. Additionally, we optimize for different modification parameters for enzyme coating and experimental conditions. We change parameters like: enzyme concentration, enzyme thickness (number of drops) and pH conditions. Interferent rejection layer (mPD-layer) coating parameters e.g scan rate, were also a research objective. Finally, a new quantification

procedure of GABA and GLU concentration from pre-experiment calibration is also needed.

2) Fabrication and characterization of wire-based sensor for GABA and GLU measurement: We will fabricate a low-cost alternative to our commercial probes that works on the same working principle and has similar dimensions. In the 8-TRK probes the eight electrodes are arranged vertically within 8mm in a ceramic-based shank. Because of these dimensions we cannot use all eight electrodes in a tissue slice experiments (slice depth ~400μm). They are unsuitable in live animal recording too as we can't implant them too deep inside the brain. Other important consideration is that, in commercial probe the electrodes are always need to be used in pairs. This makes it impossible to have a blank electrode to record environmental noise along with GABA and GLU electrode. Our wire-based electrodes need be modified to have that functionality. We will call this "sentinel channel". We will fabricate these platinum microwire channels and modify them for our *ex-vivo* and *in-vivo* application. Characterization of these wires was also an important objective.

3) Validation of microelectrode biosensors in rat tissue slice and the brain of freely-moving rats: We need to validate our probes, both 8-TRK and microwire arrays, *ex-vivo* and *in-vivo*. Very few sensors to date have been able to successfully demonstrate simultaneous detection of GABA and GLU [11], [14], [15]. We need to be able to calculate the real-time concentration of GLU and GABA in different electrical stimulation conditions in brain tissue. Investigation of excitation (E, GLU concentration) and inhibition (I, GABA concentration) ratio is also critical. Finally; we have to demonstrate the suitability of our microarray channels in awake-free moving rat. We

need to determine the basal level of GLU and GABA as well as capture the sub-second fluctuations in the concentrations.

1.4 Dissertation Format

This dissertation is divided into seven chapters including introduction and the conclusion. Chapter-2 provides the background information about the methods available for neurochemical detection and overview of microelectrodes for neurochemical detection in the literature. It also introduces our novel method for GLU and GABA detection. We discuss our material and methods in Chapter-3. In that chapter we discuss biosensor preparation method, *in-vivo* and *ex-vivo* experimental method, data acquisition, data analysis and statistical methods.

Chapter-4 discusses GLU-GABA probe development. We tune different parameters to maximize GLU and GABA sensitivity. Thorough our experiments we optimized, α-ketoglutarate concentration, enzyme concentration, enzyme thickness, pH solution and permselective interference rejection layer. Linear range for GABA was also discussed. Our novel GABA and GLU concentration calculation procedure was also introduced. Chapter-5 discusses an alternate GLU-GABA probe based on microwire array. Wire selection procedure and calibration of GABA and GLU is discussed. Chapter-6 describes the validation of our probes in mostly *ex-vivo* environments and *in-vivo* conditions. Demonstration of real-time GABA and GLU concentration, peak parameters like rise time, delay time and full duration half maximum (FDHM) is also discussed. Dynamic features like excitation-inhibition (E/I) ratio for different electrical stimulation are one of highlights of this chapter. Finally, in Chapter-7 we draw conclusions fromour research and discuss future works in our lab.

CHAPTER 2

BACKGROUND AND THEORY

2.1 Importance of L-Glutamate (GLU) and γ-Aminobutyric Acid (GABA)

GLU is the main excitatory neurochemical and GABA is the major inhibitory neurochemical in the central nervous system (CNS). Both GLU and GABA serve multiple functions in the central nerves system (CNS). Both of them are important for normal brain functions. GLU plays important roles in depolarizing postsynaptic receptors, detoxification of ammonia, memory and cognitive process. γ-Aminobuteric Acid (GABA) is one of the most important major inhibitor neurochemical that is essential for normal brain function, neuronal activity, information processing and plasticity, and for network synchronization [16]–[18]. GABA plays a critical role in several psychiatric and neurological disorders, inflammation, and immune cell function and therefore, has been a main target of a wide range of drug therapies [16], [19]–[21].

As a neurotransmitter GLU is produced and released glutamatergic neurons. GLU is transported into vesicle by vesicular glutamate transporters (vGluTs). Upon depolarization of the cell membrane due to electrochemical gradient, the vesicles fuse and release the neurotransmitter into the synaptic cleft [22]. Once in synaptic cleft, GLU can be transported further with the receptors such as N-methyl-D-aspartate (NMDA), α-

amino-3-hydroxy-5-methyl-4-isoazolepropionic acid (AMPA), and 2-carboxy-3-carboxymethyl-4-isopropenylpyrrolidine (Kainate; KA) [23]. Upon GLU binding to these receptors, sodium/calcium dependent transporter located in both glial cells and astrocytes, depolarizes the post-synaptic neurons [23]. At this final stage GLU is taken up by both glial cells and astrocytes [23]. This Na^{+} and Ca^{2+} dependent depolarization is responsible for a lot of cognitive functions [23]. However, excessive depolarization and/or GLU release gives rise to phenomenon of excitotoxicity [24]. In this process, GLU and other amino acids rapidly kill CNS neurons [24].

In addition, GLU can also act as a precursor to GABA. In presence of glutamate decarboxylase (GAD), GLU converts into GABA in the pre-synaptic terminal. The GABA-GLU cycle is illustrated beautifully in Figure 2-1.Some GABA is uptaken by the glial cells with the help of GABA- transaminase (GABA-T) enzymes. This is also shown in Figure 2-1.

GLU and GABA maintain healthy balance in the brain by means of Glutamate (GABA)-glutamine cycle. The main feature of this cycle is: upon depolarization and vesicular release of Glu, it is uptaken into astrocytes by high affinity transporters [25]. Astrocytic GLU is turned into glutamine by the amination process. Interestingly, this process can only happen in astrocytes. Glutamine is not known to be neurotoxic and therefore it can be safely transported out of the astrocytes. Intracellular and extracellular GLU concentration typically ranges in the micromolar range. However, tissue and blood fluids sometimes also show high GLU concentration. Similarly, In the brain GABA concentration is in the range of nM to lower mM [26], [27]. For rat brain slices the concentration of GABA is reported as 20-70μM [28]. However, with magnetic resonance

spectroscopy in human brain GABA concentrations was found to be 1-1.2μM [29]. Abnormal level of GABA and GLU is an underlying cause of brain disorders such as epilepsy, Parkinson's, Alzheimer's, traumatic brain injury and drug addiction [2], [6]–[8], [30].

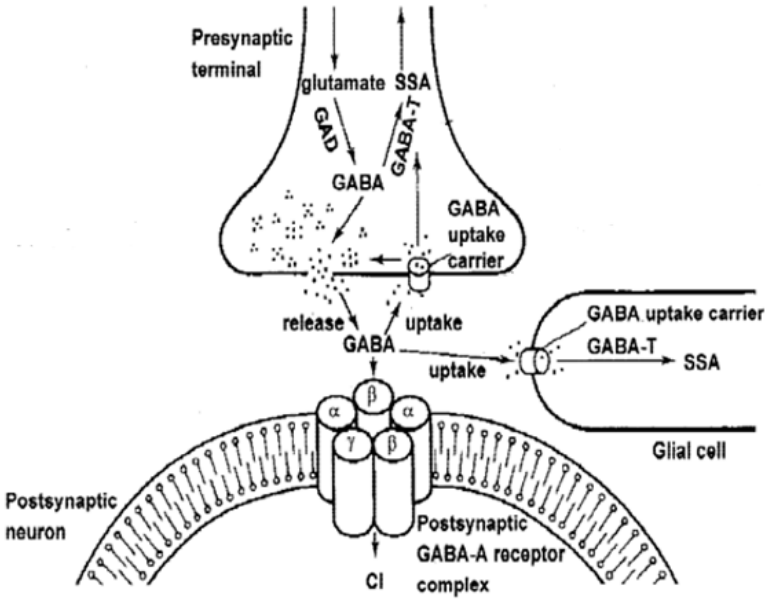

Figure 2-1: GABA cycle in the brain. Adopted from [31]

2.2 Current Methods for Neurochemical Detection

Different methods are available for measurements of neurochemicals. Based on the mechanism principles, these methods can be invasive or non-invasive. As expected, different methods have different advantages and disadvantages. The comparison helps us to select the right approach required for the particular application. Table 2-1 gives a brief overview of the current methods for neurochemical detection.

Table 2-1: Comparison of different methods for neurochemical detection adopted from [32]

Method	Advantages	Disadvantages
Electrochemical microsensors	High temporal resolution (<1 s) Low detection limit (<1 μM) High spatial resolution (<100 μM)	Invasive Limited lifetime (< 60 days) Small number of analytes
Microdialysis	Very low detection limit (<1 nM) Large number of analytes	Invasive Low temporal resolution (minutes) Complicated setup to facilitate HPLC
Nuclear magnetic resonance	Non-invasive Direct chemical structure detection	Low precision and costly large equipment High detection limit (mM) Low temporal resolution (minutes) Very low spatial resolution (cm^3)
Positron emission tomography	Non-invasive Low detection limit (<1 μM) Large number of analytes	Radioactive exposure and costly setup Low temporal resolution (minutes) Low spatial resolution (up to mm^3)
Fluorescence imaging	Very low detection limit (<1 nM) High temporal resolution (<1 s) Very High spatial resolution (<1 μM)	Indirect via biomarkers Complex chemical properties of biomarkers Separate optical equipment needed

2.2.1 Microdialysis

Microdialysis is the most widely used method for *in-vivo* measurements [32]. It is based on the principle of semipermeable membranes. These membranes restrict diffusion of the molecules by means of diffusion gradient[33]. An invasive probe is inserted in the brain and the extra-cellular fluid is pumped out for offline analysis [32] with other complementary methods like chromatography or fluorescence imaging. Microdialysis can measure small sample sizes (<10 μL) that allows for very low detection limit in nanomolar range [34]. Researchers can study simultaneous neurochemicals with this method. To date, *in-vivo* GABA levels are detected mainly via microdialysis on a high-performance liquid chromatography (HPLC) system with electrochemical (EC) and spectroscopic detection methods [35]–[38]. Since these methods are relatively insensitive to GABA, one must derivatize the solution, i.e., modifying them to be more conducive to electric signals. Several studies have been used HPLC with pre/post derivatized columns using 2,4,6-trinitrobenzenesulfonic acid, o-phthaldialdehyde (OPA)-sulfite and OPA-alkylthiols to separate GABA and other amino acids and then applied electrochemical detection on a glassy carbon electrode (GCE) to detect them at picomolar concentrations in rat brains [18] . The idea of OPA-butylthiol was first proposed by Kehr who further infused nipecotic acid and 3- mercaptopro-pionic acid to obtain a faster and more sensitive determination of GABA [35]. Rowley et al. extended this derivatization technique to separate seven amino acids and concluded that their method has the sensitivity to successfully detect stimulated levels of GABA and glutamate (Glu), a major excitatory neurochemical in a rat hippocampus[36]. Acuna et al. also used this method to separate GABA, Glu and glutamine in rat brain homogenates with higher accuracy and

repeatability [37]. Reinhoud used microbore columned Ultra-HPLC to detect catecholamines such as dopamine (DA) and serotonin (HT-5) [38].The main benefit of this method was that analytes with large differences in retention time could be separated in a single run [38].Commercial HPLC-ED systems (Alexys, Dionex) are now available that utilize GCEs at ~0.8 V for amino acid detection. This current state of the art technology is bulky and unsuitable for real-time continuous GABA monitoring, which is a key technology gap in the chemical neuroscience field. However, despite all these advantages there are several shortcomings for microdialysis when it comes to *in-vivo* application. The main disadvantage of microdialysis is the low temporal resolution. In this method the sample is collected over minutes, whereas neurochemical transmission lasts in the order of milliseconds or seconds [39]. For this reason, the events of neurochemical release and uptake gets mixed with each other, which is a loss of temporal resolution. This phenomenon also makes the study of behavior patterns and disease models that depend on sub-second resolution difficult to accomplish with this method.

2.2.2 Nuclear Magnetic Resonance (NMR)

NMR spectroscopy uses frequency spectra to specify chemical structure of molecules. The structure is used to identify chemical compounds. This is also a desirable method for clinicians since it is a minimally invasive process. The frequency spectra reveal the exact chemical structure which can visually inspected using proton imaging techniques. However, the low temporal resolution and the need for high volume sample required make this method unsuitable for some specific application. Additionally, this method can’t distinguish between molecules of similar chemical structure (e.g. glutamate and glutamine). Molecular labeling maybe required for those situations [40], [41].

2.2.3 Positron Emission Tomography (PET)

In this method a radioactive substance is perfused in the tissue. The resulting radiation is detected. Since this method is also non-invasive [32], it is of importance to the clinicians. However, the main drawback of this method is the limited availability and lifetime of the radioactive tracers. Sometimes these tracers are metabolized directly in the cells without ever detecting our molecule of interest [32]. Additionally, this method is limited by spatial resolution [42], [43] and low temporal resolution[44]. The long-term effects of these radioactive tracers also need to be evaluated.

2.2.4 Optical Methods

Optical enzymatic or non-enzymatic biosensors based on fluorescence or spectroscopy and their relevant principles is discussed widely in the literature [45], [46]. These methods are mostly restricted to animal models. Lack of appropriate dyes, optical path length and interferences often hinder optical sensor methods [32]. In recent years fluorescence markers for different neurochemicals have emerged [47], [48]. Glutamate binding protein and fluorescent protein is introduced in the cells and multiphoton microscopy is used to analyze results [49]. This gave acceptable spatio-temporal resolution [49]. However, complex mechanism to accommodate this biomarker into the organism, non-linear fluorescence signal and the need for integrating high-resolution imaging system makes these optical methods unsuitable for clinical use, especially *in-vivo* use. Spectroscopic based on UV-Vis methods has also been demonstrated for various neurochemicals [50].

2.2.5 Electrochemical Sensors

Electrochemical sensor is based on the direct/indirect oxidation/reduction of the molecules on the surface of the sensor. The sensor surface can be as small as a few microns. We call these sensors microelectrodes. Electrochemical sensors are available for most neurochemicals, including dopamine, glucose, glutamate and GABA. These are widely used in commercial purposes as well as clinical purposes. The most widely available application of electrochemical sensors is the glucose sensor.

Electroactive molecules comes in direct contact with the sensor surface and we immediately see a change in electrical signal [6], [51], [52]. The quick response in the form of change in signal gives electrochemical sensors higher temporal resolution than micro dialysis, NMR, PET. It also means we can resolve signals in behavior patterns and neuron firing in the milliseconds to seconds range. In some cases, if the molecules are not electroactive, not capable of directly oxidizing in the sensor surface, we can modify our sensor surface with appropriate materials (e.g. enzymes) to facilitate the oxidization. This capability makes electrochemical sensors powerful in detecting almost all neurochemicals. Advanced microfabrication techniques can be employed to make sensors every geometrical shape imaginable. These sensors can also be employed in *in-vivo, ex-vivo* and cell culture environments. The main disadvantage of these electrochemical sensors is that they have limited lifetime because the surface coatings foul with time [32]. In the subsequent section, we discuss electrochemical methods for neurochemical detection.

2.3 Electrochemical Methods for Neurochemical Detection

Electrochemical methods depend on the interaction between the electrode materials and molecules. The general mechanism is: when the molecule comes in contact with the sensor (electrode) surface, it gives away electrons. This electron gives rise to current which can be visualized and analyzed with advanced computational tools. This mechanism is shown in Figure 2-2.

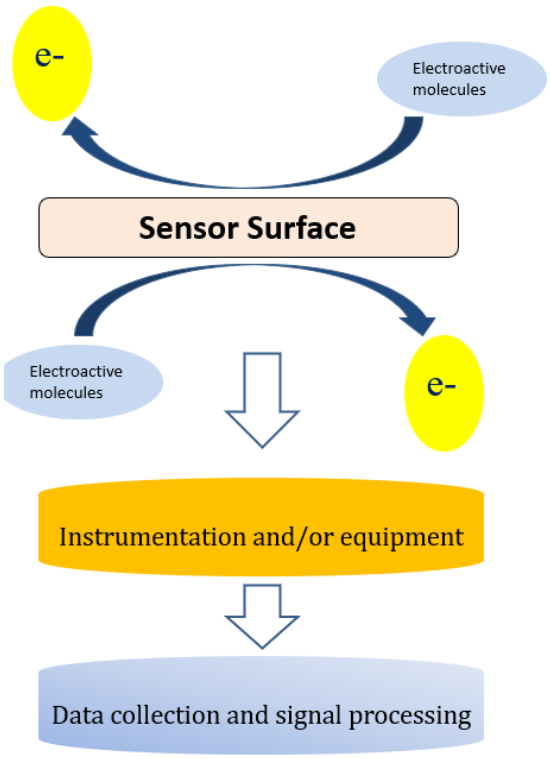

Figure 2-2: General mechanism of electrochemical process

The predominant method we use here is chronoamperometry. In chronoamperometry we bias the electrodes with a constant potential against a reference electrode. The mechanism of chronoamperometry is simple: monitor a gain or loss of electrons and measure the subsequent faradaic current. Chronoamperometry is governed by the Cottrel equation shown in **Eq. 2-1**

$$i = \frac{nFAC\sqrt{D}}{\sqrt{\pi t}} \qquad \textbf{Eq. 2-1}$$

Here, i is recorded current (A); n is the number of electrons transferred; F is the Faraday constant ($96485\ \frac{C}{mol}$); A is the electrode area (m^2); C is substrate concentration ($\frac{mol}{m^3}$); D is mass transfer coefficient ($\frac{m^2}{s}$); and t is time (s). As the equation suggests, the current depends on the concentration of our analyte. Figure 2-3 shows a sample chronoamperometry graph. As we expect when we inject our sample of interest the current level goes higher. This assumed linear diffusion of oxidized/reduced species is very desirable for a sensor.

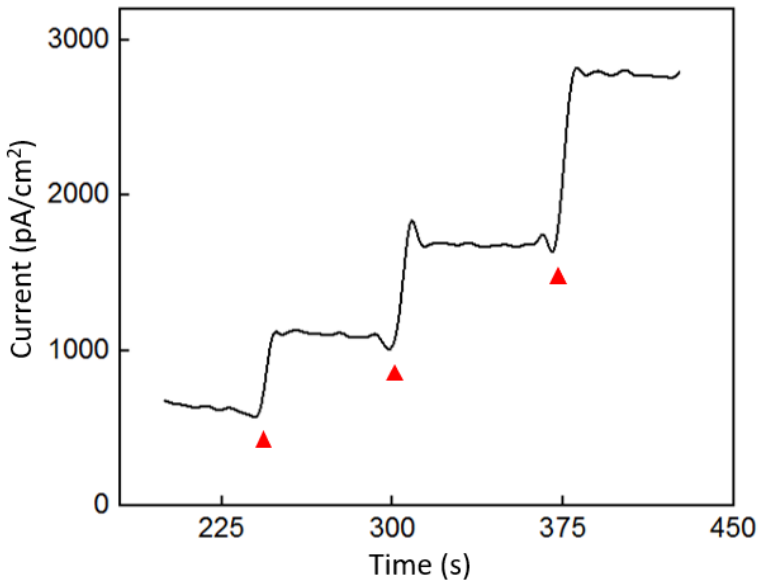

Figure 2-3: Sample chronoamperometry signal. The current level increases with each analyte addition. The red triangles indicate each analyte addition.

We can easily make the *current vs concentration* graph from the chronoamperometry plot. From the current vs concentration curve, we can get sensitivity and limit of detection (LOD) for the sensors. We can also get the linear range from the

data. The rise time ($T_{10\text{-}90}$), decay time ($T_{90\text{-}10}$) and full duration half maximum ($T_{50\text{-}50}$) of changes in current can also be determined from chronomperometry results. However, the main limitation for this method is the non-selective oxidization (or reduction) of molecules in the sensor surface. Through the fine tuning of applied voltage and judicious surface modification can remedy this problem. This method has been used in measurement in cell culture [53], [54] and in-vivo environments [55], [56].The other method we use throughout our work is cyclic voltammetry (CV A sample CV graph is shown Figure 2-4.

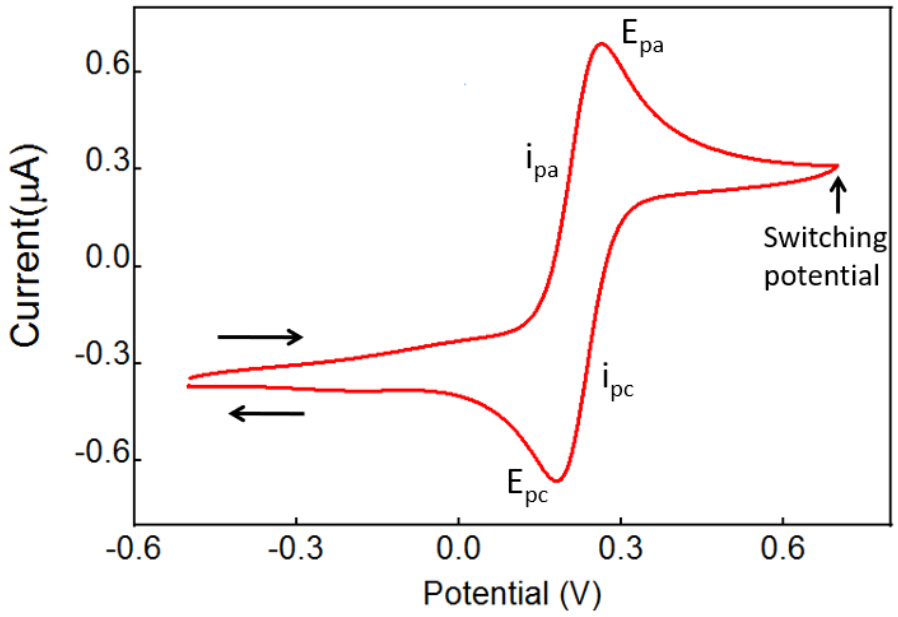

Figure 2-4: Sample CV graph. The arrows show the forward and backward sweep. E_{pa}= anodic potential, E_{pc}= cathodic potential, i_{pa}= anodic current and i_{pa}= cathodic current. CV is done in 8-TRK probes and 5mM ferro/ferri cyanide.

The peak current for forward sweep current, *i* is governed by Randle-Sevcik Equation shown in **Eq. 2-2** below:

$$i = (2.69 * 10^5)\sqrt[3]{n}\, A\sqrt{Dv}\, C \qquad \textbf{Eq. 2-2}$$

Here i is the measured current in amperes, n is the number of electrons transferred during the redox process, A is the area of the electrode's surface(cm^2), D_0 is the diffusion coefficient of the analyte ($\frac{cm^2}{s}$), v is the scan rate ($\frac{V}{s}$)and C_0 is the concentration of the analyte expressed in($\frac{mol}{cm^3}$).

CV gives information about the electron transfer kinetics, electrochemical diffusion process and adsorption process. CV and particularly a variation of CV called the fast scan cyclic voltammetry (FSCV) is very popular for *in-vivo* applications[57]. A higher scan rate facilitates rapid electron transfer on the electrode surface which is highly desirable live-animal experiments. FSCV has been used to monitor various neurochemicals like dopamine [58], serotonin and pH level changes [59]–[61]. The fast scan also suggest that this method can be used to study real-time release and uptake of neurochemicals [62], [63]. In our works we use CV for mild sulfuric acid (H_2SO_4) cleaning and permselective layer coating. CV can also be used to measure electroactive surface area. We used chronoamperometry for other sensor calibration.

2.4 Microelectrodes for Neurochemical Sensing

Microelectrodes are electrodes with dimensions typically in the micron range (≤25 μm). It has several advantages over the macroelectrodes (which are in the millimeter range)[64], [65]. Firstly, in these micro-electrodes the redox reaction in the sensor surface is independent of the analyte concentration in the solution [66]. Secondly, since ohmic voltage drop is minimal we can keep the currents in picomolar range [66]. This is highly desirable for measurement of very low concentration of neurochemical.

Finally, the dominant diffusion process in these electrodes is the radial diffusion which always result in higher charge density and higher selectivity [66].

Electoactive neurochemicals (dopamine, serotonin) oxidize directly in the electrode surface resulting in amperometric current signals. However, GLU and GABA are is non-electroactive, and it is therefore challenging to detect it in real-time using electrochemical (EC) and spectrophotometrical methods [67]. The most common approach for electrochemically detecting these molecules is to enzymatically convert them to an electroactive reporter molecule (e.g. hydrogen peroxide or H_2O_2, NADPH) with an appropriate enzyme immobilized on the surface of the electrode [3], [68], [69]. These enzymes are usually oxidase enzymes. The most famous enzyme based electrode is the glucose sensors based on glucose oxidase [4]. Glucose sensors are now a billion-dollar commercial industry that serves the diabetes patients. Additionally, lactate oxidase [70], glutamate oxidase [12] or choline oxidase [71] based sensors are also available. These enzyme-based biosensors also evolved overtime.

In the first-generation biosensor, enzymes convert the molecule, in presense of oxygen, into reporter molecule (H_2O_2). This sensor needs oxygen to function. However, oxygen is available in lower concentrations in tissues because of restricted supply by blood vessels [32]. This low oxygen concentration severely limits diffusion capability when the analyte concentration becomes too high [32]. In our works we use the first-generation biosensor.

To eliminate this oxygen dependency, researchers developed second-generation biosensors. This is a regentless sensor where they use electron acceptor instead of oxygen [72]. Basically, in this method enzyme is reduced and substrate turns to product. This

reduced form of enzyme reduces the mediator and then oxidized by electron from nearby molecule [32]. The final step involves oxidation of mediator in the electrode surface [32]. Redox polymers which are capable of containing both enzyme and mediator molecules are used in this type of sensors [73], [74]. The third-generation biosensors the electron transfer happens directly in the surface from the enzyme without any oxygen or mediator molecule. However, Wang et. al., 2008 showed in from their work these sensors are severely limited in their efficiency [72].

Our sensors are based on the first-generation sensor working principle. There are several GLU sensor based on this principle is available [75]–[77]. In Figure 2-5, we show several pathways for GABA detection scheme. However, because of absence of an oxidase enzyme that can directly oxidize GABA, GABA detection is more challenging. Biosensors selectively oxidize GABA into a secondary product (GLU) and then oxidized into a reporter molecule in the presence of enzymes, similar to the detection method used for Glu [78] or acetylcholine [79]. Electroactive reporter molecules such as β-nicotinamide adenine dinucleotide phosphate (NADPH) or hydrogen peroxide (H_2O_2) are usually generated through a series of enzymatic reactions by adding nicotinamide adenine dinucleotide phosphate (NADP), a co-factor or by adding α-ketoglutarate and then electrochemically detecting them on a modified glassy carbon electrode GCE. The current generated by electrochemically oxidizing them can be used as an index to quantify GABA. In AM-based GABA biosensors, GABASE, which consists of two enzymes, γ-aminobutylate ketoglutarate aminotransferase (GABA-T) and succinic semialdehyde dehydrogenase (SSDH) converts GABA into GLU (henceforth called GLU_{GABA}) and succinic semialdehyde (SSA) in the presence of α-ketoglutarate (reaction 1). For reaction 1 to occur,

α-ketoglutarate must be present in the sample. The α-ketoglutarate can be added to the sample externally or it can be obtained from oxidizing Gluthat is ubiquitously present in the brain microenvironment (henceforth called Glu_E/GLU_E) using the glutamate oxidase (GOx) enzyme (reaction 2). Subsequently, there are two pathways by which reaction-1 can proceed to generate electrochemically or optically active molecules that are detected as a GABA signal. The first approach is based on SSA reacting with NADP in the presence of SSDH to form NADPH that is then detected optically (UV spectrophotometry or colorimetry [50]) or electrochemically (reaction 3). Mazzei et. al. developed a GABA biosensor based on reaction 3 using a horseradish peroxidase-modified GCE [80] However, the main disadvantage of reaction 3 are that the electrode surface fouls rapidly due to the irreversible nature of $NADP^+$ adsorption. Sekioka et. al., partially addressed this challenge using an electron cyclotron resonance (ECR) sputtered carbon electrode [13]. Since there is a critical need for ex vivo and in vivo studies to detect GABA long term and NADP to NADPH conversion is irreversible, NADP must be continuously replenished. Badalyan et.al., addressed this problem of continual NADP additions by employing periplasmatic aldehyde oxidoreductase instead of SSDH and mediators such as ferricyanide, phenoxazines, ferrocene derivatives, quinones and bipyridinium salts instead of NADP[81]. The SSA generated in reaction 1 is converted to SA when periplasmatic aldehyde reductase is present on the electrode surface (reaction 5) [26].

Niwa et al. employed a very different approach that relied on GOx to convert the Glu_{GABA} generated in reaction 1into α-ketoglutarate and H_2O_2 (henceforth called $H_2O_{2(GABA)}$, i.e. H_2O_2generated from the Glu that in turn is generated from GABA) (reaction-4) and then detecting it on an osmium-poly(vinylpyrridine) gel-horseradish

peroxidase-modified GCE [11]. Applying reactions-1 and reaction-4, researchers were able to detect GABA with adequate sensitivity and selectivity in the presence of DA, serotonin (HT-5) and ascorbic acid (AA). However, both approaches are incapable of continuously monitoring the changes in GABA levels in real-time since they require additions of reagents such as NADP and α-ketoglutarate. A biosensor technology that can accurately measure GABA in real-time and continuously without any external intervention is technically challenging and therefore as yet unrealized. Detailed recation pathways are shown in Figure 2-6.

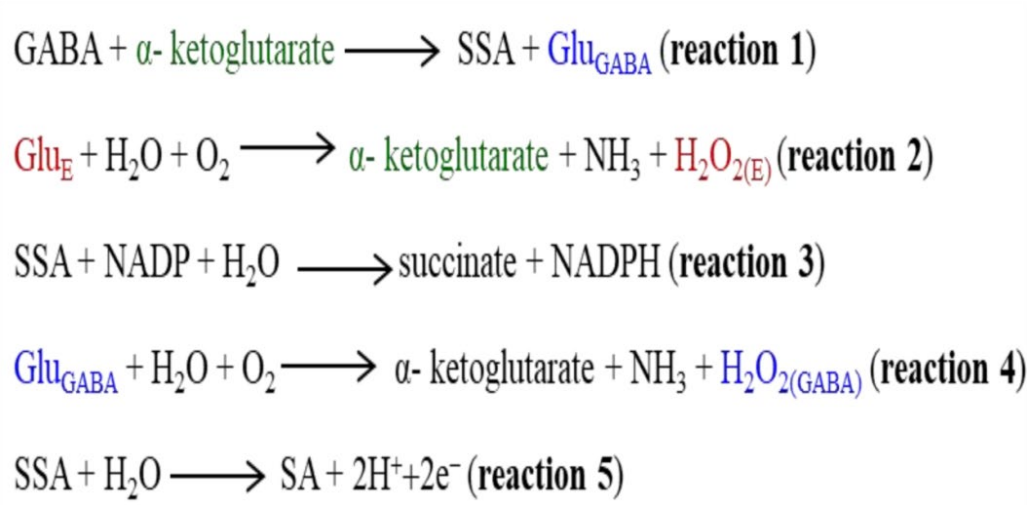

Figure 2-5: Reaction pathways and detection mechanism for GABA and GLU detection [14]

2.5 Working Mechanism and Sensor Design Considerations

2.5.1 Reaction Pathways

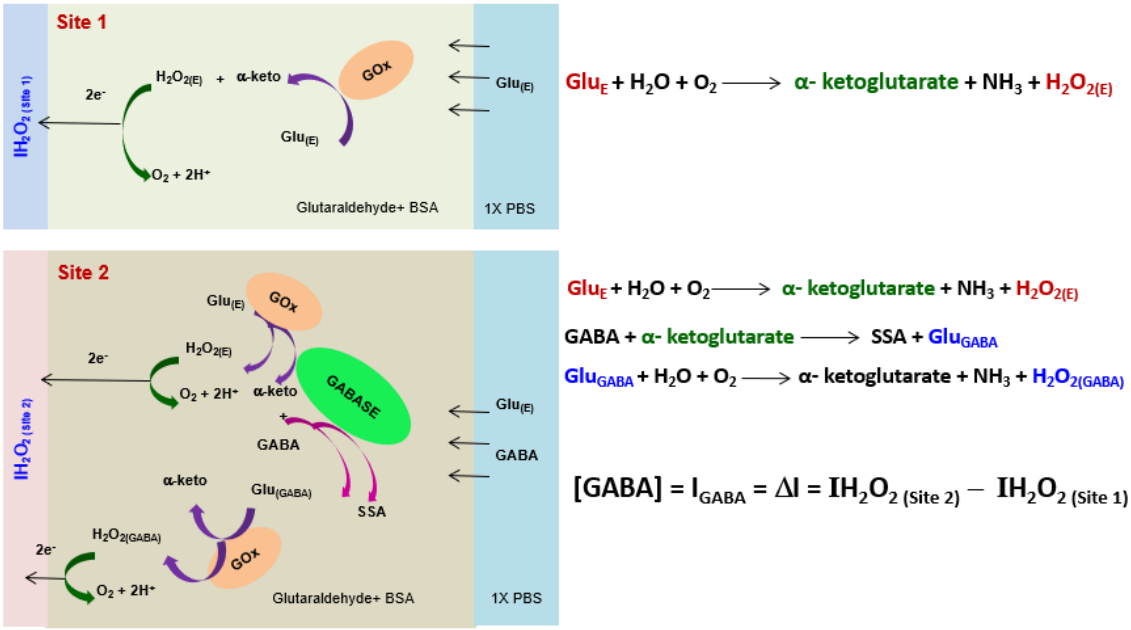

Figure 2-6: Reaction pathways for different sites and related reactions [14].

In this work, we report the development of a novel GABA probe based upon platinum (Pt) microelectrode array (MEA). The GABA probe uses two types of microbiosensors, namely a GLU microbiosensor located in Site 1, Figure 2-6) and a GABA microbiosensor (located in Site 2, Figure 2-6) that are uniquely modified with GOx only at Site 1 for reaction 1 to occur and with GOx and GABASE at Site 2 for reactions 1, 2 and 4 to occur. The two sites should be very close to each other, distance between them should be close. By simultaneously measuring and subtracting the oxidation currents of H_2O_2 generated from the two microbiosensors, current of $H_2O_{2(E)}$ at Site 1 (henceforth called $H_2O_{2(Site\ 1)}$) and H_2O_2 from $H_2O_{2(E)}$ and $H_2O_{2(GABA)}$ at Site 2 (henceforth called $H_2O_{2(Site\ 2)}$) GABA ($I_{GABA} = \Delta I = H_2O_{2(Site\ 2)} - H_2O_{2(Site\ 1)}$) can be

detected in real-time continuously (Figure 2-6) without adding α-ketoglutarate externally (Figure 2-6). This is possible because α-ketoglutarate generated in reaction 2 is used in reaction 1. This scheme can be readily implemented *in vivo* because the ubiquitous presence of Glu allows *in-situ* generation of α-ketoglutarate and thus, reaction 1 to occur continuously. Additionally, we prepare a blank electrode without any enzyme as our control. This electrode will detect neither GABA nor GLU. This electrode will only detect signals resulting from common, electrically active intereferent molecules like ascorbic acid. In case of wire we call this the "sentinel channel", which is further described in CHAPTER 5. In presence of a sentinel channel, our probe becomes truly self-referencing. The current at the sentinel channel is then subtracted from the GABA and Glu channels at each time point. This minimizes the effects of these environmental signals, thereby greatly improving the selectivity of the GABA and GLU channels.

Our material of choice for our sensors is platinum because it has high catalytic activity for oxidation of H_2O_2 (our reporter molecule). Platinum is also a general choice in enzymatic biosensors [12], [68], [69], [78]. Platinum electrodes are fabricated and commercialized in both shank style probes and microwire-based platform devices. Combining a series of microfabrication techniques platinum electrodes have been implemented in substrates like silicon [71] and ceramic [82]. Sensors based on polymer substrates are also available[83], [84]. The main concern with these sensors is their fragility. These probes break during penetration in the tissue. Other limitation is most of the times these sensors are arranged vertically which make spatial recording impossible. For those reasons sometimes wire based electrodes are used. Wires are easily modifiable, low- cost alternative to commercial sensors. It is also easily implantable in brain and

applications are available in literature [85], [86]. However, microfabricating wires for simultaneous monitoring of more than one neurochemical still remains a challenge. Other limiting mechanism is the enzyme coating procedure. Dip coating is generally used which allows for only partial spatial control [32].

2.5.2 Enzyme Immobilization

Immobilization of enzyme in the sensor is the most important step of any biosensor integration. The enzyme needs to form a stable layer in the sensor surface without loss of activity. A simple layer of enzyme is kinetically limited because of catalytic occupation of its molecules [32]. To solve this problem, we need a protein matrix that has higher loading (for enzymes) without loss of signals. In literature immobilization is done by cross-linking with a homo bifunctional molecule (glutaraldehyde) and protein matrix (bovine serum albumin, BSA) [12], entrapment in hydrogel matrix [87] or integration into a electrodeposited polymer [88], [89]. Comparison of these methods is presented in literature [32]. Cross-linking with BSA and glutaraldehyde gives the highest sensitivity in commercial platinum electrodes. The main drawback of cross-linking method is the limited lifetime of these sensors. A decrease in sensitivity is reported in the literature [83]. However, fine tuning enzyme concentration a sensor which is stable for at least a month have been reported [90].

2.5.3 Selectivity and Interference Rejection

Typically, selectivity refers to the ability of the sensors to produce high signal for the measured analyte and low signal for the unspecified molecules. It is an important consideration for in-vivo measurement because lots of chemical are present in the brain. Chronoamperometry is not selective method, meaning if any electroactive molecules

come in the contact of the surface, they get oxidized and produces current in constant potential. To maximize selectivity, we need mechanism that can stop the reaction between interferent molecule and the sensor surface. The most frequently used method is the use of size-exclusion layer like m-phenyldiamine (mPD [91]) or nafion [92]. These layers work on a simple method: it lets small molecule like H_2O_2 pass and blocks bigger molecules like ascorbic acid. Typically, these polymers are deposited electrochemically (cyclic voltammetry). While this method can prevent the interferent molecules, the trade-off here is the loss of sensitivity. Selectivity is measured by the ratio of sensitivity for the analyte divided by sensitivity of interferent. Higher the value suggests greater selectivity. Typically, selectivity value of $\geq$35 is desirable. Other commonly used method for interference rejection is the blank electrode or self-referencing method. In this method, an electrode without enzyme is placed in proximity to another enzyme-based working sensor. In the final phase, the current from this blank is subtracted from the working sensor. In the *in-vivo* application where background signal fluctuate often, blank electrode can be useful.

Throughout this dissertation we used various platforms for our sensors. The enzyme immobilization was done using the matrix of BSA and glutaraldehyde. An mPD layer was electrochemically coated for selectivity improvement.

CHAPTER 3

MATERIALS AND METHODS

3.1 Chemicals and Enzymes

Phosphate buffered saline (PBS), bovine serum albumin (BSA), glutaraldehyde, GABA, GABASE from Pseudomonas fluorescens, *L*-glutamic acid monosodium hydrate, ascorbic acid, hydrogen peroxide, choline, acetylcholine, dopamine, uric acid, seratonin (5-HT) and α-ketoglutarate disodium salt was purchased from Millipore-Sigma (MO, United States). All chemicals were reagent grade unless otherwise specified. Glutamate oxidase, recombinant lyophilized powder (9.3 U/mg), was purchased from Cosmo Bio Co., LTD (Carlsbad, CA, USA).

3.2 Microelectrode Array

3.2.1 8-TRK Commercial Platinum Microelectrode Array

Microsensors were prepared based on 8-TRK-type microelectrode arrays (Center for Microelectrode Technology, University of Kentucky, Lexington, KY). 8-TRK MEA consisted of eight platinum sites (50 μm × 100 μm, 100 μm boundary-to-boundary spacing for sites within a pair and 1, 1, 2 mm distance for between pairs, Figure 3-1) on a ceramic substrate (127 μm Al2O3) that employed a thin polyimide as a passivation layer. The fabrication process of these commercially available electrodes is described in

literature [3], [82], [93]. Electrode sites, connecting lines, and bonding pads were patterned onto a photoresist-coated 2.5 cm × 2.5 cm ceramic substrate by exposing the photoresist with collimated UV light through a mask. Using sputter coating system, a 500 Å adhesion layer of titanium and a 2300 Å layer of elemental Pt (Pt°) were coated in the ceramic substrate to perfectly define the electrode site, connection line and bonding pads. Besides the MEAs, all circuits were insulated with approximately 1.2 μm layer of polyimide to protect against aqueous environments and reduce charging current. Individual microelectrodes were sawed from patterned wafers using a computer-controlled diamond saw and were connected to printed circuit boards. Eight contact pads were located on the other side of the ceramic substrate which enables the probe to connect with our electrochemical system (FAST system, mkIII, Quanteon, KY, USA).

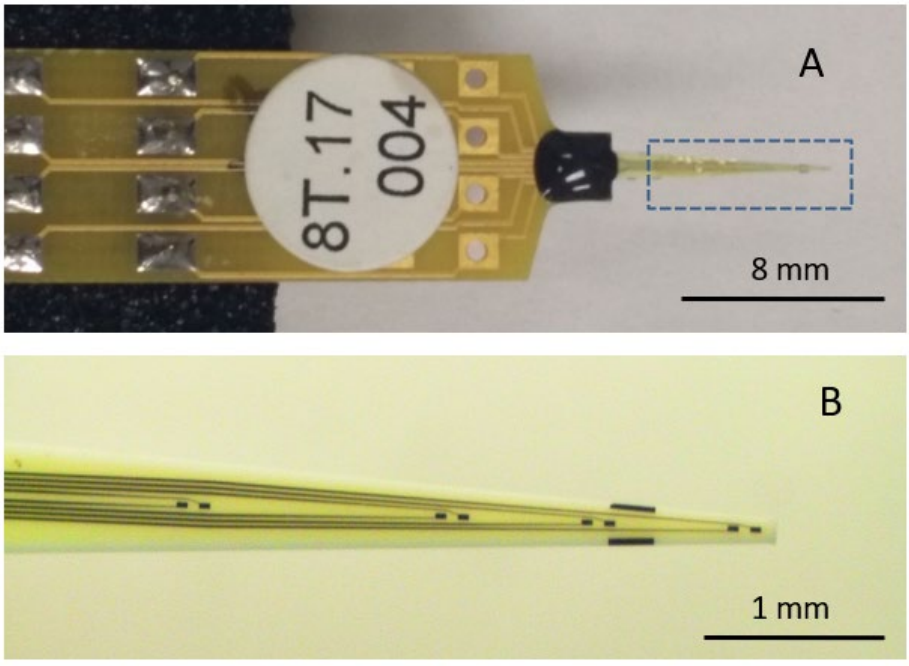

Figure 3-1: Optical picture of 8-TRK-type microelectrode arrays. A. Shows the whole probe with the connection pads, electrode sites. B. Shows zoomed in version of the eight electrode sites [14].

Some salient features of this probe in the context of our research are:

1. eight individually electrically addressable Pt microelectrodes that can easily be multiplexed to simultaneously measure other important neurochemicals, such as Glu, DA, adenosine and HT-5, through suitable surface modifications, which is not possible with other commonly available electrodes for chemical sensing, e.g., carbon fiber microelectrodes;
2. GABA and GLU microbiosensors can be placed in close proximity to provide precise measurements of local GABA level changes;
3. The ability to detect GABA-GLU in real-time without adding reagents (i.e., truly self-contained);
4. The location of MEAs along the long shank allows GABA sensing at multiple depths in the brain; and
5. Allows simultaneous sensing of neurochemicals and field potentials for multimodal recordings, which is not possible with the current neurochemical technologies.

In our initial sensor development phase, we exclusively used these MEA shown in detail in Chapter-4. Initial ex-vivo experiments to get GABA and GLU concentration from a rat hippocampus was also demonstrated using these MEA shown in detail in CHAPTER 6.

3.2.2 Wire based Platinum Microelectrode array

We have developed a platinum (Pt) microwire biosensor probe that can is easily fabricated in a lab that has electrochemistry expertise. Our biosensor probe is composed of three Pt microwires to detect GABA, GLU, and interferents respectively. The GABA biosensor is based on a novel process that does not require the addition of substrates, which makes it easier to use for *in-vitro*[94] and *ex-vivo*[14] applications and which enables in vivo recordings[15], [94]. Additionally, when the ends of the microwires are in the same plane, as we report here, the geometry is suitable for placement into cell culture dishes and brain slices. It is also optimal for in vivo recording in brain regions with laminar structure, such as the cerebral cortex and hippocampus in animals.

Our microwire biosensor design is not only advantageous for future, longitudinal in vivo recording, its geometry has distinct advantages over shank-style neural recording probes for brain slice and cell culture models. Shank-style probes are designed to record electrical signals from different regions of the brain for in vivo studies. In contrast, brain slices are cut thin and placed horizontally in a recording chamber to extend tissue viability and function. Thus, a geometric profile in which all of the microwire biosensor sites contact the slice in the same horizontal plane provides an advantage. Similarly, cultured cells for in vitro models grow in a thin layer on a flat cell culture dish. Again, a microwire biosensor in which all probe sites are in a horizontal plane equidistant from the cells is a desirable arrangement. In our previous studies, we experienced difficulties in using shank-style microbiosensor arrays when recording from brain slices[14] and cultured cells[94]. When recording in brain slices, we could only use two of the eight sensor sites on a shank-style probe; the same was true for cell culture recording.

Fabrication of microwire biosensors in-house offer several advantages. They are as follows:

1. The mPD layer can be coated on the outside for longer sensor life for in vivo applications, or on the inside for higher sensitivity, short-term use.
2. Additional wires can be added and placed at different depths for recording in more than one brain area or region.
3. Pt microwires are relatively inexpensive and easy to coat compared to high-density shank arrays.
4. It is relatively easy to change the geometrical area of the biosensors by simply changing the Pt microwire diameter.
5. A high-density probe (up to 8 biosensors) can be assembled with thinner wires to create a probe diameter of less than 300 microns. This should result in minimal inflammation, which is a desirable biosensor characteristic for *in vivo* recordings. The ease of handling the microwire biosensor with the microwires banded together provided the strength and stability to insert it into a cannula for real time in vivo recording. The ability to remove it and replace it with a fresh biosensor facilitated a pilot long-term study of GLU and GABA dynamics with high temporal resolution in the hundreds of ms.

The details of fabrication, wire selection and characterization are described in detail in Chapter-5. The *ex-vivo* and *in- vivo* results from our wire-based microarray is discussed in Chapter-6.

3.3 Biosensor Preparation

3.3.1 Electrode Preparation

To coat the 8-TRK probe for GABA and GLU electrodes, we modify two sites (pairs). Site-1 is designated for GLU electrode and is coated with Glutamate oxidase (GOx) only. Site-2 is designated for GABA electrode and is coated with GOx and GABASE. This is shown in Figure 3-2.

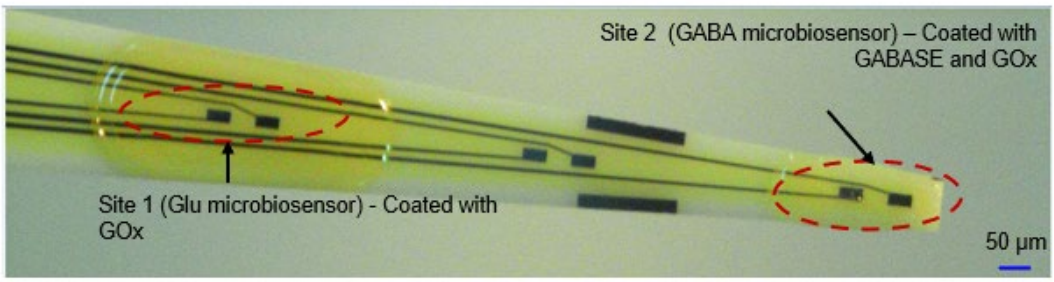

Figure 3-2: The probe at higher magnification showing 6 of 8 Pt microelectrodes. Each site has two modified microelectrodes. For this work, Site 1 is modified with Gox (Glu microbiosensor) and Site 2 is modified with GOx and GABASE enzymes (GABA microbiosensor). Each Pt microelectrode is 100 µm × 50 µm. The distance between the sites is 1 mm [14]

In case of wire-based microelectrode arrays, we modify first wire as the GABA channel with GABASE and GOx, second wire as GLU channel with GOx only and third wire as sentinel channel with BSA and glutaraldehyde (no enzymes). We discuss the fabrication and characterization in Chapter-5.

3.3.2 Enzyme Aliquot Preparation

The GOx enzyme with the BSA and glutaraldehyde was coated in Site 1 as per literature [12]. For GLU sites (channels), the GOx enzyme was mixed in DI water to prepare aliquots of 0.5 U/µL and stored in -80°C. Prior to coating, they were thawed first at 4°C and then at room temperature. DI water (985 µL) was added to 10 mg BSA in a 1

mL centrifuge tube. After allowing the BSA to dissolve, 5 µL of glutaraldehyde (25% in water) was added to the solution. We kept the solution mixture (1% BSA and 0.125% glutaraldehyde) at room temperature for ~5 min. A 4 µL of the mixture was added to 1 µL of GOx (0.5 U/µL) and centrifuged to form the final enzyme-matrix mixture of 0.1 U/µLGOx/0.8% BSA/0.1% glutaraldehyde.

Similarly, for GABA sites (channels), DI water (986.7 µL) was added to 13.33 mg BSA in a 1 mL centrifuge tube. After allowing the BSA to dissolve, 6.67 µL of glutaraldehyde (25% in water) was added to the solution. We kept the solution mixture (1.33% BSA and 0.166% glutaraldehyde) at room temperature for ~5 min. Next, 3 µL of the mixture was added to 1 µL of GOx (0.5 U/µL) and 1 µL GABASE (0.5 U/µL) and centrifuged to form the final enzyme-matrix mixture of 0.1 U/µLGOx/0.1 U/µL GABASE/0.8% BSA/0.1% glutaraldehyde. For the GABASE-only site, the procedure used for GLU site (channel) was followed except that GABASE instead of GOx was used.

For sentinel channels, in case of wires, DI water (985 µL) was added to 10 mg BSA in a 1 mL centrifuge tube. After allowing the BSA to dissolve, 5 µL of glutaraldehyde (25% in water) was added to the solution. We kept the solution mixture (1% BSA and 0.125% glutaraldehyde) at room temperature for ~5 min. At this point, we coat the wires with this solution. No enzymes were present in this mixture.

3.3.3 Enzyme Coating Procedure

Under a Nikon stereomicroscope (Model, SMZ18), three drops (0.05 µL/drop) of the respective enzyme-matrix mixture was applied manually at each site using a

microsyringe (Hamilton®, Model 701 N). Then the probe was stored for 48 h in an aluminum foil covered storage container with no exposure to light prior to use.

3.4 Reference Electrode

Ag/AgCl is used as our reference electrode for amperometric measurements. Teflon-coated Ag wire was purchased for this purpose (wire diameter-200 µm bare, 280 µm coated; A-M Systems, Carlsberg, WA, USA). To prepare this reference wire, one side of the silver wire was exposed 2 mm using a scalpel and then soldered to a copper connection pin (Tin soldering, Radioshack, USA) and the other side of the silver wire was exposed approximately 1 cm. This silver wire was then used as an anode with the silver part immersed in saturated NaCl in 1 M HCl, and a platinum wire was used as a cathode. A +9 V potential was applied to this 2-electrode system using a Gamry reference 600 workstation for 20 minutes. Prepared Ag/AgCl wire was then rinsed with DI water before use. This Ag/AgCl is stored in room temperature at 3MNaCl solution.

3.5 Electrochemical Measurements

For amperometry measurements, a multichannel FAST-16mkIII® potentiostat (Quanteon, LLC, Nicholasville, KY, United States) in a 2-electrode setup was used with an Ag/AgCl electrode as the reference electrode, our microelectrode array (8-TRK/microwires) is our working electrode. The general setup and the experimental setup are shown in Figure 3-3. The applied potential was set at +0.7 V for H_2O_2 detection. Note: This applied potential can be reduced to +0.3 V vs. Ag/AgCl when modified using platinum black as reported in the literature [95]. The recording frequency was 2 Hz. All solutions were freshly prepared on the same day that the experiments were conducted. The experiment was carried out in a 40 mL buffer solution. The analytes were introduced

into the solution using a syringe pump (KD Scientific, Legato® 100 syringe pump) to obtain the desired concentrations (M). The solution was continuously stirred at 200 rpm and maintained at 37°C. All measurements were repeated at least 3 times. In amperometry calibration for the beaker experiments, 5-10 mins was usually given to obtain a stable baseline.

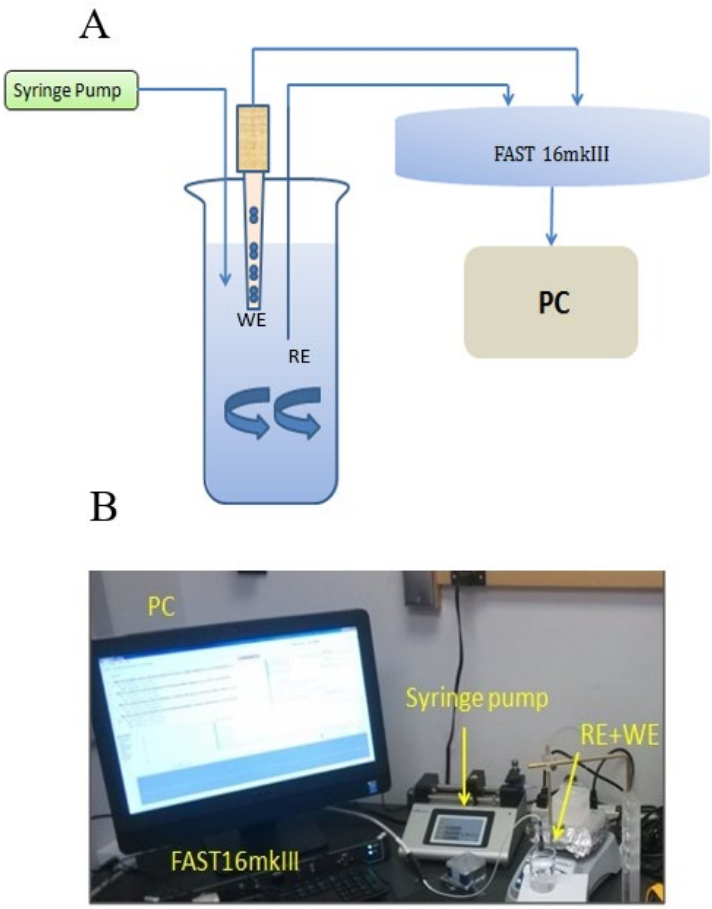

Figure 3-3: Chronoamperometry experimental setup A. shows the schematic diagram of our setup. B. Experimental setup of our beaker experiments. WE: working electrode (8-TRK/microwires), RE: reference electrode (Ag/AgCl).

3.6 Recording GABA and GLU in Brain Tissue

3.6.1 Animal Care and Use

Male Sprague Dawley rats were housed on a 12 h on – 12 h off cycle with food and water provided ad libitum, according to a Louisiana Tech University IACUC protocol, the Guide for the Care and Use of Laboratory Animals and the AVMA Guidelines on Euthanasia.

3.6.2 Hippocampal Slice Preparation

Hippocampal slices were prepared from an adult Sprague Dawley rat that was anesthetized using 5% isoflurane gas prior to decapitation and rapid removal of the brain. The brain was immediately placed into ice cold artificial cerebrospinal fluid (aCSF) containing (in mM): 135 NaCl, 3 KCl, 16 $NaHCO_3$, 1 MgCl, 1.25 NaH_2PO_4, 2 $CaCl_2$, and 10 glucose, bubbled with 95% O_2/5% CO_2 (carbogen) [96]. The slicing chamber of an OTS-5000 tissue slicer (Electron Microscopy Sciences) was filled with aCSF at 4° C and then 500-μm thick coronal sections were cut and transferred to a holding chamber filled with aCSF maintained at 35°C and bubbled with carbogen. Slices were incubated for at least 60 min prior to recording. Thereafter, one slice was transferred to a liquid-air interface of a BSC1 chamber (Scientific Systems Design, Inc.) with the slice suspended on nylon net at the liquid-air interface with continuously dripping aCSF (37°C) bubbled with carbogen. Waste products were removed by continuous suction from the recording chamber Figure 3-4.

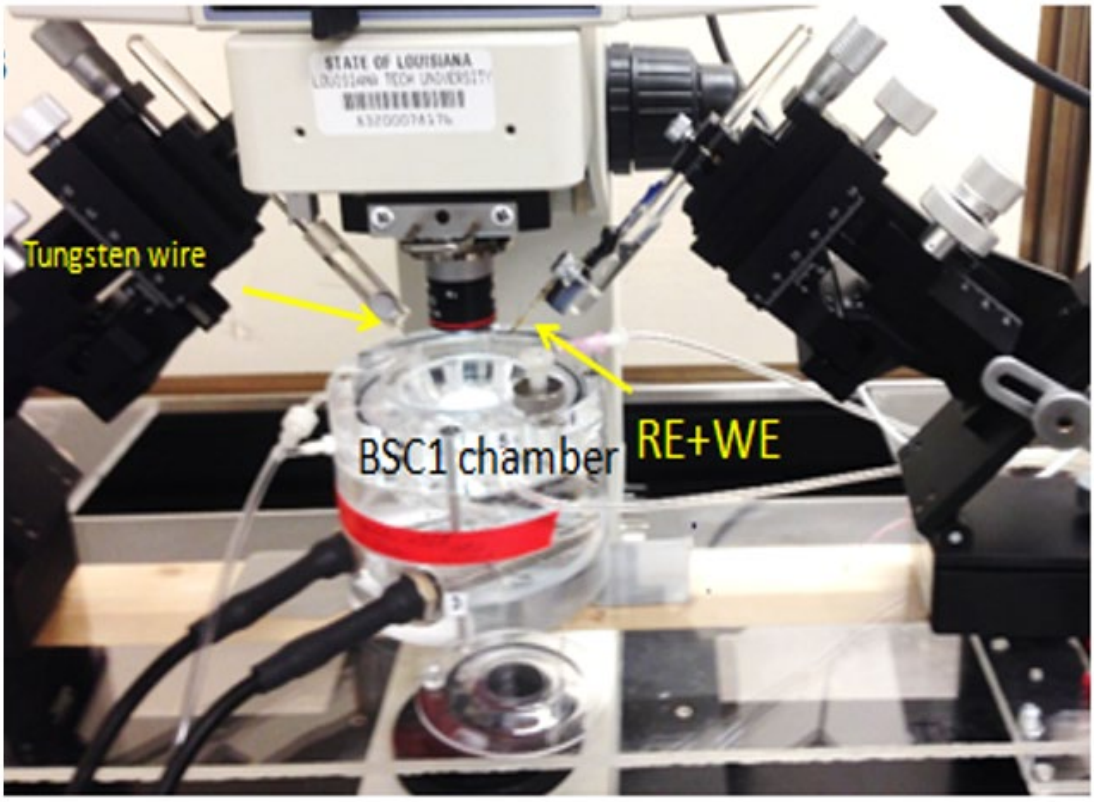

Figure 3-4: Setup for our *ex vivo* experiments in a working chamber consisting of modified probe (microwire/8-TRK), Ag/AgCl wire and tungsten wire as stimulus electrode, Photograph provided by P.T Doughty and T.A Murray, 2018 [14].

3.6.3 GABA Recording in Rat Hippocampal Slices

The microbiosensors were coated with a size-exclusion polymer (m-phenylenediamine, mPD) to prevent the interferents reaching the microbiosensor surface and to enhance the probe selectivity [97]. Chapter-4 and Chapter-5 shows the effectiveness of mPD layer to block intereferents. However, the trade-off is that we see a loss of sensitivity as well. The mPD layer was electrochemically deposited (cycling between +0.2 V and +0.8 V, 50 mV/s, 20 min in 10 mM mPD solution). A pair of 160 µm diameter tungsten stimulation electrodes was placed in the Schaffer collateral CA1 pathway within 200 µm of the microbiosensor probe sites [96]. A home-built, Arduino-based signal generator [98] and a stimulus isolator (A365, World Precision Instruments,

USA) were used to deliver 100 μA current pulses to the slices. Two micromanipulators (M3301, World Precision Instrument, Hessen, Germany), an upright brightfield microscope (Eclipse E600FN, Nikon, Japan), and a custom, acrylic stage facilitated placement of the microwire biosensor in the pyramidal layer of hippocampal region CA1. Paired tungsten wire stimulation electrodes, 160-μm in diameter, were placed within the Schaffer collaterals, ~150μm from the microwire biosensor, as previously reported [14],[96]. For tissue slices recording with our 8-TRK probe we used five different types DC-signals with varying pulse-widths (duration of the pulse). However, for our tissue experiments with the microwire channels we programmed three types of 5 s pulse trainswith1-ms pulse width were programmed to deliver 10 Hz, 50 Hz, and 140 Hz stimulation and a single, 100 ms control pulse was also programmed. All these pulses were programmed and verified with an oscilloscope prior to our experiments. The motivation for selecting these stimulation frequencies were purely driven by clinical experience where 140 Hz stimulation is often used in deep brain stimulation (DBS) therapy against seizure or tremor, 50 Hz stimulation is used in direct cortical stimulation (DCS) to induce seizure while 10 Hz stimulation is used in transcranial alternating current stimulation (tACS) therapy. Current detected at the probe sites was plotted in real time. After the response current returned to baseline, we delivered a single 100 ms control pulse to assess the health of the slice and to verify that stimulations were not inducing potentiation. When the response current to a single pulse reached 80% or less than the mean response of the first three control pulses, the slice was discarded.

3.7 Awake-Free Rat Behavior Recording

3.7.1 Microwire Guide Cannula Fabrication

Each guide cannula was constructed from a 20-gauge stainless steel hypodermic needle with a plastic luer lock fitting (BD305125, Becton, Dickson and Company, Franklin Lakes, NJ). The hypodermic needle was blunt cut to a length of 2.8 mm, which allowed for its insertion into the hippocampus at the desired depth. A 25-gauge hypodermic needle (BD305175, Becton, Dickson and Company) was fashioned into a filler for the lumen of the guide cannula; the filler keeps blood and tissue from infiltrating into the guide cannula. To facilitate the insertion of the filler, most of the plastic luer lock fitting was removed using a Dremel Multipro™ using a circular 3.4 cm diameter cutting bit, leaving approximately a 1-2 mm section of the plastic fitting that surrounds the top of the needle. A 1mm hole was drilled into the center of a luer lock screw cap (51525K311 nylon quick-turn cap, McMaster-Carr). The needle was passed through the hole in the cap until it reached the remaining portion of the plastic fitting. Cyanoacrylate adhesive was used to secure the needle to the cap. The needle was cut to a length that filled the guide cannula but did not protrude through it. For our guide cannula, the filler needle was cut to 2.8 cm in length. Needles were cut with a Dremel 3.4 cm diameter cutting bit and the ends were smoothed with a flat mill file of fine coarseness. An Ag/AgCl reference electrode was attached to the outside and parallel to the metal portion of the guide cannula using cyanoacrylate adhesive. The implanted end of the reference electrode was positioned at the end of the cannula. The connector end of this electrode was fashioned into a loop and pressed flat against the top of the luer lock fitting. The insulation on the

loop portion was removed to facilitate contact with the microwire biosensor for recording. When not recording, the filler cap covers the loop to prevent damage.

3.7.2 Cannula Implantation

A cannula, with the filler inserted, was implanted into the CA1region of the hippocampus, following a protocol approved by the Louisiana Tech University IACUC. To reduce stress, Male Sprague-Dawley rats were lightly anesthetized using isoflurane before an intramuscular injection of 75mg ketamine HCl and 0.25 mg dexmedetomidine HCl per 1kg of animal weight. Using aseptic techniques, a 3.5 mm diameter craniotomy was made 5.0 mm posterior from Bregma, 2.3 mm right lateral to the midline, and 2.8mm deep measured from the top of the skull. Four 1.50 mm stainless-steel anchor screws (Stoelting Co.) were implanted bilaterally along the outer edge of the scalp incision and a fifth screw located just anterior to lambda and 2.0mm laterally to the right of the sagittal suture as anchors for the implant. The cannula, with the filler inserted, was attached to a custom, 3D printed holder on a stereotaxic frame and lowered at 100 μm per min to the desired depth. The cannula and screws were secured using dental acrylic (Ortho-Jet BCA) which was applied to completely cover the bone screws, encapsulate the lower part the guide cannula fitting and sealed the exposed skull. Skin incisions were closed with interrupted sutures, and topical powder (Neo-Predef, Zoetis) was applied for antibiotic, anti-inflammatory, and analgesic effects. After this, the rat was given an IM injection of 1mg/kg Atipamezole hydrochloride to bring the animal out of anesthesia and then monitored until it regained sternal recumbency. Rats were housed individually after surgery. Animals were given at least two weeks to heal before recording.

3.7.3 *In vivo* Recording

Prior to recording, a rat was anesthetized in a chamber using 5% isoflurane for 5 min. Immediately after removing the rat from the chamber, the filler needle was removed from the guide cannula and a sterile microwire biosensor array was inserted into the guide cannula. It was secured by twisting the luer lock cap on the microwire array; this also ensured contact with the reference electrode. (The filler was stored in 91% isopropyl alcohol during surgery. After recording, it was dried with a sterile tissue and reinserted.) The pin connector on the microwire biosensor array was inserted into the FAST potentiostat system and the reference wire connector pin was inserted into a separate channel on the potentiostat fitting. The rat was placed in a standard, clear plastic housing cage without a cover for recording. Corn cob bedding (Envigo, Madison, WI) was used to line to bottom of the cage. Two to three pieces of dry chow and a water bottle were placed in the cage.

3.8 Data Acquisition and Analysis

3.8.1 Key Sensor Parameters from Beaker Experiments

The Fast analysis® software provided by Quanteon was used for data analysis. Sensitivity was defined as the change in current for each unit of analyte addition. Sensitivity was calculated from the slope (pA/μM) of the calibration curves (current density vs concentration curves). Then the slope was converted into $nA\mu M^{-1}cm^{-2}$ by dividing it by the Pt microelectrode area (5×10^{-5} cm^2 in case of 8-TRK probes and $1.27 \times 10^{-4} cm^2$ in case of microwire channels). The limit of detection (LOD) was calculated by dividing (3 times the standard deviation of 10 points from the baseline) by the least squares slope, which is based on the FAST 2014 software manual provided by

Quanteon. The baseline is the signal that was obtained when no electroactive analyte was present in the solution.

3.8.2 Data Storage for *ex-vivo* and *in-vivo* Recordings

For *ex-vivo* and *in-vivo* recordings the FAST system was set to acquire current data at 1000 Hz (biased at +0.7 V). An entire data file is too large for traditional software, such as Microsoft Excel. Therefore, we used the Fast Analysis software which is integrated into the FAST recording system to store time and current data in 1000 s segments as csv files for offline analysis.

3.8.3 Definitions and Determination of Key Peak Parameters

Current data were imported into ORIGIN-PRO 2019B for analysis. Individual responses were isolated based on noted stimulation times. The current from interferents on the sentinel channel was subtracted from the GLU channel to derive the current due to GLU. An example plot is shown in with the raw signals for GLU and the sentinel channels in Panel A and the subtracted GLU signal ($I_{GLU} - I_{Sentinel}$) in Panel B. Similarly, the current from interferents on the sentinel channel and signal in the GLU channel was subtracted from the GABA channel to derive the current due to GABA. An example plot is shown in Figure 3-5 with the raw signals for GABA channels in Panel A and the subtracted GLU signal and sentinel signal ($I_{GABA} - (I_{GLU} - I_{Sentinel})$ in Panel B. Response current was allowed to return to baseline before each subsequent stimulation; the mean of the last 10 s of each response was used to define that response's baseline. Maximum, 10%, 50%, and 90% values of the peak response were then determined as shown in Figure 3-5. The time between 10% and 90% of the rising peak were used to determine the rise time (T_R). Squares in Figure 3-5; A&B shows the peak of each signal.

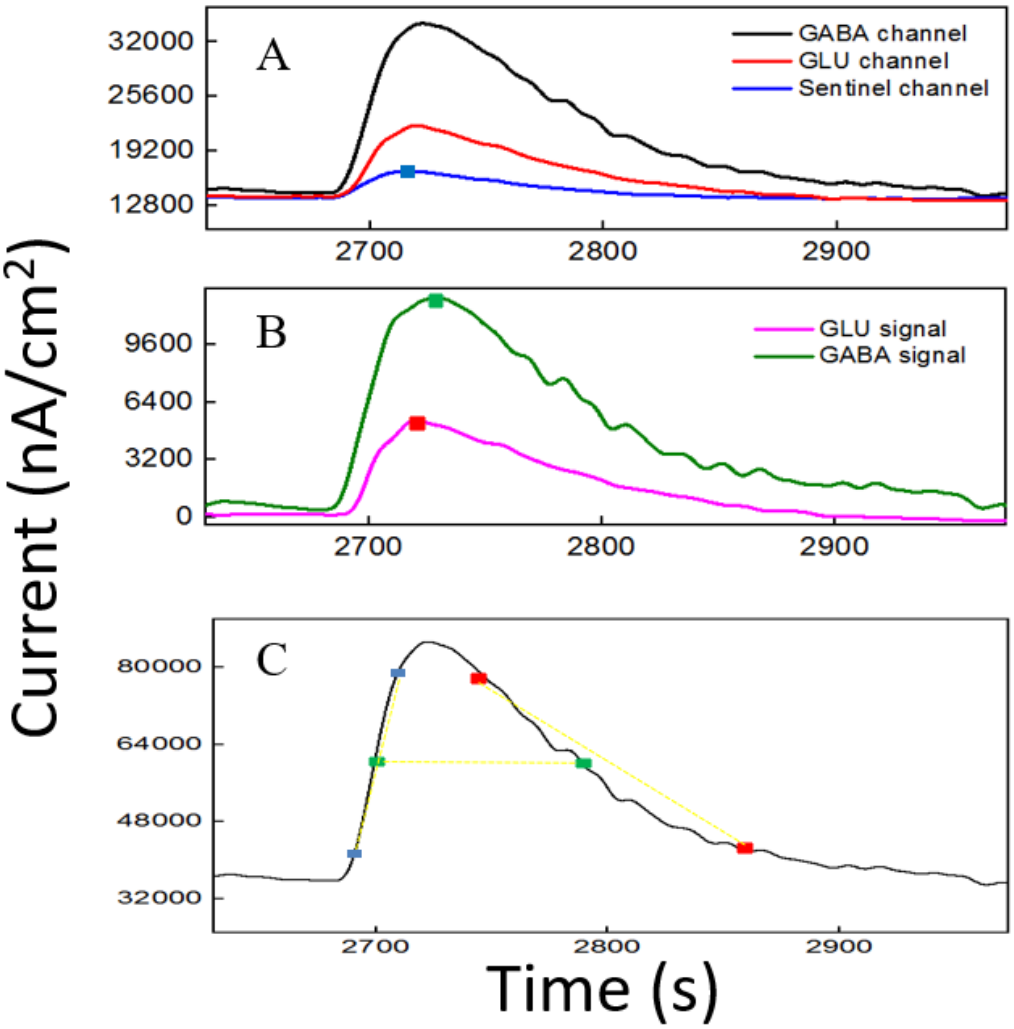

Figure 3-5: Sample plot of current response to electrical stimulation. A. Raw current recorded from the GABA, GLU and sentinel channels. B. Resulting GLU and GABA signal after the relevant subtraction are done. C. Shows Rise time (T_{R10-90}, time between blue squares), decay time (T_{D10-90}, time between red squares) and full duration at half maximum (FDHM, time between green squares).

The time between 90% and 10% of the falling peak were used to calculate the decay time (T_D). The time between the rise and fall of the peak at 50% of the maximum current was used to measure the full width and half maximum (FDHM). Responses were discarded if features were indistinguishable from noise (< 2X noise) or if the sentinel signal increased above the GLU channel. GABA current was obtained by subtraction of both the sentinel and GLU channel current. Peak values were converted into μM concentration based on calibration curves.

3.9 Thickness Measurement

Keyence 3D Laser Scanning Confocal Microscope (model VKX150, Keyence, Osaka, Japan) was used for thickness measurement. Using the accompanying visual software *VKViewer* we measured the average roughness in the electrode area where there was enzyme coating. We subtracted this roughness from the average roughness without the enzyme coating. The result is our enzyme coating thickness. Thicknesses were measured and averaged from three sets of data (n=3).

3.10 Statistics

Error value is shown as mean ± SEM. Two-tailed Students t-test was performed at 95%confidence interval ($p<0.05$) to compare means. One-way ANOVA was performed with significance defined as $p < 0.05$ to verify if sensor-to sensor variation (in the same site) is significant. All other normally distributed data were analyzed using ANOVA, with significance at $\alpha = 0.05$. For the *ex-vivo* and *in-vivo* data, evaluation of peak concentration values indicated that they were not normally distributed, and the independent Wilcoxon test was used to determine significant effects for $\alpha = 0.001$, $\alpha = 0.01$ and $\alpha = 0.05$.

CHAPTER 4

SENSOR DEVELOPEMENT

4.1 Surface Cleaning

First part of our development of the GABA sensor is to clean the 8-TRK microelectrode surface. When we receive the microelectrodes from the manufacturer, the surface may have some dust particles or unwanted surface deformities. To remove those, we need to clean the surface. One other aspect of these dust particles is that, they may reduce the sensitivity of microelectrodes (sensors). One good way to track the surface conditions is to calibrate hydrogen peroxide (H_2O_2) in the microelectrodes. As H_2O_2 is also our reporter molecule (responsible for the current) the increased sensitivity towards H_2O_2 also means our surface will be more responsive towards GABA/GLU.

In our studies we have cleaned the surface with methanol first and then electrochemically with mild sulfuric acid. After each step we calibrated the sensors for 1-5 μM H_2O_2 (n=4). The as-received microelectrodes have a sensitivity of 1680± 102 nA/μMcm^2 . However, after methanol cleaning this number increased to 1900 ± 110 nA/μMcm^2 . This corresponds to almost 15% increase from our initial sensitivity. Further electrochemical cleaning in 0.05 M sulfuric acid (cyclic voltammetry, [−0.3 V, +1.0 V], 20 mV/s, and 15 cycles) in a 2-electrode setup using a saturated calomel electrode as the

RE, shows more increase in our sensitivity. The sensitivity after CV cleaning is: 3180 ± 134 nA/μMcm^2. We show these results in Figure 4-1.

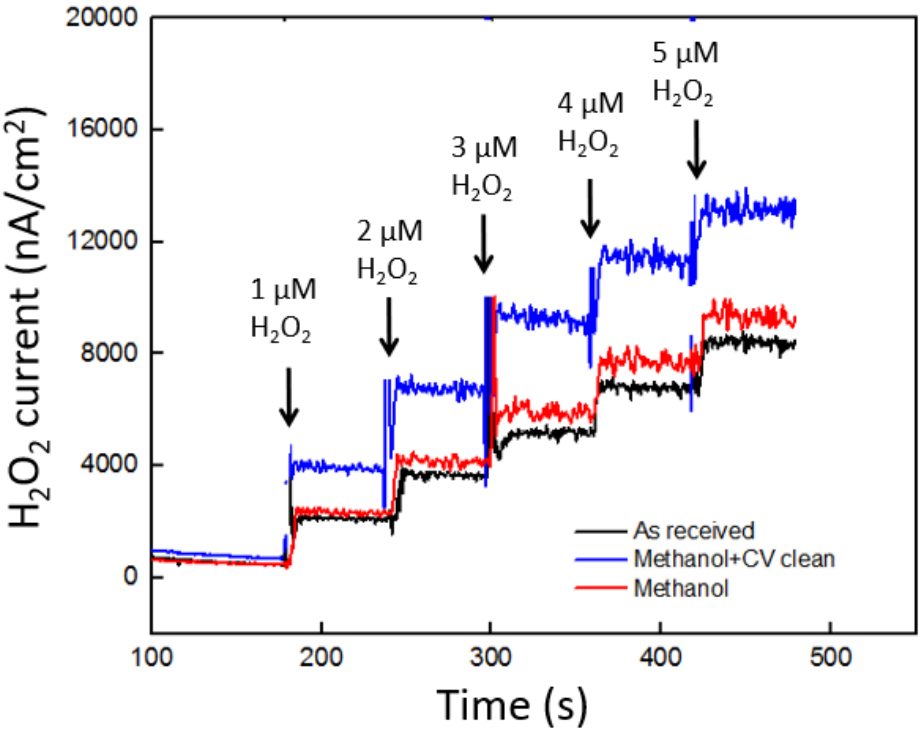

Figure 4-1: Comparison of cleaning methods. H_2O_2 calibration for as-received(black); with methanol clean (red) and methanol +echem cleaning (blue). Amperometry parameters: + 0.7 V *vs* Ag/AgCl wire in 1X PBS beaker in room temperature; the solution was always stirred at 200 rpm

As the results show we get almost 90% increases in our H_2O_2 sensitivity after this two-part cleaning. The reason for can be attributed to increased porosity and surface roughness due to electrochemical treatment. One more reason for this behavior can be found in the works of Chao et.al.,who show, by electro-impedence-spectroscopy (EIS), that with CV cleaning, charge transfer resistance reduces and electron transfer between the electrode and electrolyte happens more rapidly. From their experiments they also found that, CV cycling completely etches off grain boundaries which in turn make the

grains more conducive than grain boundaries. The etched grain boundaries may also be the cause of atomic scale heterogeneity [90].

4.2 GABA Calibration in α-ketoglutarate

Studies have shown dependence of the GABA current response (pA) on concentration of *α*-ketoglutarate [11], which is an important molecule in physiological functions, for example in the Krebs cycle[99]. Therefore, we first studied the electrochemical response of the Glu and GABA microbiosensors (Sites 1 and 2) in the presence of different amounts of α-ketoglutarate (1 μM – 500 μM) in the solution. Figure 4-2 shows the typical AM responses at Sites 1 and 2 in 1X PBS supporting electrolyte (background or control, blue dashed, red dashed curves), and to varying concentrations of GABA (5, 10, 20 and 40 μM) in 100 μM α-ketoglutarate solution prepared in 1X PBS (blue solid, red solid curves).These values of concentration in the micromolar range. They were chosen because of their relevance to the ones encountered in the brain microenvironment where GABA is typically present [26].For example, GABA levels are in the range of 20-70μM in rat brain slices, [28],and up to 1.25 μM/cm^{3}in the human brain[29]as measured by proton magnetic resonance spectroscopy. The response was recorded in different concentrations of α-ketoglutarate solution, first by allowing the microbiosensors to stabilize in the solution for up to 240 s, and then injecting GABA at 1 min time intervals to obtain the desirable concentration Figure 4-2. From Figure 4-2, as expected, we observe that the GLU microbiosensor at Site 1 did not exhibit a response to GABA because of the absence of the GABASE enzyme. Also, there was no enzymatic activity of GOx in converting GABA into Glu and then into H_2O_2. This indicates that the GABA conversion is highly selective at Site 2 that has GABASE and not at Site 1. The

GABA microbiosensor at Site 2 responded to GABA when the α-ketoglutarate concentration was at least 40 µM (Figure 4-2).

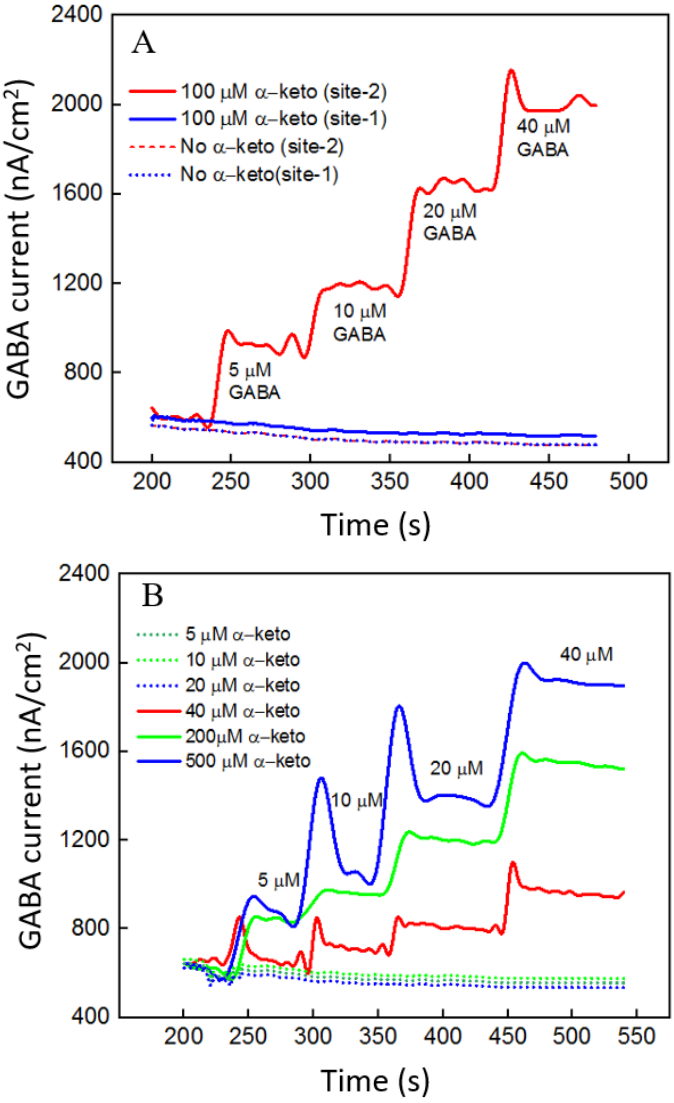

Figure 4-2: GABA probe calibration (5-40 µM GABA) in different concentrations of α-ketoglutarate (5, 10, 20, 40, 100, 200, and 500 µM) in 1X PBS. A. Current response at GABA microbiosensor in Site 2 and Glu microbiosensor in Site 1 in PBS only (background or control – red dashed curve, blue dashed curve, respectively) and in 100 µM α-ketoglutarate in 1X PBS (red and blue solid curves, respectively). B. Current response at GABA microbiosensor for other concentrations of α-ketoglutarate. The lower concentration at which there was no GABA response is shown in dotted lines. GABA responses of 40,200 and 500 µM are shown in red, green and blue. The microbiosensors were biased at + 0.7 V vs Ag/AgCl reference. The solution was stirred at 200 rpm and maintained at 37°C [14].

A transient spike in the signal was observed during the injection of the solution in the beaker. However, the signal was stabilized a few seconds following the injection of the solution. Sometimes the time to stabilization was a bit longer (e.g. in the case of 40 μM and 500 μM α-ketoglutarate experiments). This might be due to a few bubbles in the micro syringe pump that disturb the solution, more in certain experiments than others. The other data points for the same α-ketoglutarate concentrations did not show similar spikes. The highest sensitivity was observed at 100 μM. From Figure 4-3, the sensitivity is36±2.5 pA μM^{-1} cm^{-2} and the LOD is 2±0.12μM(*N*=6), which is 10-fold higher than that of similar amperometry-based microsensors[11].The sensitivities at 40 μM,200 μM and 500 μM of α-ketoglutarate were 12±1.7, 20±2.4 and 28±2.5 respectively, and the LOD was 7±0.7, 4.0±0.4 and 3±0.24, respectively (Table 4-1). This GABA response to α-ketoglutarate concentration is in agreement with previously published literature [11].

One possible reason for the decrease of GABA sensitivity at highest α-ketoglutarate concentrations could be due to their scavenging of H_2O_2 as suggested by previous studies [100], [101]. Another study [26] showed a similar trend where the GABA sensitivity was highest at 1mM α-ketoglutarate and then decreased at much higher concentrations. The LOD achieved using the non-optimal GABA microbiosensor is 2-7 μM, which is lower than the clinically-relevant concentrations [28] and similar to the values achieved by alternative methods [29] in the human brain.

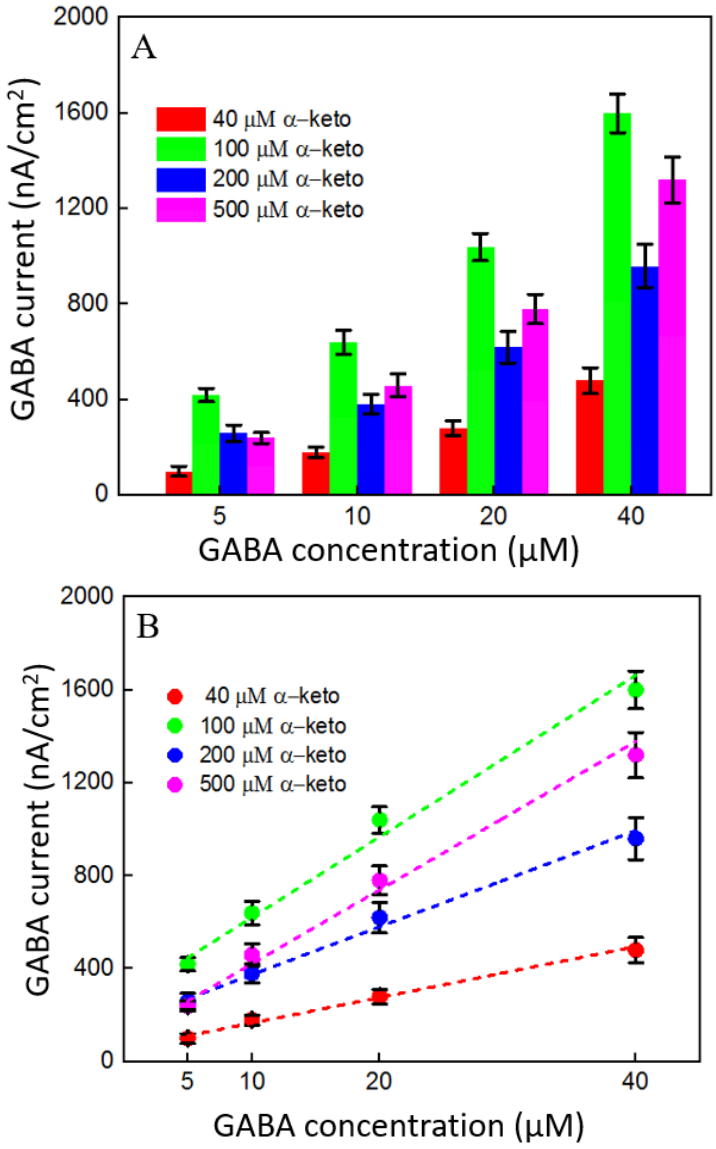

Figure 4-3: Current response and linear fitting at GABA microbiosensor for different GABA concentrations and α-ketoglutarate concentrations at ≥ 40 µM. A. shows the currents in bar-charts. B. Shows the linear fit. Linear fit parameters obtained: 40 µM α-keto sensitivity = (12 ± 1.5 nA/µMcm^2), R^2 = 0.99728; 100 µM α-keto sensitivity = (36 ± 3 nA/µMcm^2), R^2 = 0.99582; 200 µM α-keto sensitivity = (20 ± 2.6 nA/µMcm^2), R^2 = 0.99582 and 500 µM α-keto sensitivity = (28 ± 2.8 nA/µMcm^2); R^2 = 0.99582 at GABA microbiosensor. Legends: 40 µM (red), 100 µM (green), 200 µM (blue) and 500 µM (magenta). Error bars are shown as mean± SEM [14].

Sensitivities differ slightly between microelectrodes, which are likely due to variations in the quantity of enzymes that are manually applied to each site. Any potential defects in the surface of the electrodes may also lead to a difference in sensitivity. But this could be remedied by employing an array of GABA and Glu microbiosensors and by applying appropriate statistics (e.g. averaging the current values etc.). This sensitivity variation can be further minimized by employing micro spotting techniques that are fully automated and dispense very precise volumes of enzyme solutions.

Table 4-1: GABA sensitivity and LOD for different α-ketoglutarate concentration [14]

α-ketoglurate concentration (μM)	**Sensitivity (nA $\mu M^{-1}cm^{-2}$)**	**LOD (μM)**
40	12±1.7	7±0.7
100	36±2.5	2±0.12
200	20±2.4	4±0.4
500	28±2.5	3±0.24
40	12±1.7	7±0.7

4.3 Effect of Enzyme Concentration

Sensitivity is the most key factor when designing any kind of sensors. In our case we have two neurochemicals GABA and GLU. We want to design a sensor that gives highest sensitivity to both GABA and GLU. For these experiments we use different concentrations of GOx (0.1, 0.2, 0.3, 0.4, 0.6 and 0.8 unit/μL) and different concentrations of GABASE (0.05, 0.1, 0.2, 0.3, 0.4 and 0.8 unit/μL). We modify our

GABA electrode with certain combinations (ratio) of these enzymes. However, the GLU electrode we modify with only GOx. We did a calibration of 20-60 μM GABA and 20-60 μM GLU to check for the sensitivity of both GABA and GLU.

For our first experiments, we observe the responses with increasing GABASE concentrations, keeping the GOx constant. The GLU electrodes in these cases have the same GOx concentration. We see that, the GABA response is highest when GABASE concentration is 0.1 unit/μL and the GABA responses decreases with increasing GABASE concentrations. Meanwhile, the GLU responses remain somewhat similar across GABA and GLU electrodes. Although, when the GABASE concentration increases (e.g. 0.8 GABASE+0.1 GOx) the signal quality worsens. We show these results in Figure 4-4.

In the next step we do the reverse experiments. We observe signals with increasing GOx concentrations keeping the GABASE concentration constant. In these cases, GOx concentrations increase in the GLU electrodes. We see that, for both GABA and GLU electrode GLU response increases from 0.1-0.4 unit/μL. It is shown in Figure 4-5.

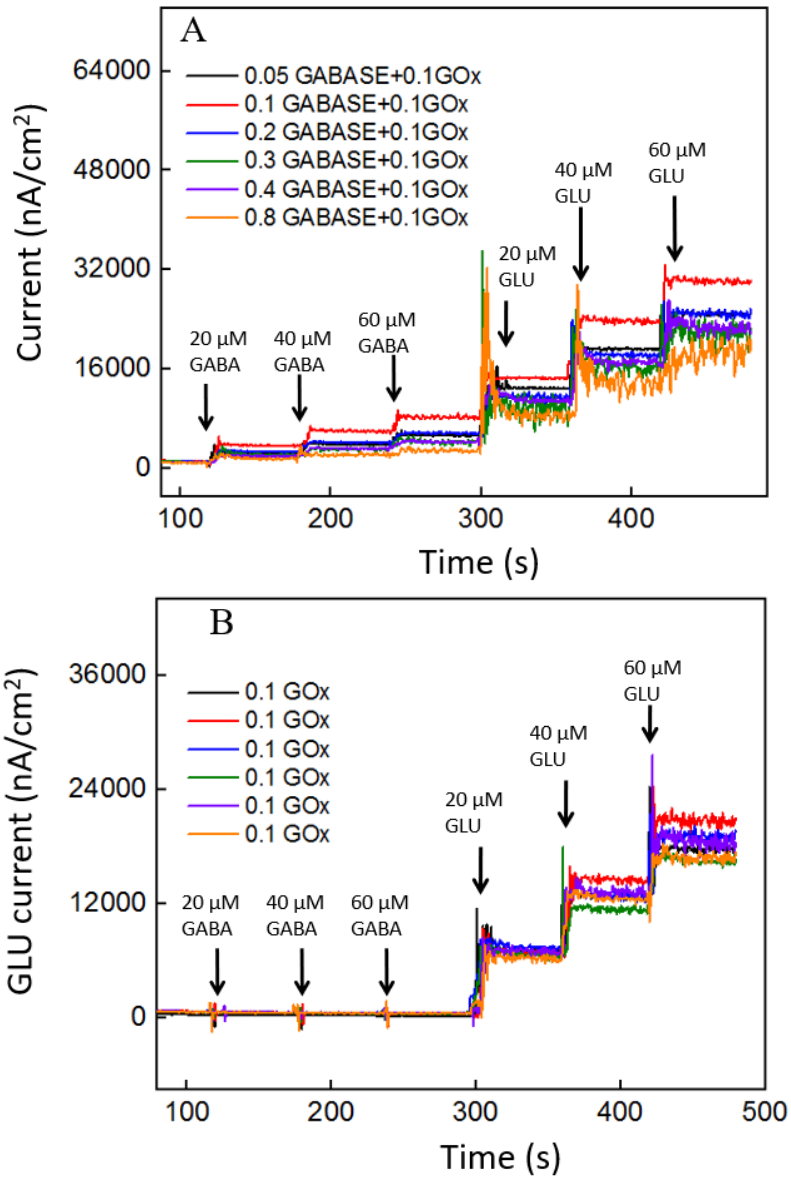

Figure 4-4: The comparison of GABA and GLU sensitivities. A. Shows GABA and GLU calibration in GABA electrode. B. Shows the GABA and GLU calibration GLU electrode. These experiments were done in 100 µM α-ketoglutarate+1X PBS. The microbiosensors were biased at + 0.7 V vs Ag/AgCl reference. The solution was stirred at 200 rpm and maintained at 37°C. Legends: 0.05 GABASE+0.1 GOx (black); 0.1 GABASE+0.1 GOx (red); 0.2 GABASE+0.1 GOx (blue); 0.3 GABASE+0.1 GOx (green); 0.5 GABASE+0.1 GOx (violet) and 0.8 GABASE+0.1 GOx (orange).

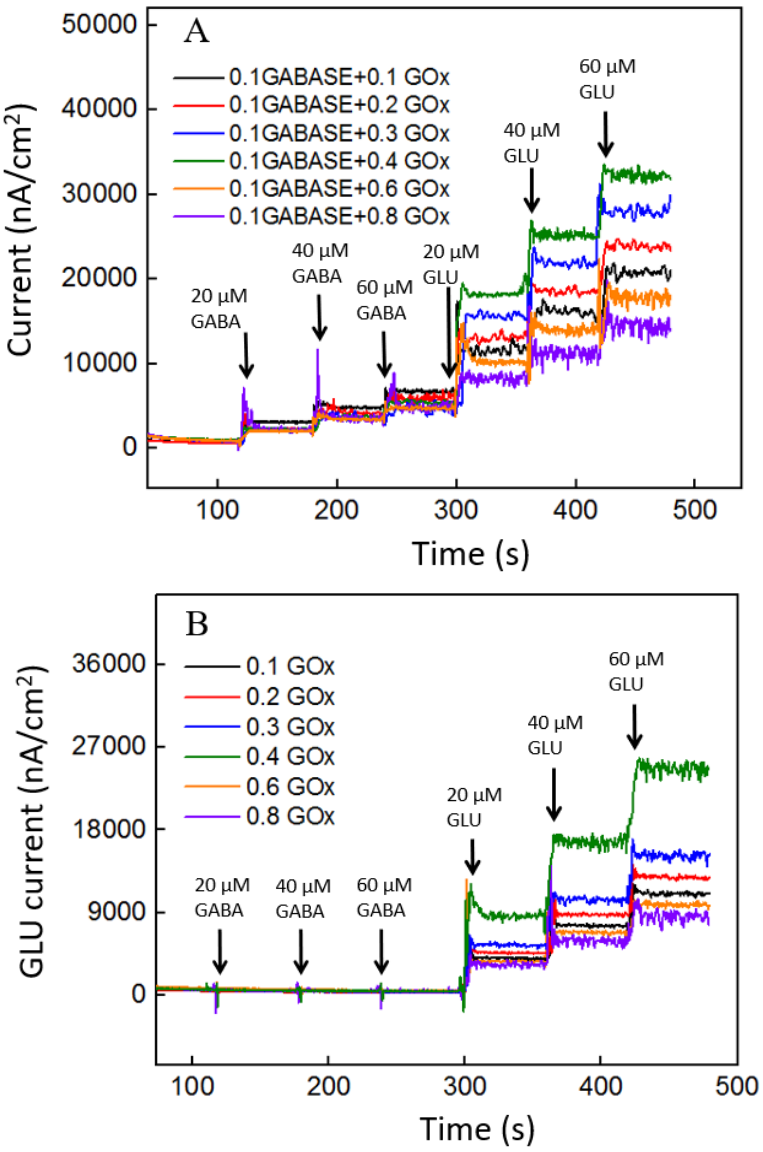

Figure 4-5: GABA and GLU signals in different conditions. A. Shows GABA and GLU signal when GABASE concentration is kept constant and GOx concentration increases in GABA electrode. Legends: 0.1 GABASE+0.1 GOx (black); 0.1 GABASE+0.2GOx (red); 0.1 GABASE+0.3 GOx (blue); 0.1 GABASE+0.4 GOx (green); 0.1 GABASE+0.6 GOx (orange); 0.1 GABASE+0.8 GOx (violet). B. shows the GABA and GLU signal in GLU electrode with increasing GOx concentration. Legends: 0.1 GOx (black); 0.2 GOx (red); 0.3 GOx (blue); 0.4 GOx (green); 0.6 GOx(orange); 0.8 GOx (violet). These experiments were done in 100 µM α-ketoglutarate+1X PBS. The microbiosensors were biased at + 0.7 V vs Ag/AgCl reference. The solution was stirred at 200 rpm and maintained at 37°C.

The highest GLU sensitivity is at 0.4 unit/μL and GLU sensitivity decreases after that point. The GABA response, however, remains somewhat similar; even though signal quality decreases. The GLU and GABA sensitivity in terms of enzyme concentration can be seen in Figure 4-4, Figure 4-5 and Figure 4-6. It can be explained with Michaelis-Menten theory (APPENDIX A). It states that, reaction rate (in our sensitivity) depends on enzyme concentration. The signal is maximized at the transition point of diffusion limitation and kinetic limitation [32]. It is understandable that for a certain enzyme a certain concentration will give highest sensitivity. In our studies the GABA signal is highest when GABASE concentration is 0.1unit/μL and GLU response is highest when GOx concentration is 0.4 unit/μL. High (more than the optimal) enzyme concentration can lead to low solubility and high viscosity of enzyme aliquots [32]. This leads to thicker enzyme membrane layer and thus limits the diffusion of analyte in the enzyme membrane [32]. In higher enzyme concentration, both GABASE and GOx, the signals become noisy because the enzyme layer becomes diffusion-limiting (see APPENDIX B for all the sensitivity values).

In literature they have used GABASE concentration of 0.0125 unit/μL in similar electrode geometry[15]. The sensitivity in that case was 40±8 nA/μMcm^2 [15]. In our studies we got the highest GABA sensitivity at 84±11nA/μMcm^2 which is almost 2 times the literature. Appendix-B shows the GABA and GLU sensitivity in all enzyme concentrations. For our subsequent experiments we use the concentration of 0.1 unit/μL GABASE and 0.1 unit/μLGOx in the GABA electrode because it gives the highest GABA sensitivity and acceptable GLU sensitivity. In the GLU electrode we keep 0.1 unit/μLGOx constant.

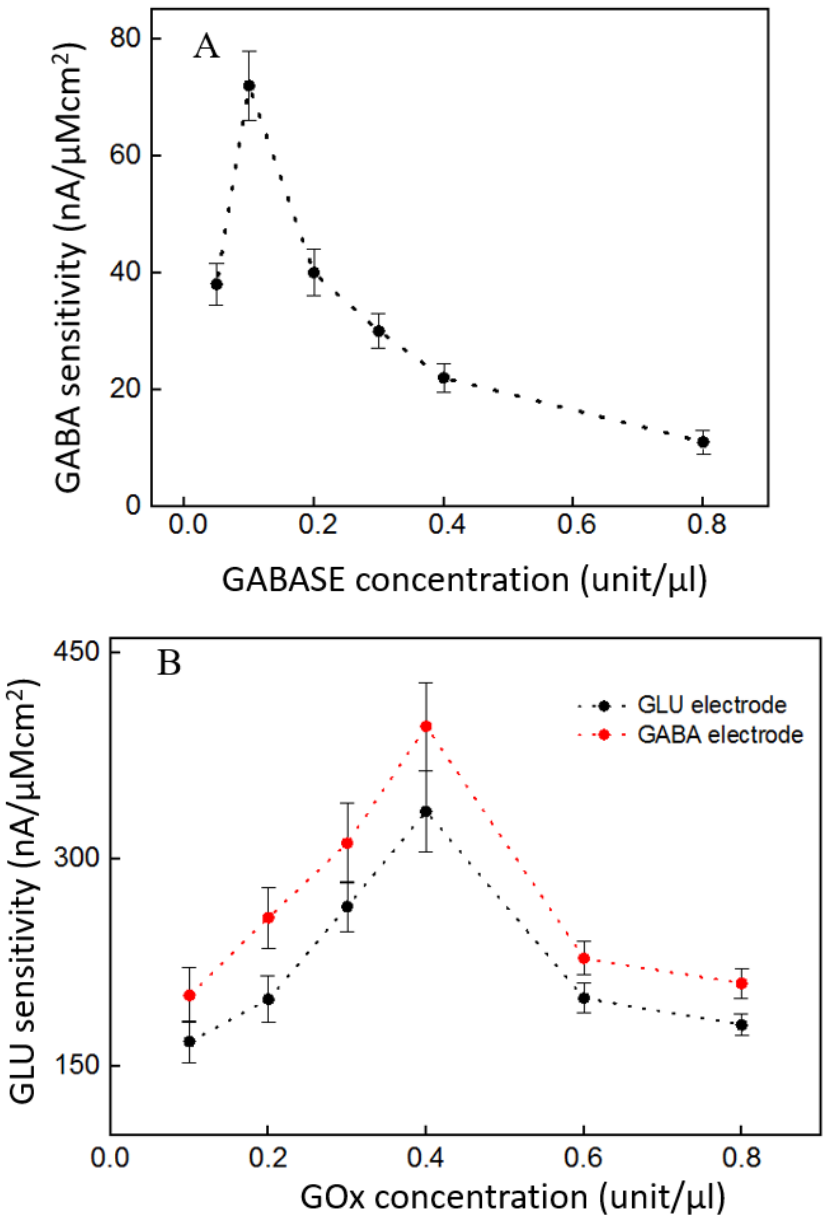

Figure 4-6: A. Shows the GABA sensitivity with increasing GABASE concentration. GOx concentration is 0.1unit/µL. B. Shows the GLU sensitivity with increasing GOx concentration. GABASE concentration is 0.1unit/µL.

4.4 Effect of Enzyme Loading (thickness)

The next experiments we performed were to study the enzyme loading/thickness on the platinum surface. With each drop our enzyme layer thickness increases. Thicknesses were measured and averaged from six sets of data (n=6) using a Keyence 3D Laser Scanning Confocal Microscope (model VKX150, Keyence, Osaka, Japan). Wechange number of drops from 1 to 8 in the platinum surface and observed the response. We did a calibration of 20-60 μM GABA and 20-60 μM GLU to check for the sensitivity of both GABA and GLU in both the electrodes. We observed with the increasing number of drops the thickness of the enzyme increases in both the GABA and GLU electrode surfaces. shows the thickness of both the GABA and GLU electrode surfaces.

Table 4-2: Thickness variation with # of drops

# of drops	Thickness of GABA electrode site (μm)	Thickness of GLU electrode site (μm)
1 drop	0.49±0.03	0.38±0.05
2 drops	0.89±0.07	0.81±0.06
3 drops	1.41±0.32	1.39±0.25
4 drops	2.13±0.74	2.06±0.56
8 drops	4.29±0.81	4.12±0.78

In site-1(GLU sensors) we can only observe current for GLU as shown in Figure 4-7. Injection of GABA in these sites has no effect on the current. As there is no GABASE, GABA can't react with α-ketoglutarate and subsequently produce H_2O_2. However, in site-2 we observe sensitivity for both GABA and GLU because of the presence of both GABASE and GOx as shown in Figure 4-7.

In case of the GABA electrode we observe the sensitivity for GABA is 138±21 nA/μMcm^2 when we have only one drop of enzyme but the sensitivity decreases to 76±13nA/μMcm^2 if we have 4 drops of enzyme. This is almost 70% decrease sensitivity. This is shown in Figure 4-8.

Similar trend is observed for GLU sensitivity in both the GABA and GLU electrode. For GABA electrode the GLU sensitivity decreases from 297±42 nA/μMcm^2 to 179±42 nA/μMcm^2 when we increase the number of drops from 1 to 4. This is a decrease of 65%. Similarly, for GLU electrode the GLU sensitivity decreases from 267±40 nA/μMcm^2 to 152±22 nA/μMcm^2 when we increase the number of drops from 1 to 4. This is a decrease of 75%. This is shown in Figure 4-8.

The reason for this trend can be found in the diffusing mechanism of the enzyme layer. When the enzyme is layer is thin the molecules can diffuse freely into the layers and react with them but if the layer is thick then the molecule cannot diffuse easily. Thus, results in less sensitivity. Previous works have explained this phenomenon by doing the H_2O_2 calibration in different thickness of enzymes [102]. They found that if the enzyme layer is thick the H_2O_2 sensitivity will be low too. That can explain our decreasing sensitivity with thicker enzyme layer.

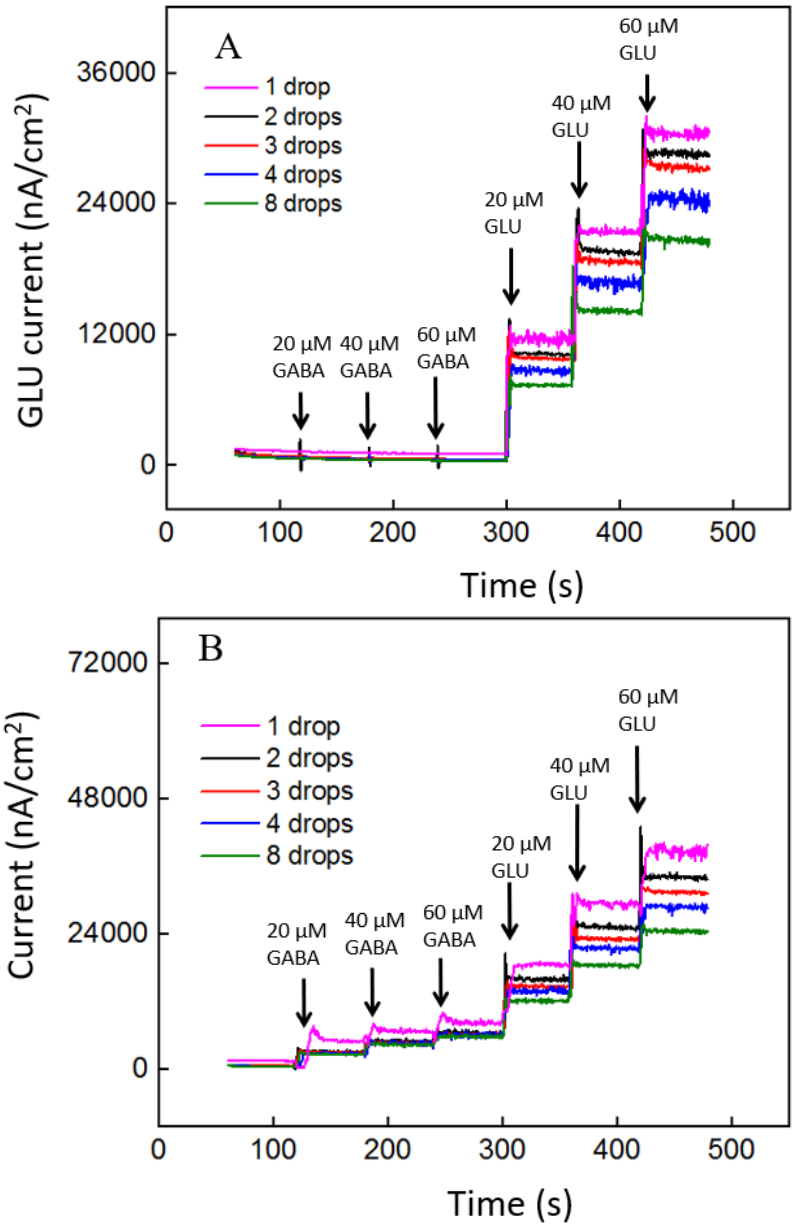

Figure 4-7: GABA and GLU signals in different enzyme thickness (#of drops) A.Shows GABA and GLU signals when in GLU electrode coated with 0.1 unit/µLGOx . B. Shows the GABA and GLU signal in GABA electrode coated with 0.1 unit/µLGABASE and 0.1 unit/µLGOx. These experiments were done in 100 µM α-ketoglutarate+1X PBS. The microbiosensors were biased at + 0.7 V vs Ag/AgCl reference. The solution was stirred at 200 rpm and maintained at 37°C. Legends: 1 drop (magenta);2 drops (black), 3 drops (red), 4 drops (blue), 8drops (green).

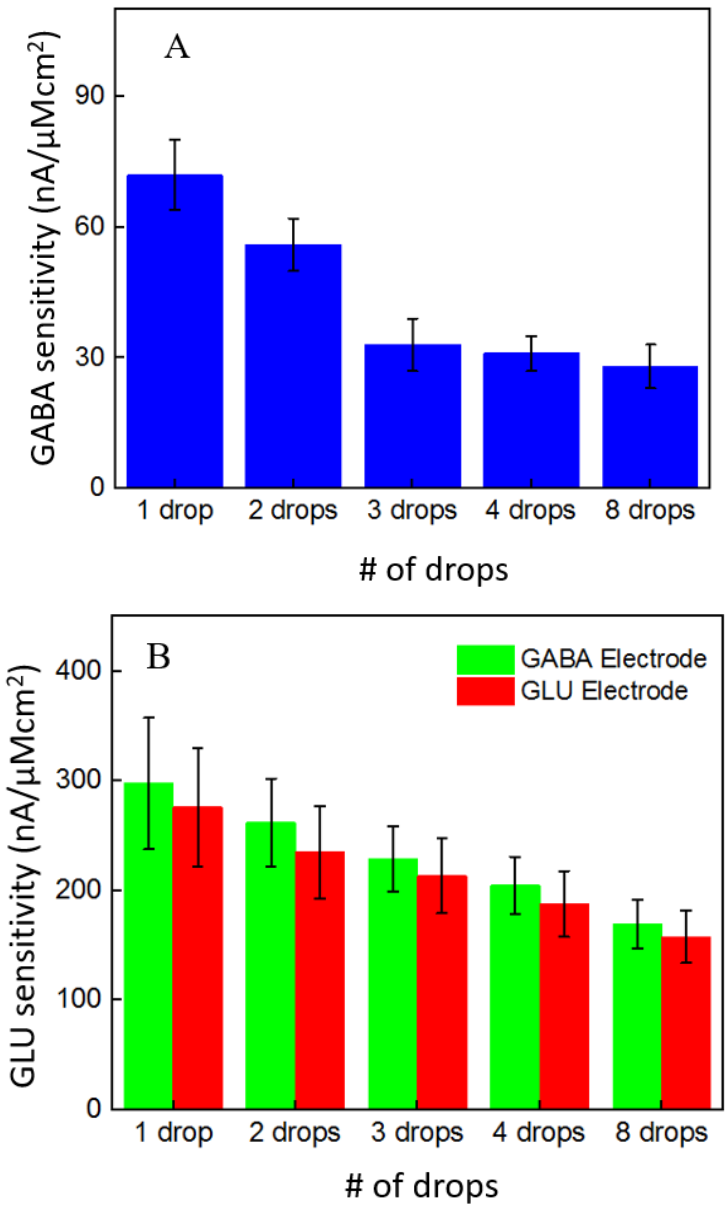

Figure 4-8: GABA and GLU sensitivity for both the electrodes. A. Shows the GABA sensitivity of the GABA electrode (blue bars). B. Shows the GLU sensitivity GABA electrode (green bars) and GLU sensitivity GLU electrode (red bars). Error bars are shown as mean±SEM.

4.5 Effect of pH

Solution pH plays an important role in any kind of enzymatic sensors. Moreover, each enzyme has different "working pH", pH at which the enzyme is most reactive. Since we used two enzymes to modify the electrode surface, we had to examine at which pH the enzymes work best. In our normal lab condition 1X PBS always has a pH of 7 (6.95-7.1). To get pH=5 we make the solution acidic with 1×10^{-5}M $HClO_4$. We start off with 0.1M $HClO_4$ and reach our desired concentration after a series of dilutions. To get pH=11 and pH=9 we make solution alkaline with 1×10^{-3}M and 1×10^{-5}M KOH respectively. In this case too we start off with 0.1M KOH and reach our desired concentration after a series of dilutions. We did a calibration of 20-60 μM GABA and 20-60 μM GLU to check for the sensitivity of both GABA and GLU in both the electrodes.

As expected, the GLU electrodes don't respond to GABA but responds to GLU whereas GABA electrodes respond to both GABA and GLU. This is shown Figure 4-9. In case of GABA sensitivity in GABA electrode, we see that GABA sensitivity is highest at pH=9, 72±11 nA/μMcm^2 and lowest at pH=11, 20 ±6 nA/μMcm^2. This is shown in Figure 4-10. In contrast, GLU sensitivity is highest at pH=7 in both the GABA electrode, 156±22 nA/μMcm^2 and in GLU electrode, 104±20 nA/μMcm^2. However, GLU sensitivity is lowest at pH=11 in both the GABA electrode, 36±6 nA/μMcm^2 and in GLU electrode, 28±4 nA/μMcm^2. These results are shown in Figure 4-10. The low sensitivities of GABA and GLU in pH=11 can be attributed to the extreme alkalinity of the solution.

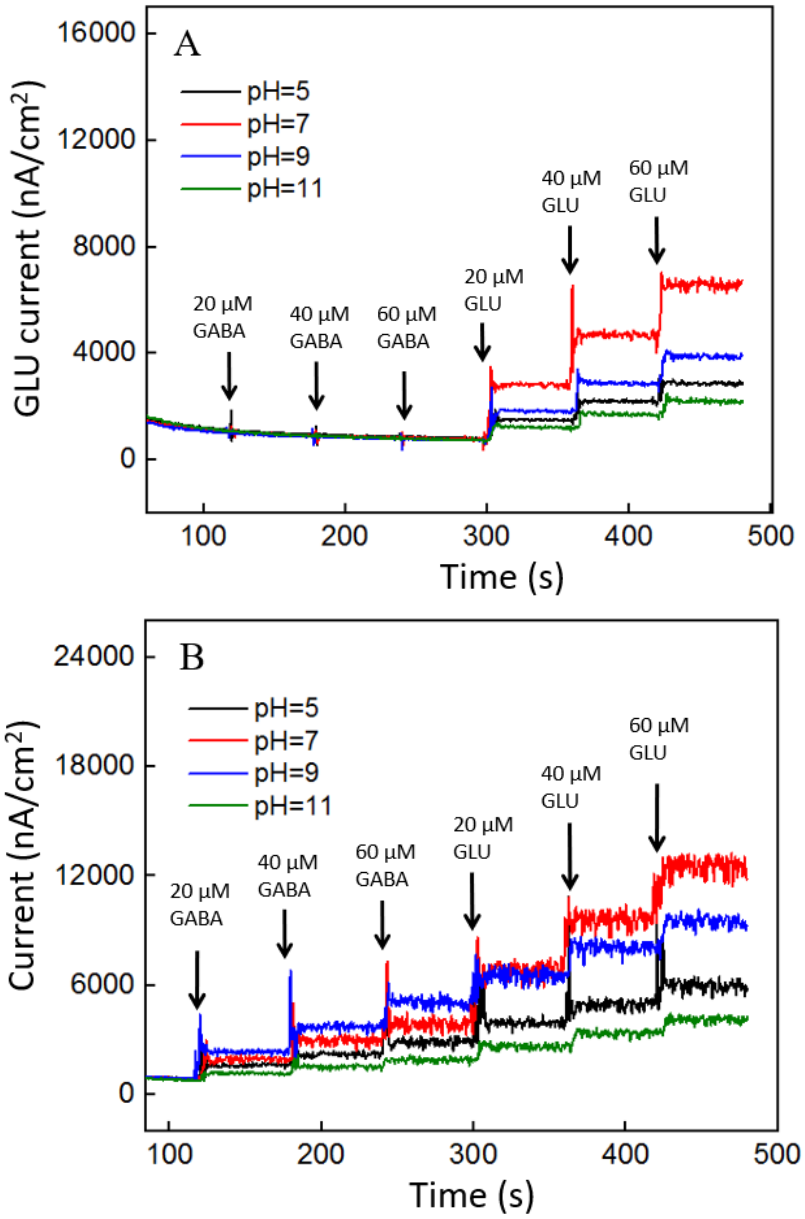

Figure 4-9: GABA and GLU signals in pH conditions A. Shows GABA and GLU signals when in GLU electrode coated with 0.1 unit/µLGOx . B. Shows the GABA and GLU signal in GABA electrode coated 0.1 unit/µL GABASE and 0.1 unit/µLGOx. These experiments were done in 100 µM α-ketoglutarate+1X PBS. The microbiosensors were biased at + 0.7 V vs Ag/AgCl reference. The solution was stirred at 200 rpm and maintained at 37°C. Legends: pH=5 (black), pH=7 (red), pH=9 (blue), pH=11 (green)

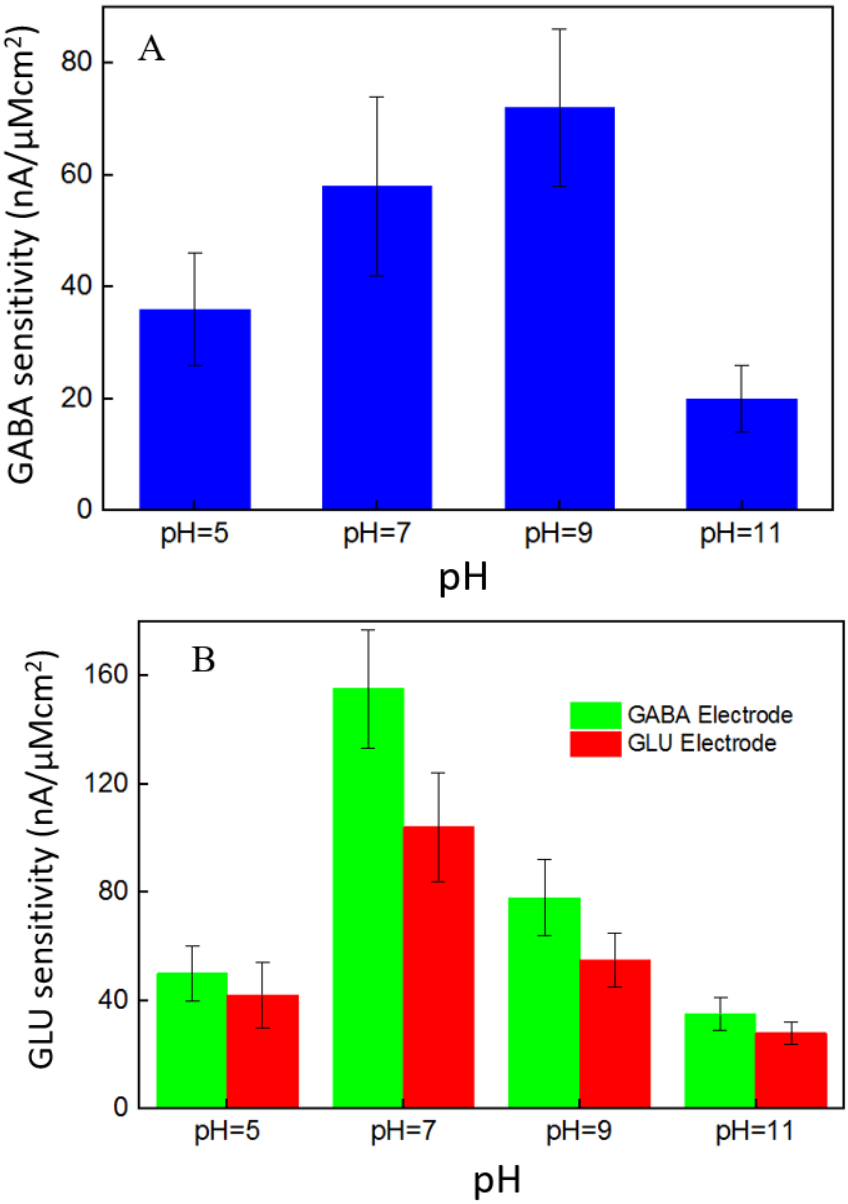

Figure 4-10: GABA and GLU sensitivity for both the electrodes. A. Shows GABA sensitivity of the GABA electrode (blue bars). B. Shows the GLU sensitivity GABA electrode (green bars) and GLU sensitivity GLU electrode (red bars). Error bars are shown as mean±SEM.

These results can be explained by the inherent qualities of the enzymes. According to manufacturer label and prior literature optimum GABASE condition is pH=8.6 [15]. This may be the reason why GABA sensitivity is highest at that pH. We note that GABA is a neutral molecule so the GABA sensitivity is assumed to be dependent upon GABASE and α-ketoglutarate as discussed in earlier sections. On the otherhand the GLU sensitivity is highest at pH=7 because this is the GOx optimum condition. It is highly likely that in various tissue and live brain conditions we will come across pH conditions that are not neutral, pH=5. In those cases, we can use these results to interpolate the GABA and GLU sensitivity in different *ex-vivo/in-vivo* pH conditions.

4.6 Linear Range Determination

To determine the linear range of the GABA sensors, we generated the plots for 5-500 μM GABA concentrations versus different α-ketoglutarate concentrations. We observe that the GABA current values saturate, and saturation depends on the α-ketoglutarate concentration as shown in Figure 4-11. For example, at 40 μM α-ketoglutarate, the GABA signal saturation is at 50 μM shown in Figure 4-12, whereas in 100, 200 and 500 μM α-ketoglutarate concentrations, the GABA signal saturation occurs at 100 μM as shown in Figure 4-12.The trend in sensitivity in the linear range is the same as before. For 100 μM α-ketoglutarate, the GABA sensitivity is highest and decreases at other concentrations of α-ketoglutarate. The linear range for GABA also depends on the α-ketoglutarate concentration. For 40 μM α-ketoglutarate, the GABA signal is linear upto 50μM shown in (Figure 4-12:inset) for other concentration the GABA signal is linear upto 100 μM shown in Figure 4-12 (inset).

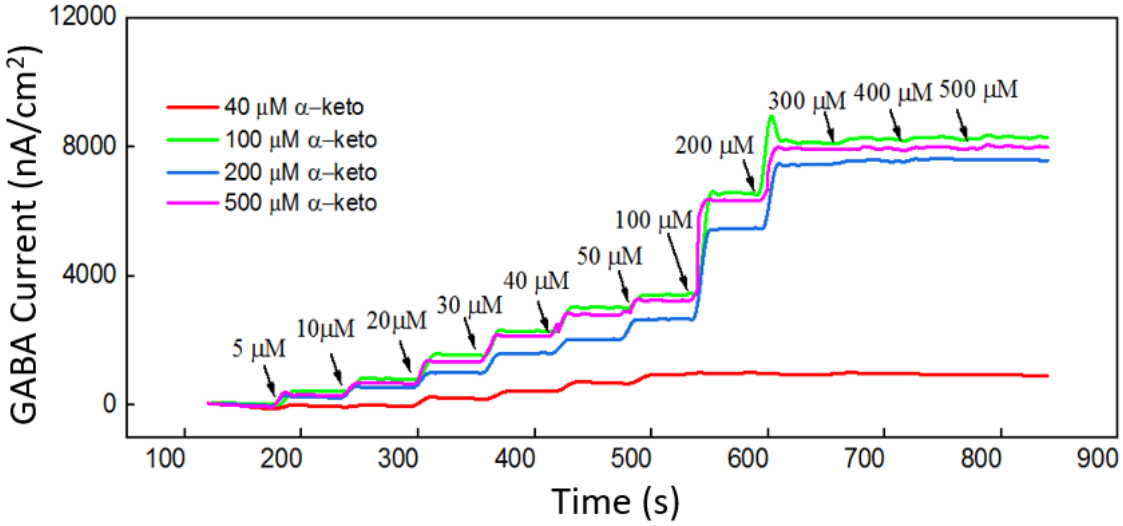

Figure 4-11: Calibration of GABA (5-500 µM GABA) in the presence of different concentrations of α-ketoglutarate in site 2 (GABA microbiosensor). Legends: Current response at GABA microbiosensor in Site-2 in 100 µM α-ketoglutarate (green curve), 40 µM α-ketoglutarate (red curve), 200 µM α-ketoglutarate (blue curve) and 500 µM α-ketoglutarate (magenta curve). GABA electrode coated 0.1unit/µLGABASE and 0.1unit/µLGOx [14]. * α-keto= α-ketoglutarate

This phenomenon can be explained by Michaelis-Menten theory (see APPENDIX A). It states that, enzyme-based reactions remain linear until the reaction rate reaches half its maximum value ($V_{max}/2$). The concentration at which the maximum reaction rate is half the maximum value, is called K_m. In all our calibration curves we have shown the $V_{max}/2$ and K_m (Figure 4-12). K_m value represents the concentration where our current is linear. Usually after the K_m value the current increases non-linearly or saturates (no current increase with increasing concentration. As expected in our K_m value is dependent on the α-ketoglutarate concentration. The K_m value for 40,100,200 and 500 µM α-ketoglutarate is 50,100,100 and 100 µM GABA respectively.

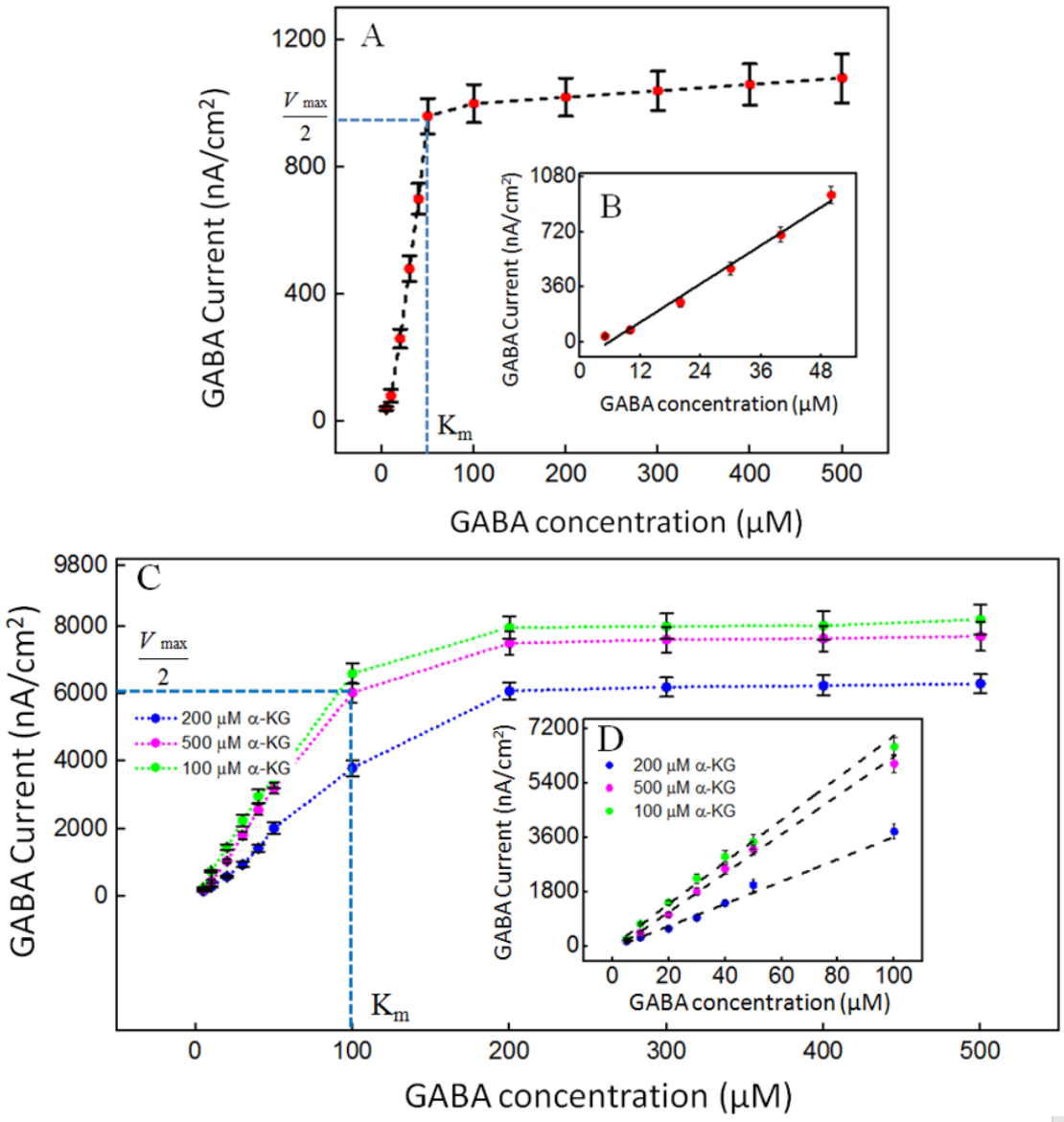

Figure 4-12: Current response of GABA (5-500 μM GABA) at different α-ketoglutarate concentrations and the linear range. A. Current response of GABA at 40 μM α-ketoglutarate (red dots). B. Linear range up to 50 μM GABA (solid line). Linear fit parameters GABA sensitivity: 14±1 nA/μMcm^2, R^2=0.99486.
C. Current response of GABA at 100 μM (green dots), 200 μM (blue dots) and 500 μM (magenta dots) α-ketoglutarate. D. Linear range up to 100 μM GABA for all α-ketoglutarate (solid black line) concentration. Linear fit parameters GABA sensitivity in 200 μM α-ketoglutarate: 32±4 nA/μMcm^2, R^2=0.99692. Linear fit parameters GABA sensitivity in 500 μM α-ketoglutarate: 47±10 nA/μMcm^2, R^2=0.9982. Linear fit parameters GABA sensitivity in 100 μM α-ketoglutarate: 61±14 nA/μMcm^2, R^2=0.99692 [14]. *α-KG= α-ketoglutarate

4.7 Effect of Size-Exclusion Layer

Selectivity is a key characteristic of any kind of sensor. This is especially true for neurochemical sensors. Since the eventual goal of our neurochemical sensor is to implant this sensor *in-vivo* or *ex-vivo* where a lot of interferents are present, our sensor must be selective to GABA (and GLU). A platinum surface without any selective layer will oxidize all the interferents like Ascorbic Acid (AA), Dopamine (DA) which are electroactive species that could contribute to faradaic signal if they are present in the solution. We observe similar signals in our electrode surfaces too as shown in Figure 4-13. As expected GLU electrode doesn't react to GABA but reacts to all other chemicals. GABA electrode shows response to all neurochemicals as shown in Figure 4-13. Cellulose acetate or polyphenol is commonly used as size exclusion layer. The main principle behind is that, this layer blocks large intereferent molecules while still allowing penetration of smaller molecules like H_2O_2. These size exclusion layer works on the basis of electrostatic repulsion between ions. For example, nafion is a negatively charged polymer that can block negatively charged ascorbate ions.

For this study we used 1,3-phenylenediamine (mPD) as our perm-selective layer. We selected mPD because mPD is a well know polymer to be used as a perm-selective layer [12]. In this work 10 mM mPD was prepared in 1 M NaCl and then purged with nitrogen for 30 min. Cyclic voltammetry scans between +0.2 V and +0.8 V, using a saturated calomel electrode as a reference electrode, were performed to form a size-exclusive mPD layer. In later sections we discuss two different scan rates for coating and their effects on the selectivity and sensitivity. These mPD coated MEAs were rinsed with DI water and stored for use.

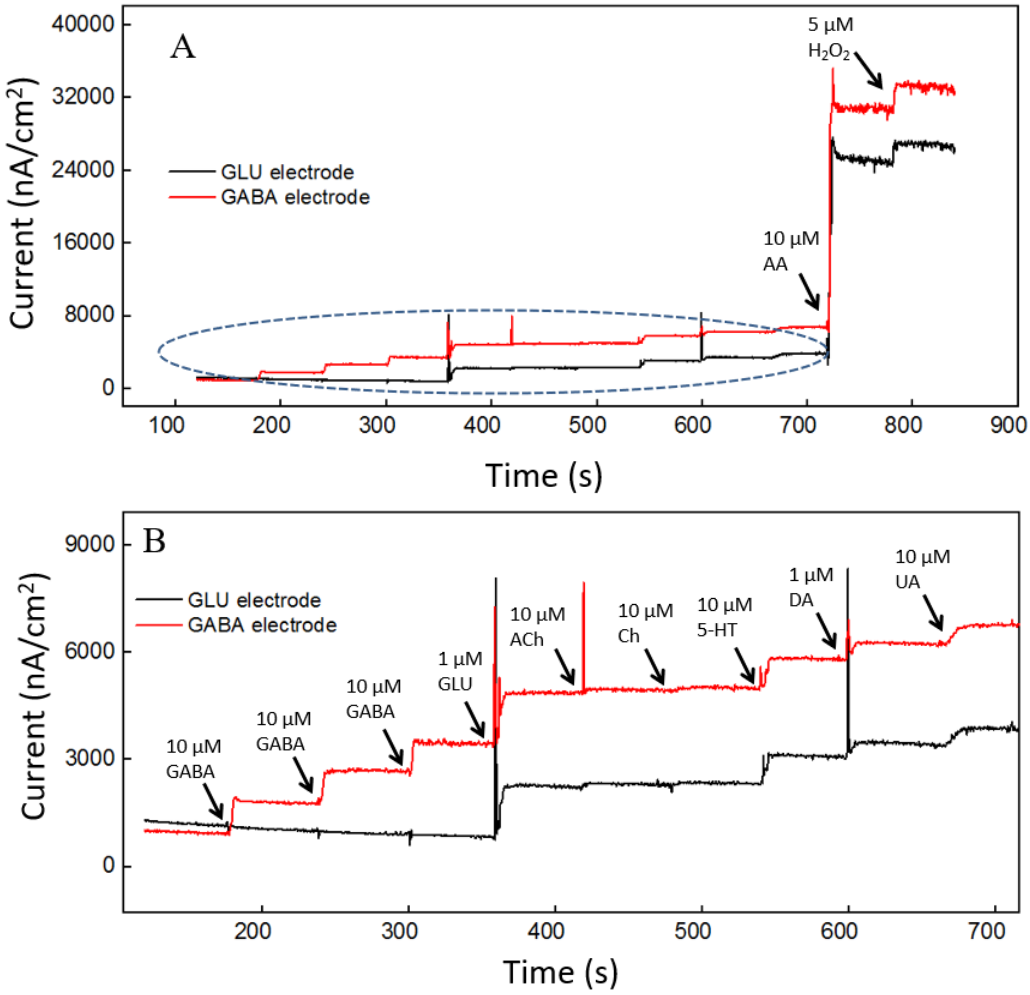

Figure 4-13: A. shows the signals for all chemicals in both GABA (red curve) and GLU electrode (black line). B. Shows the zoomed in version of the signal in blue circle (100-700 sec range; Legends: Ach= acetylcholine, Ch=choline, 5-HT=serotonin, DA=dopamine, UA=Uric acid, AA=Ascorbic acid.

As we can see from above, all molecules oxidize in the electrode surfaces producing current. The current is especially high in case of AA. In the brain AA is ubiquitous. To improve that problem we coat the surface with mPD using two different scan rates 50 mV/s and 5mV/s. As expected, we see signal from interferents (especially AA) decreased rapidly. This is shown in Figure 4-14. A zoomed in version of this can also be seen in Figure 4-15. However, we observe from Figure 4-15 that, both the GABA and GLU sensitivity decreases when we have the selective layer. The sensitivity for GABA decreases 40% in case of 50 mV/s scan rate and decreases 53% in case of scan rate 5 mV/s. The sensitivity and selectivity values for all neurochemicals are summarized in Table 4-3.

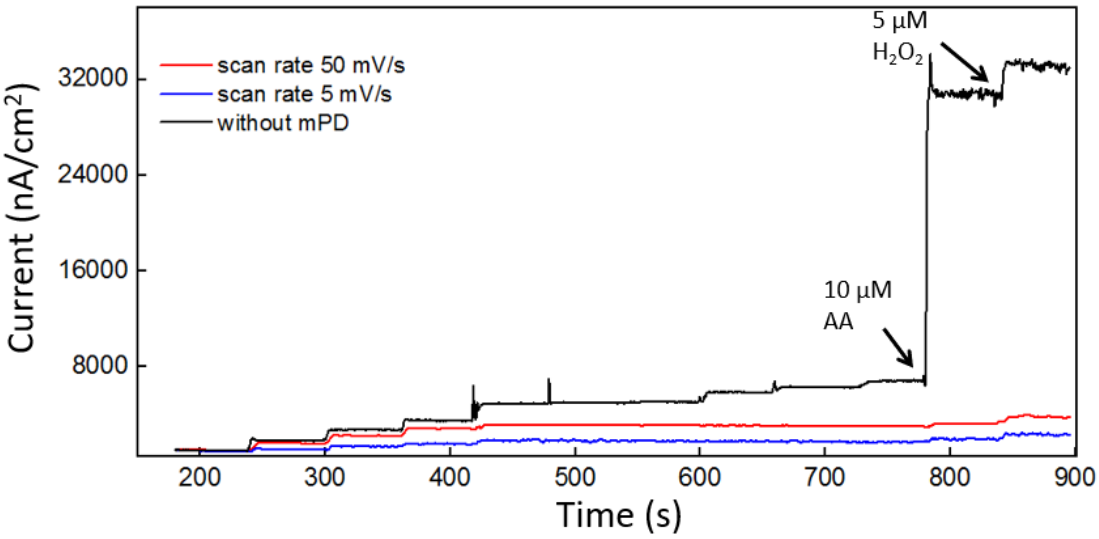

Figure 4-14: Interferent rejection signals for chemicals in GABA electrode. We show the signals when the electrode had no exclusion layer (black curve), the scan rate for the selective coating was 50 mV/s (red curve) and the the scan rate for the selective coating was 5 mV/s (blue curve) in GABA electrode coated 0.1 unit/µL GABASE and 0.1 unit/µLGOx. The solution had 100 µM of α-ketoglutarate. The microbiosensors were biased at +0.7 V vs Ag/AgCl reference. The solution was stirred at 200 rpm and maintained at 37° C. mPD coating uses CV [+0.2 to +0.8 V]

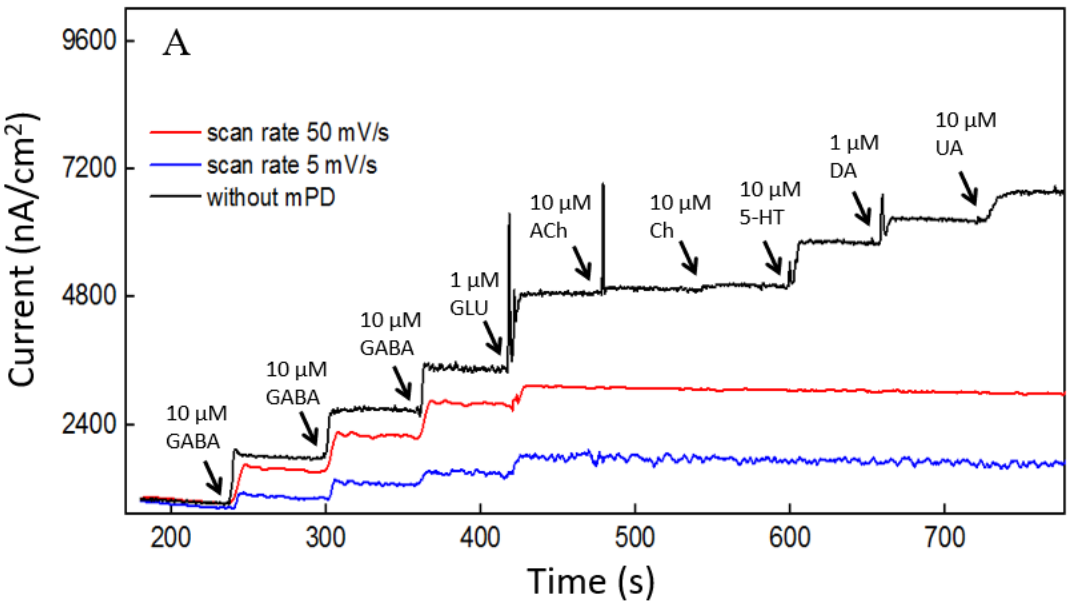

Figure 4-15: Shows the detailed versions of Figure 4-14. The experimental conditions remained the same. We show the 200-700 sec range. We show the signals when the electrode had no exclusion layer (black curve), the scan rate for the selective coating was 50 mV/s (red curve) and the the scan rate for the selective coating was 5 mV/s (blue curve) in GABA electrode coated 0.1 unit/µL GABASE and 0.1 unit/µL. mPD coating uses CV [0.2, 0.8 V].
*Ach= acetylcholine, Ch=choline, 5-HT=serotonin, DA=dopamine, UA=Uric acid, AA=Ascorbic acid.

The decrease in sensitivity in different scan rates can be attributed to the thickness difference in the surface. Thickness was measured using the confocal microscope (VK X-100, Keyence Company, Osaka, Japan). We observe if we coat at 50 mV/s the thickness is 26±5 nm. In contrast if we coat at 50 mV/s the thickness is 71±5 nm. This changing thickness can also be verified by observing the H_2O_2 sensitivity. The H_2O_2 sensitivity in 50 mV/s scan rate is 780±56 nA/µMcm^2. However, The H_2O_2 sensitivity in 5 mV/s scan rate is 420±67 nA/µMcm^2. This contrast in sensitivity suggests that thicker layer block more

H_2O_2 and results in lower sensitivity. In case of 5mV/s, the signals are noisier, than 50 mV/s signal. This is due to the thicker layer and diffusion limiting mechanism.

Table 4-3: Effect of mPD in GABA and GLU sensitivity (nA/ μMcm^2) [second and third column] and acetylcholine (Ach.), choline (Ch.) and serotonin (5-HT) selectivity against GABA (no unit) [third, fourth and fifth column]

Conditions	GABA	GLU	Ach	Ch.	5-HT
No mPD	65±13	708 ±79	11.3±2	11.3±3	1±0.5
Scan rate 50 mV/s	40 ±7	381±53	∞	∞	∞
Scan rate 5 mV/s	28 ±11	223±31	∞	∞	∞

We see from Table 4-3 that, the sensitivity for GABA and GLU decreases with high scan rates. Even though the sensitivity decreases we know from previous studies [90] that thicker layer of mPD lasts longer. We see from Table 4-4 that, the selectivity for AA increases with high scan rates. According to literature AA selectivity value of 35 is acceptable [15]. Our GLU selectivity is 189±32 and 256±47 respectively, which comparable to earlier work [102].

Table 4-4: Effect of mPD on dopamine (DA), uric acid (UA), ascorbic acid (AA) and H_2O_2 selectivity against GABA (no unit)

Conditions	DA	UA	AA	H_2O_2
No mPD	0.2±0.05	1.5±0.03	0.03±0.01	0.2±0.001
Scan rate 50mV/s	∞	∞	57±14	0.3±0.002
Scan rate 5mV/s	∞	∞	85±12	0.5±0.008

4.8 GABA Calibration in Presence of Glutamate

The GABA probe was calibrated in the presence of (5-80 μM) range of concentrations of GLU, which mimics the brain microenvironment both in healthy and diseased states. For example, the basal concentration of GLU in the extracellular space is up to 20 μM[103], while GLU concentrations in cerebrospinal fluid are~10 μM. During seizures, GLU levels increase 4-fold and GABA levels decreases [104]–[106].GLU is a major excitatory neurochemical that is ubiquitously present as L-glutamate in its anionic form (glutamic acid) in the brain environment (henceforth called GLU_E)[103].One of the objectives of this study was to monitor GLU_E as an *in-situ* source for the generation of α-ketoglutarate, which aids in the continuous real-time GABA monitoring at Site 2, and thus does not rely on the addition of α-ketoglutarate externally. Firstly, we calibrated the two microbiosensors by injecting GLU at various concentrations (5 μM, 10 μM, 20 μM, 40 μM and 80 μM) in 1X PBS buffer solution. Figure 4-16 shows the response of the two microbiosensors. The GABA microbiosensor (Site 2) consistently exhibited a slightly

higher GLU response than that of the GLU microbiosensor (Site 1). The GLU sensitivity of Site 2 and Site 1 are 132±10 $nA\mu M^{-1}cm^{-2}$ and 94±5 $nA\mu M^{-1}cm^{-2}$, respectively. The difference in the current response from the two microbiosensors increases with higher GLU concentrations (Figure 4-16). To further understand this, we modified Site 2 with only GABASE and no GOx. Ideally, there should not be any response from the GABA microbiosensor. However, a small response was observed (Figure 4-16). This confirms our hypothesis that some non-selective activity of GABASE is due to GLU oxidation. Others have made similar observations where GABASE showed weak enzyme activity towards Glu compared to GOx [11].

The large response could also be due to the presence of more enzymes per unit volume (0.2 U/µl) that somehow collectively create more active sites [107].To account for this difference in the Glu response, henceforth called the background noise, $\mathbf{I}_b$ (shown in Figure 4-16), the $\mathbf{I}_b$ has to be subtracted from the difference in the currents (I_{GABA}) at the two sites to obtain the final current response to GABA (details discussed later).

The next calibration step was to experiment with different GABA solutions (0, 5, 10, 20 µM) in 1X PBS buffer and repeat the above GLU calibration (Figure 4-17). These experiments were performed without adding α-ketoglutarate externally. At Site 1, Glu_E is oxidized to α-ketoglutarate and $H_2O_{2\,(E)}$ (reaction 2, shown in Chapter-2). This α-ketoglutarate then reacts with GABA at Site 2 and produces GLU_{GABA} (reaction 1, shown in Chapter-2) followed by reaction 4 (shown in Chapter-2), which generates $H_2O_{2(GABA)}$ and more α-ketoglutarate. These reactions and pathways were shown in earlier chapter. At the GABA microbiosensor (Site 2), in the case of no GABA in the solution, the current response ($H_2O_{2\,(Site\,2)}$) is due only to the changing GLU levels in the solution

(Figure 4-17, red curve). When GABA is present in the solution, the H_2O_2 (Site 2) response is from both GABA and GLU oxidation and we expect it to be larger than the response when there was no GABA. Therefore, higher GABA concentrations appear to induce a greater response (Figure 4-17, blue, green, magenta curves) at Site 2 and greater I_{GABA}, which is the GABA signal as shown in Chapter-2, shows the sensitivity of the GABA microbiosensor at different GABA and GLU concentrations.

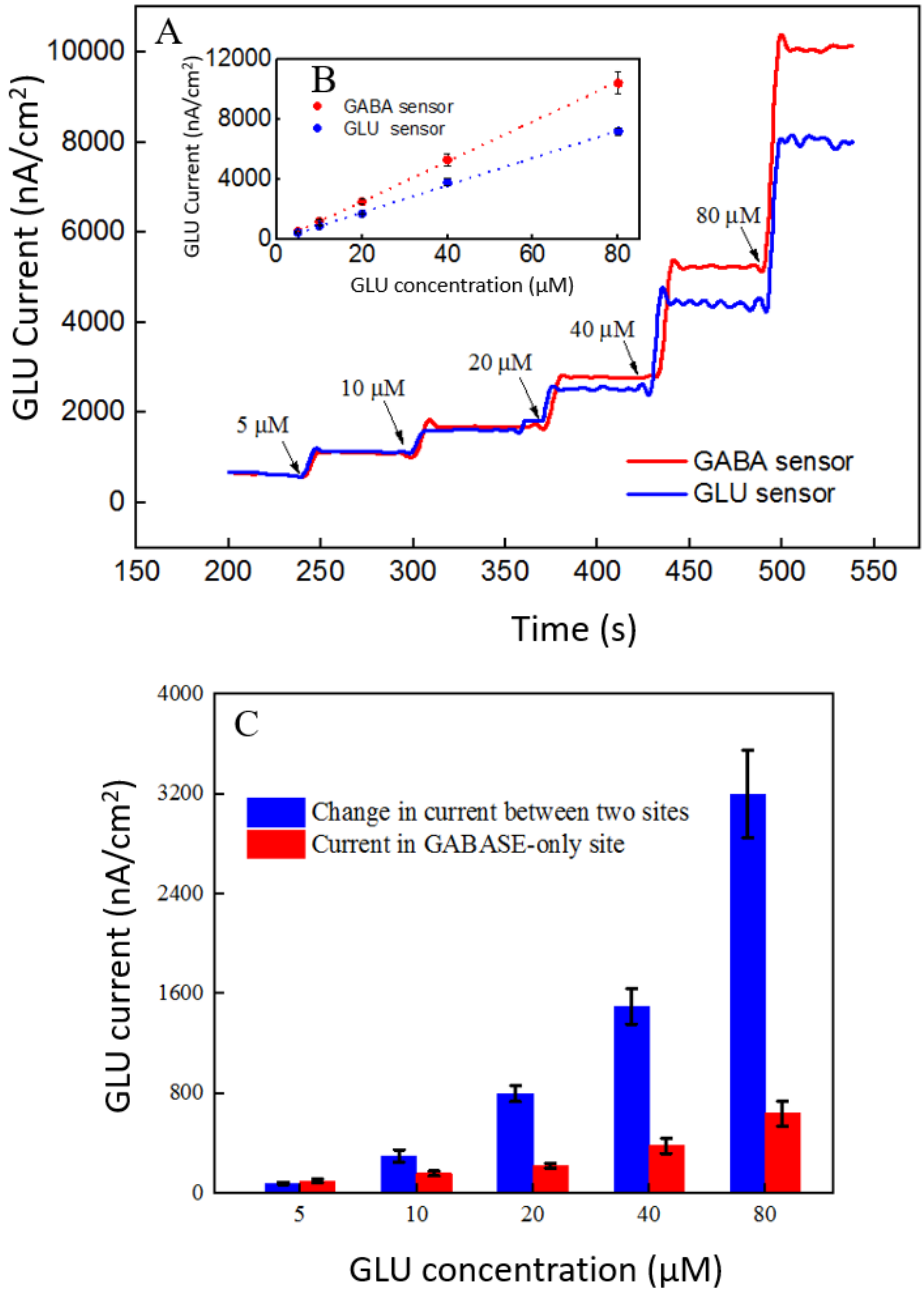

Figure 4-16: A. Current response at GABA microbiosensor in Site 2 and Glu microbiosensor in Site 1 (red and blue solid curves, respectively). Arrows indicate GLU infusion. B. Inset showing the linear fitting for GABA and Glu microbiosensors (red and blue dotted lines) C. The difference in the current response between the microbiosensors (blue bars). The current response at GABA microbiosensor (that was coated with GABASE enzyme only; no GOx enzyme) (red bars). No α-ketoglutarate added during all the experiments [14].

With increasing GABA and Glu concentrations, the sensitivity of the GABA microbiosensor increases and this is because of increased availability of α-ketoglutarate. The sensitivity and the LOD of the two microbiosensors are shown in Table 4-5 and Table 4-6. The GABA sensitivity increased by ~25% at 20μM GABA concentrations. The sensitivity reported here is greater than that of the Pt based GLU sensors published in the literature [108] The LOD is comparable to other Glu sensors [109].

Table 4-5: Sensitivity(SS, nA.μMcm^2) of GLU (SS_{GLU}) and GABA (SS_{GABA}) sites

GABA concentration	**SS_{GLU}**	**SS_{GABA}**
0	94±5	132±10
5	101±8	148±7
10	100±10	156±8
20	102±12	168±21

The difference in current, shown in Figure 1-17**,** is caused by the presence of GABA in the solution. The GABA signal was quantified as $\mathbf{I}_{GABA} = H_2O_{2\,(Site\text{-}1)} - H_2O_{2(Site2)}$. The $\mathbf{I}_{GABA}$ is plotted for varying GABA and GLU concentrations Figure 4-18 after subtracting the $\mathbf{I}_b$ noise.

Table 4-6: Limit of detection (LOD, μM) of GLU (LOD_{GLU}) and GABA (LOD_{GABA}) sites

GABA concentration	LOD_{GLU}	LOD_{GABA}
0	0.23±0.01	0.08±0.007
5	0.22±0.01	0.07±0.008
10	0.23±0.02	0.07±0.009
20	0.23±0.01	0.08±0.007

The positive values for $\mathbf{I}_{GABA}$ at all concentrations of GABA and GLU confirm GABA detection at Site 2. As expected, the $\mathbf{I}_{GABA}$ increases as GABA concentrations increase. The GABA calibration curves, following linear approximation of $\mathbf{I}_{GABA}$ at various GLU concentrations, is shown in Figure 4-18. A steeper slope is evident at higher GABA concentrations. Values of the slope are 42±4 $nA\mu M^{-1}cm^{-2}$, 49±6 $nA\mu M^{-1}cm^{-2}$ and 70±11 $nA\mu M^{-1}cm^{-2}$ for 5 μM, 10 μM and 20 μM GABA, respectively.

To better understand the GABA signal dependence on GLU concentrations, $\mathbf{I}_{GABA}$ values were plotted in terms of different molarity ratios of GABA:GLU (1:1, 1:2, 1:4 and 1:8) for different GABA concentrations (Figure 4-18).It is known that GABA and GLU maintains a certain balance in the human brain through the glutamate-glutamine(GABA) cycle[110] And they exist in a certain molarity ratio based upon the state of the brain. For example, in epilepsy, this cycle becomes imbalanced and GLU levels are elevated [104]–[106].

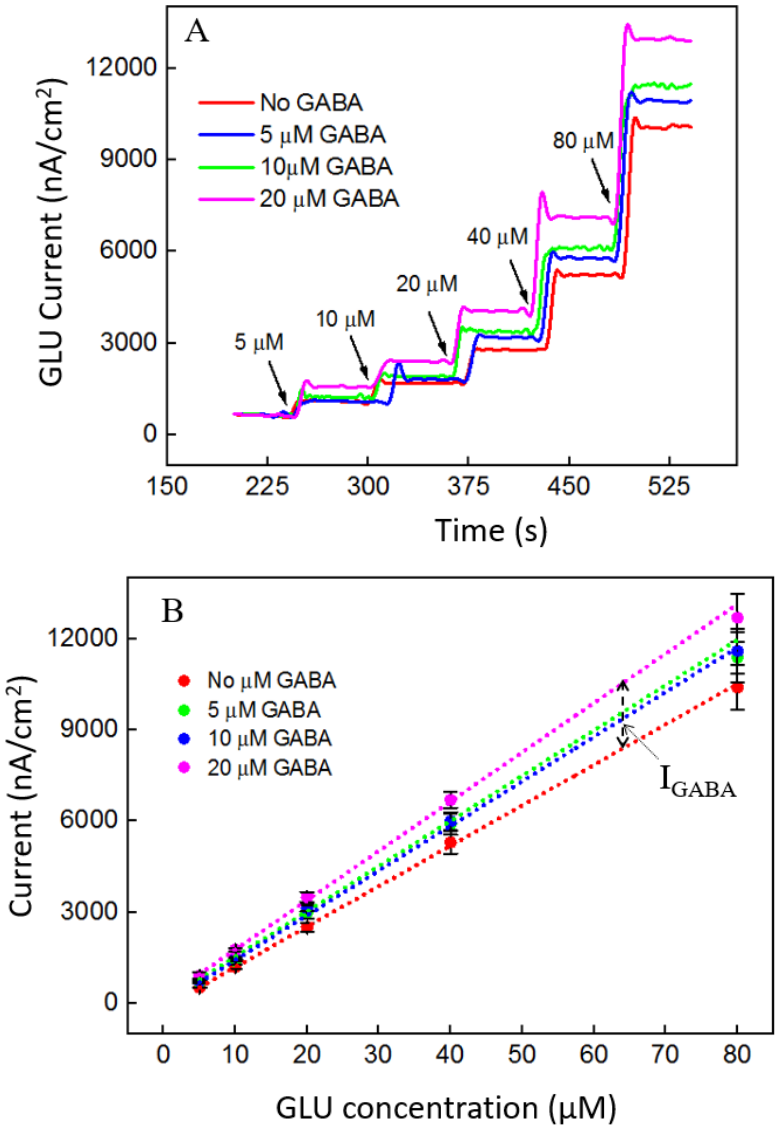

Figure 4-17: GABA probe calibration in different concentrations of Glutamate, GLU (5, 10, 20, 40, 80 µM). A, B. shows current response and linear fitting at GABA microbiosensor in Site 2 with and without GABA. Arrows indicate GLU infusion Legends: no GABA (red solid curve), 5 µM GABA (blue), 10 µM GABA (green) and 20 µM GABA (magenta). Linear fit parameters obtained for GLU with different concentration of GABA : no/0µM GABA (red line), GLU sensitivity = (132 ±9 $nA\mu M^{-1}cm^{-2}$), R^2 =0.99973; 5µM GABA (blue line) GLU sensitivity = (146±7 $nA\mu M^{-1}cm^{-2}$), R^2 =0.99921; 10µMGABA (green line),GLU sensitivity = (156±12 $nA\mu M^{-1}cm^{-2}$); R^2 =0.99927 and and20µM GABA (magenta line), GLU sensitivity = (168±19 $nA\mu M^{-1}cm^{-2}$); R^2 =0.99863 at GABA microbiosensor. The microbiosensor was biased at + 0.7 V vs Ag/AgCl reference. The solution was stirred at 200 rpm and maintained at 37 ° C. No α-ketoglutarate added during all the experiments [14].

The data clearly suggest that the I_{GABA} increases as GABA and GLU levels increases. This is evident from Figure 4-18**,** which shows that, for a given GABA concentration, the I_{GABA} value is larger for higher GABA: GLU ratios. So, in this approach, for a given I_{GABA} value, the GABA concentration can vary. To get the GABA concentrations we also need the GLU concentration of the outer environment. To get the GLU and GABA concentration we propose our novel method in the next section.

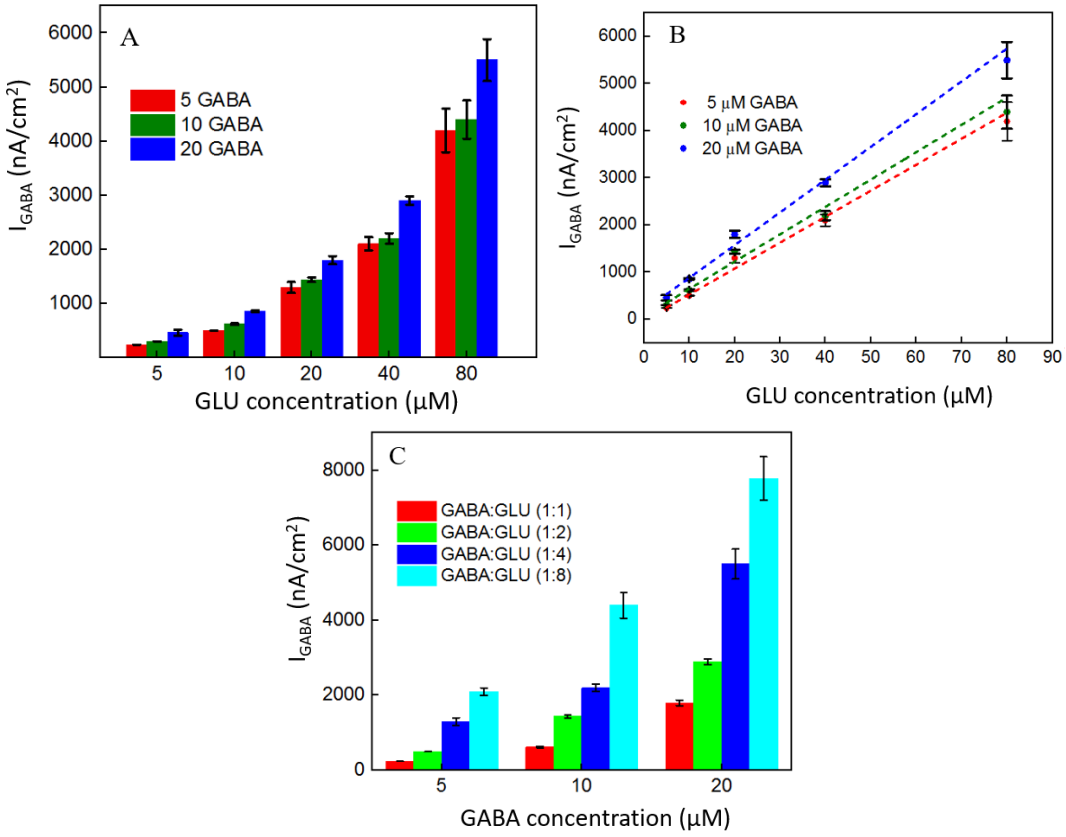

Figure 4-18: A&B: shows the I_{GABA} values for different GABA (5, 10 and 20 µM) and Glu concentrations (5, 10, 20, 40, 80 µM). Legends: 5 µM GABA (red bar/line), 10 µM (green bar/line) and 20 µM (blue bar/line). B.10, 20, 40 and 80 µM Glutamate. C.The I_{GABA} values at different GABA: GLU molarity ratios. Legends: GABA:GLU= 1:1 (red), 1:2 (green), 1:4 (blue) and 1:8 (cyan bar) [14].

4.9 Quantification of GABA and GLU

Since our GABA sensor is based on GLU concentration, only **I**$_{GABA}$ value cannot give GABA concentration. We need determine the local GLU concentration first to get our GABA concentration. The steps are explained with examples below. Figure 4-19 shows the total calculation steps.

1. GLU concentration [GLU] is derived from 1-18-(B), *e.g. for 4200 nAcm^{-2}, [GLU$_E$]= 45 µM*
2. This is also the x-coordinate of 1-18-(C); *e.g. [GLU$_E$]= 45µM*
3. We get I$_{GABA}$ from (D). I$_{GABA}$ is the difference in current recorded from the GABA and GLU microbiosensor in the presence of known GABA concentration. *At 20 µM GABA, current is 7400 nAcm^{-2} and for 0 µM GABA the current is 4200 nAcm^{-2} (GLU only). Thus, I$_{GABA}$ is 3200 nAcm^{-2}.* We Use this value for step 4.
4. The intersection of x-y coordinates in (C) gives [GABA]. In this case *45 µM (x) and 3200 nAcm^{-2} (y) intersect at the 20 µM GABA line.* (4)
5. Therefore, GLU concentration in this case is *45µM and* GABA concentration *is 20 µM.*

Ideally, we do the calibration values (for GABA and GLU) before the *ex-vivo* and *in-vivo* experiments. However, with time our electrodes foul and the sensitivity values deviate from pre-experiments calibrations. We can solve this problem by installing a microfluidic flow channel in our probe which can help us do *in-situ* calibration.

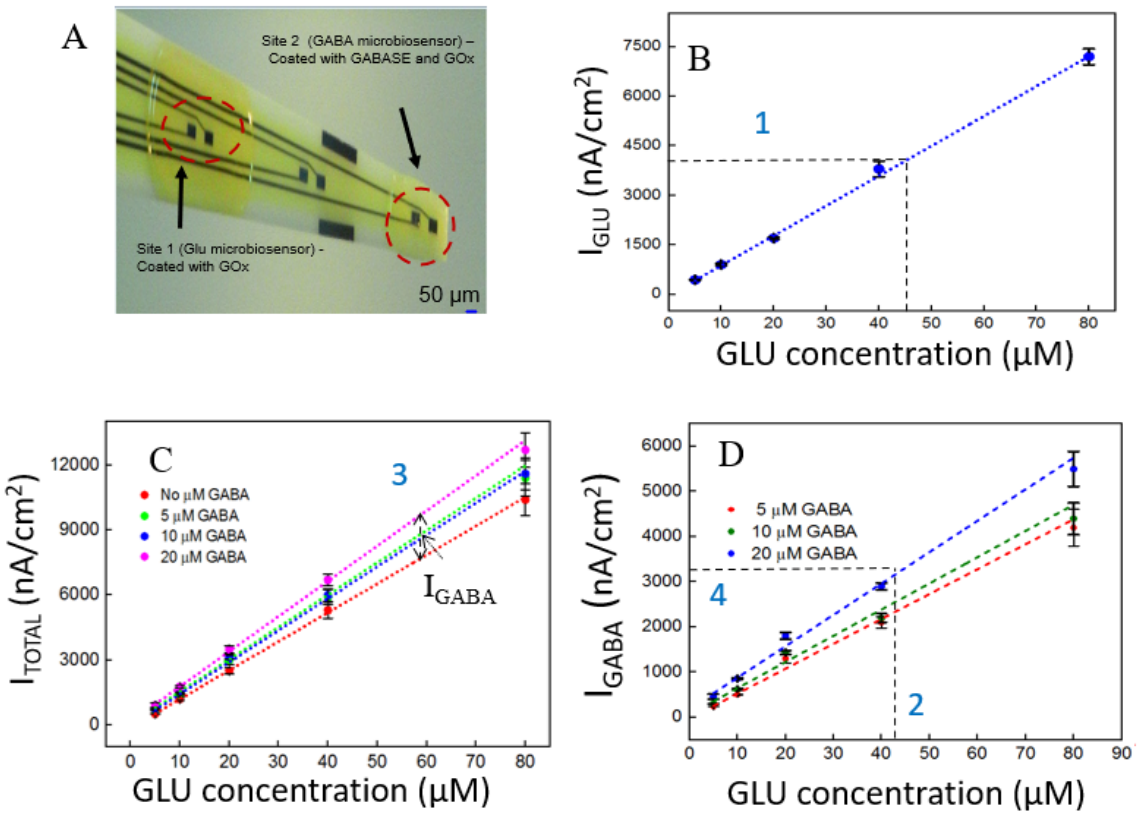

Figure 4-19: Scheme for calculating GLU and GABA calculation. A. Shows the sensor positions. B, C and D. show different steps to determine the eventual GLU and GABA concentration [14].

CHAPTER 5

WIRE BASED SENSOR FOR NEUROCHEMICAL DETECTION

5.1 Sensor Fabrication

In the first step, Teflon® coated, 127-µm diameter Pt wire (#77300, AM-systems, Sequim, WA) was cut into 4-cm lengths with a PXC058 tube cutter (Coilhouse Pneumatics, East Brunswick, NJ). One cut end served as the recording side. On the other, non-recording side, a 1-cm length of Teflon® coating was gently stripped away using a steel scalpel blade. This end was wrapped around a gold coated nickel electrical connector pin (#3128-4-00-15-00-00-08-0, Mouser Electronics, Mansfield, TX). The contact region between the wire and the connector pin was then covered with a 3/64" heat shrink wrap (HS-TBG 3/64" 2:1 CL, Mouser Electronics, Mansfield, TX) to provide an adequate, seamless electrical contact between the biosensor and the pin that was eventually in contact with the connector (ED 3013-ND, Digi-key, Thief River falls, MN) that is in contact with the potentiostat (FAST-16MkIII ,Quanteon, LLC, Nicholasville,KY).The exposed Pt microwires were electrochemically cleaned using cyclic voltammetry (CV) method. The CV was run in a 2-electrode setup using Ag/AgCl reference in a 0.05 M H_2SO_4 electrolyte solution and the potential was cycle between –0.3 V to +1.0 V at a 20 mV/s scan rate for 15 cycles. After the microwire cleaning, they

were heated in an oven at 65° C for 20 min. The Pt microwires were then calibrated to measure their sensitivity towards H_2O_2, the electroactive by-product of the microbiosensor shown in Figure 5-1. This initial calibration helps to make sure the three different channels (GABA, GLU and sentinel) have same sensitivity towards H_2O_2.Different H_2O_2 sensitivity will suggest different electroactive area. This is not acceptable since we need uniform area in all three wires. The microwires were stored dry at room temperature in a clean plastic container until ready for the enzyme coating.

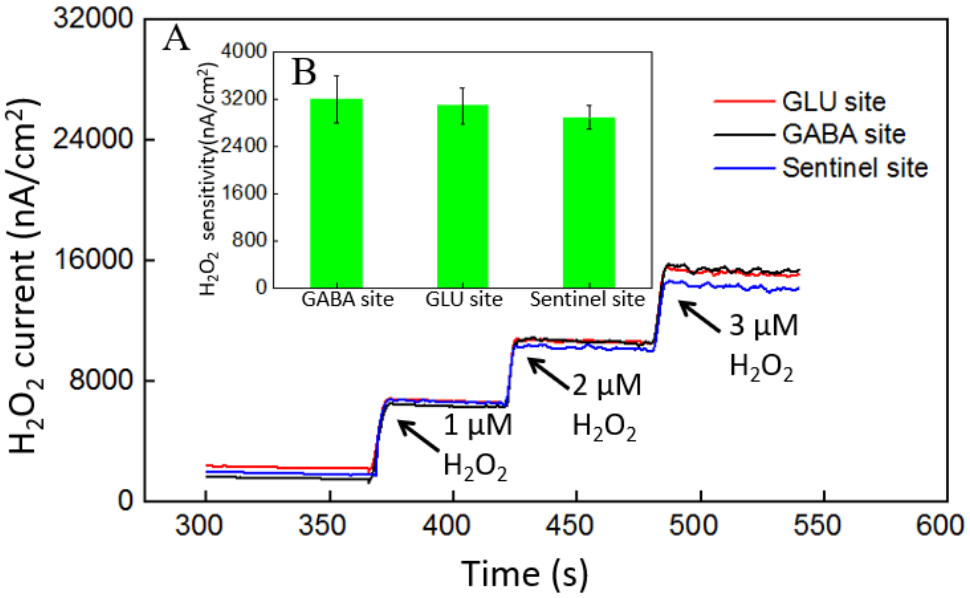

Figure 5-1: H_2O_2 calibration and sensitivity in different sites. A. Calibration of different sites with 1, 2 and 3 µM H_2O_2, GABA site (black), GLU site (red) and sentinel site (blue). Amperometry*:* + 0.7 V *vs* Ag/AgCl wire in a stirred 1X PBS beaker; the stir rate was 200 rpm. B. shows the H_2O_2 sensitivity in different sites (Green bars). Error is shown as mean± SEM.

After the completion of the H_2O_2 calibration, enzyme solutions were drop-casted onto the recording end of the Pt microwires (details in Hossain et.al., [14]). Briefly, a fresh enzyme matrix solution was prepared that contains BSA (1%) and glutaraldehyde (0.125%) in DI water. This solution was mixed with 0.1 U/mL GOx for the GLU

microbiosensor and a mixture of 0.1 U/mL GOx and0.1 U/mL GABASE for the GABA microbiosensor. The third microwire, called a sentinel microsensor, was constructed by applying only the enzyme matrix solution (i.e., it does not contain any GOx or GABASE enzymes). The sentinel microsensor plays an important role in measuring the amounts (and concentrations) of all the electroactive molecules present in the vicinity of the biosensor probe such as ascorbic acid (AA) and that can be easily oxidized at the +0.7 V applied to all three microsensors. The enzyme coated microwires were stored in the dark at room temperature for 48 hours.

Once the enzyme is cross-linked with the enzyme matrix, a size-exclusion layer of m-phenylenediamine (mPD) was electrochemically coated onto all three coated microwires. 10 mM mPD was prepared in 1 M NaCl and then purged with nitrogen for 30 min before use. Cyclic voltammetry scans between +0.2 V and +0.8 V, scan rate 50 mV/s for 100 cycles (40 minutes), using a saturated calomel electrode as a reference electrode, were performed to form a size-exclusive mPD layer. This provides selectivity or specificity to the microbiosensor by preventing the diffusion of the interferents, primarily AA, that are present in high concentrations (up to millimolar range [97]). After the coating, the freshly prepared microbiosensors are stored in a dry, dark cool place until they are assembled into a probe.

Finally, the ends of the three coated microwires were bound together with a bigger heat shrink wrap shown in Figure 5-2 and inset (#103-0246, Nordson Medical, Salem, NH).The shrink wrap provided protection of the thin Teflon® wire coating against abrasion, and it placed the wires very close to each other (Figure 5-2) and held the ends of the wires in the same recording plane. It also added rigidity to the microwire

probe for improved handling during experiments. Electrical continuity for each biosensor channel was confirmed using a FAST-16MkIII potentiostat (Quanteon, LLC, Nicholasville, KY).

For *in-vivo* recording, A barbed leur lock cap (51525K125 nylon quick-turn barbed plug 3/16" inside diameter, McMaster-Carr, Elmhurst, IL) was used to secure the biosensor to a permanently implanted guide cannula with a male luer lock fitting. The microwires were inserted through the opening in the cap so that the end of the microwire bundle would protrude 100-μm beyond the end of a permanently implanted guide cannula for in vivo recording. For our system, this length was 4.0 cm. A Teflon-insulated Ag/AgCl wire was also inserted through the cap to connect to the reference electrode integrated into the cannula. 6 cm of insulation was stripped from the end of the wire and then the wire was twisted into a loop around the luer lock cap so that the stripped portion will make a secure electrical contact with a similar loop of Ag/AgCl wire integrated into the connector of the cannula. The remainder of the Ag/AgCl wire was threaded through the cap and cut 0.3 cm above the top end of the cap. This end of the wire was stripped and soldered to a male pin connector (520200, A-M Systems, Sequim, WA). We secured the wires into the cap using dental acrylic (Ortho-Jet BCA, Lang Dental Manufacturing Company, Inc., Wheeling, IL). Electrical continuity for each biosensor channel was confirmed using a FAST-16MkIII potentiostat (Quanteon, LLC, Nicholasville, KY). The packaging is shown in Figure 5-2.

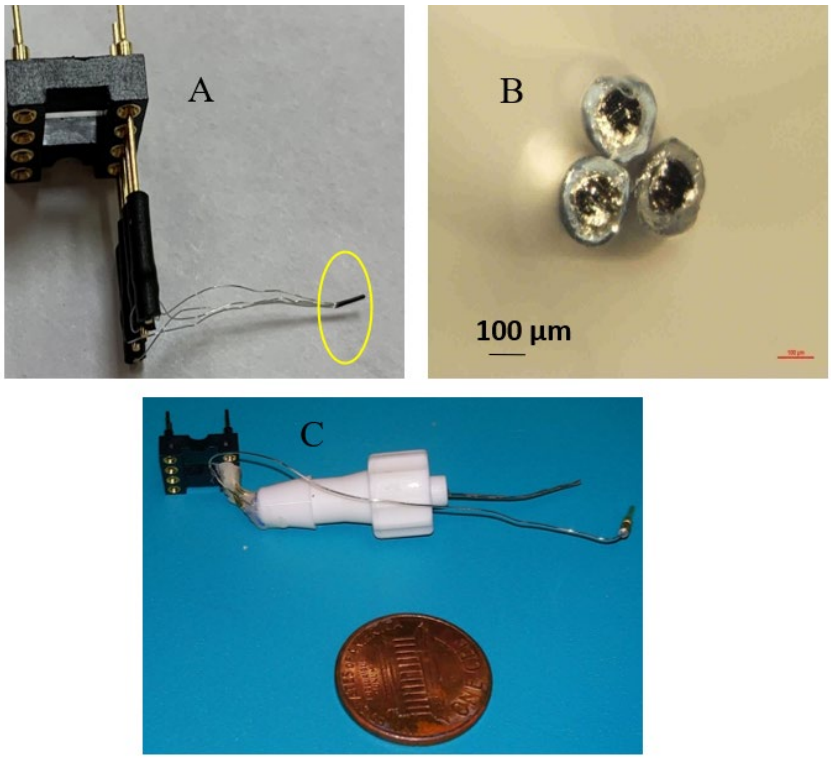

Figure 5-2: Sensor packaging. A. Shows the sensor after heat shrink wrapping and connecting to digi-key connector that eventually connects to the potentiostat. B. Shows optical microscopy image of the three sensor sites. The probe consists of three surfaces modified platinum microwires that are packaged using heat shrink tubing. Those three microwires eventually become GABA, GLU and sentinel sites. C. Sensor packaging for *in-vivo* application.

5.2 Wire Characterization

After the sensor is packaged, we do our first electrochemical characterization for the wires (sites) shown in Figure 5-3. This characterization is to make sure all our enzymes are active and the size-exclusion layer blocks interferent molecules, in our case Ascorbic acid (AA) is the main intereferent. For our calibration we calibrated the wires using 20-80 µM GABA and 5-20 µM GLU. We also use 100 µM AA to examine the effectiveness of our mPD layer.

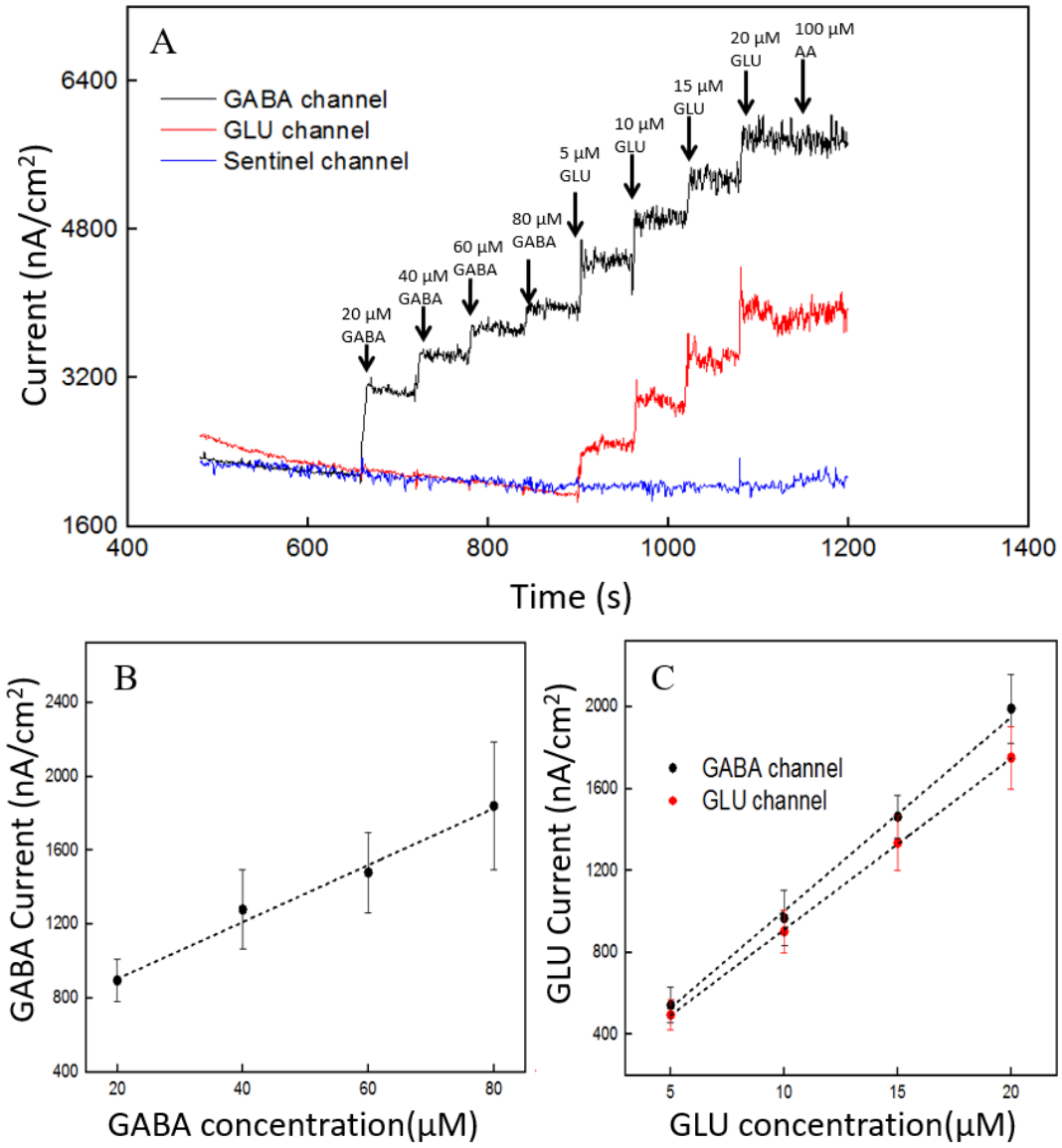

Figure 5-3: Characterization of the different channels (sites) in our packaged sensor. A. Shows the GABA and GLU signal in all the channels. GABA channel (black line), GLU channel (red line) and sentinel channel (blue line). GABA channel is coated with 0.1 unit/µL GABASE+0.1 unit/µLGOx and GLU channel is coated with 0.1 unit/µLGOx. Sentinel channel has no enzymes. The experiment is done in 1mM α-ketoglutarate with a stirring rate is 200 rpm at 37°C temperature. Amperometry parameters: +0.7V vs Ag/AgCl. B. Shows the signal against GABA concentration in GABA channel (black dots). Slope: 16.92±1.12 nA/µMcm^2 ; R^2=0.9807 C. shows the signal against GLU concentration in GABA channel (black dots) Slope: 94.64±9.12 nA/µMcm^2 ;R^2=0.996and GLU channel (red dots). Slope: 83.64±6.4 nA/µMcm^2 ; R^2=0.998. Error values are shown as mean± SEM. The microwire probes are stored at 4°C.

As we expect, the GABA channel is sensitive towards GABA and GLU but the GLU channel is sensitive towards GLU only. This is due to the fact that, GLU channel does not have GABASE enzyme. In contrast, the sentinel wire is not responsive to any of the neurochemicals for lack of enzymes. Therefore, it has neither sensitivity nor selectivity against GABA or GLU. Additionally, all the channels show low sensitivity towards AA demonstrating effectiveness of our mPD layer. Table 5-1 shows the sensitivity, selectivity and limit of detection (LOD) in different wires.

Table 5-1: Shows the sensitivity (nA/μM.cm^{-2}) of GABA (SS_{GABA}) and GLU(SS_{GLU}), selectivity(no unit) of GABA (SE_{GABA}) and GLU(SE_{GLU}), and LOD (μM) values of GABA (LOD_{GABA}) and GLU (LOD_{GLU}) for different channels.

Channel	**SS_{GABA}**	**SE_{GABA}**	**SS_{GLU}**	**SE_{GLU}**	**LOD_{GABA}**	**LOD_{GLU}**
GABA	17±2	29±7	95±10	123±27	2 ±0.66	0.20 ±0.01
GLU	-	-	84±7	106±21	-	0.25 ±0.01
Sentinel	-	-	-	-	-	-

5.3 GABA Working Range Determination

As we have done with our 8-TRK probes, with the wires we need to determine the linear range for GABA and see if the response follows Michealis-Menten theory. To do this experiment we coat the GABA channel with GABASE and GOx, GLU channel with GOx and sentinel with no enzymes just like before. After that we calibrate all of these channels in our beaker. For GABA we do the calibration in 50-2200 μM range. These concentrations are relevant for tissue stimulation study, discussed in subsequent chapters.

Figure 5-4 shows the response against GABA in all the channels. As we expect, we only observe GABA response in the GABA channel because of presence of GABASE. The GLU and sentinel channel does not give this response. The GABA response all follows Michealis-Menten theory. The GABA response is linear from 0-500μM GABA but after that range the response is not linear anymore as shown in Figure 5-4 (inset). It shows if GABA concentration is less than or equal to 1800 μM the GABA channel responds. However, Figure 5-4 also shows when GABA concentration is >1800 μM the sensor saturates (no increase in signal with increasing GABA concentration). From these experiments, we can say 50-1800 μM is the working range for GABA channels. However, the GABA linear range is 0-500 μM and in the linear range the sensitivity is $1 \pm 0.16 nA/\mu M cm^2$.

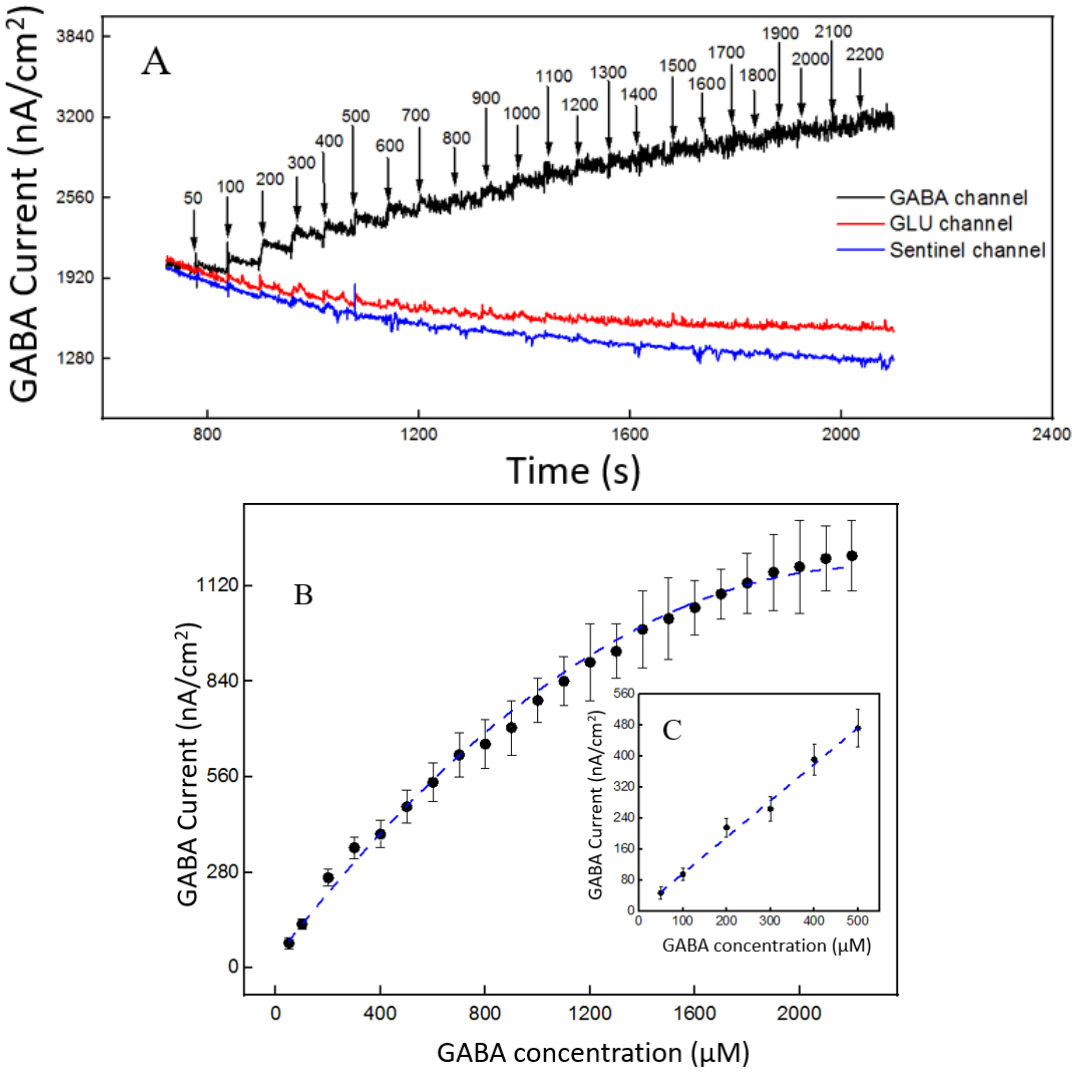

Figure 5-4: GABA response in all the channels. A. Shows response at 50-2200 µM GABA. The arrows show the infusion point and the numbers represent GABA concentration in µM. GABA channel (black line), GLU channel (red line) and sentinel channel (blue line). GABA channel is coated with 0.1 unit/µL GABASE+0.1 unit/µLGOx and GLU channel is coated with 0.1 unit/µLGOx. Sentinel channel has no enzymes. The experiment is done in 1mM α-ketoglutarate with a stirring rate is 200 rpm at 37°C temperature. Amperometry parameters: +0.7V vs Ag/AgCl. B. Shows response against GABA concentration. C. Shows response against GABA concentration in the linear range. Linear fitting parameter: slope 0.96±0.15 nA/µMcm^2; R^2= 0.982. Error values are shown as mean± SEM. The microwire probes are stored at room temperature.

5.4 Glutamate Working Range Determination

To keep consistency with our earlier works, with the wires we need to determine the linear range for GLU and see if the response follows Michealis-Menten theory. To do this experiment we coat the GABA channel with GABASE and GOx, GLU channel with GOx and sentinel with no enzymes just like before. After that we calibrate all of these channels in our beaker. For GLU we do the calibration in 20-1200 μM range. These concentrations are relevant for tissue stimulation study, discussed in subsequent chapters.

Figure 5-5 shows the response against GLU in all the channels. As we expect, we observe GLU response in both GABA and GLU channel because of presence of GOx. The sentinel channel does not give this response. The GLU response all follows Michealis-Menten theory. The GLU response is linear from 0-300μM GLU in both GABA and GLU channel but after that range the response is not linear anymore as shown in Figure 5-5 (inset). It shows if GLU concentration is less than or equal to 1000 μM both the GABA channel and GLU channel responds to GLU. However, Figure 5-5 also shows when GABA concentration is greater than 1000 μM the sensor saturates (no increase in signal with increasing GABA concentration). From these experiments, we can say 0-1000 μM GLU is the working range for both GABA and GLU channels. However, the GLU linear range is 0-300μM and in the linear range the sensitivity is 144±20 nA/μMcm^2 for GABA channel and 112±17 nA/μMcm^2 for GLU channel. These microwire probes are stored at room temperature.

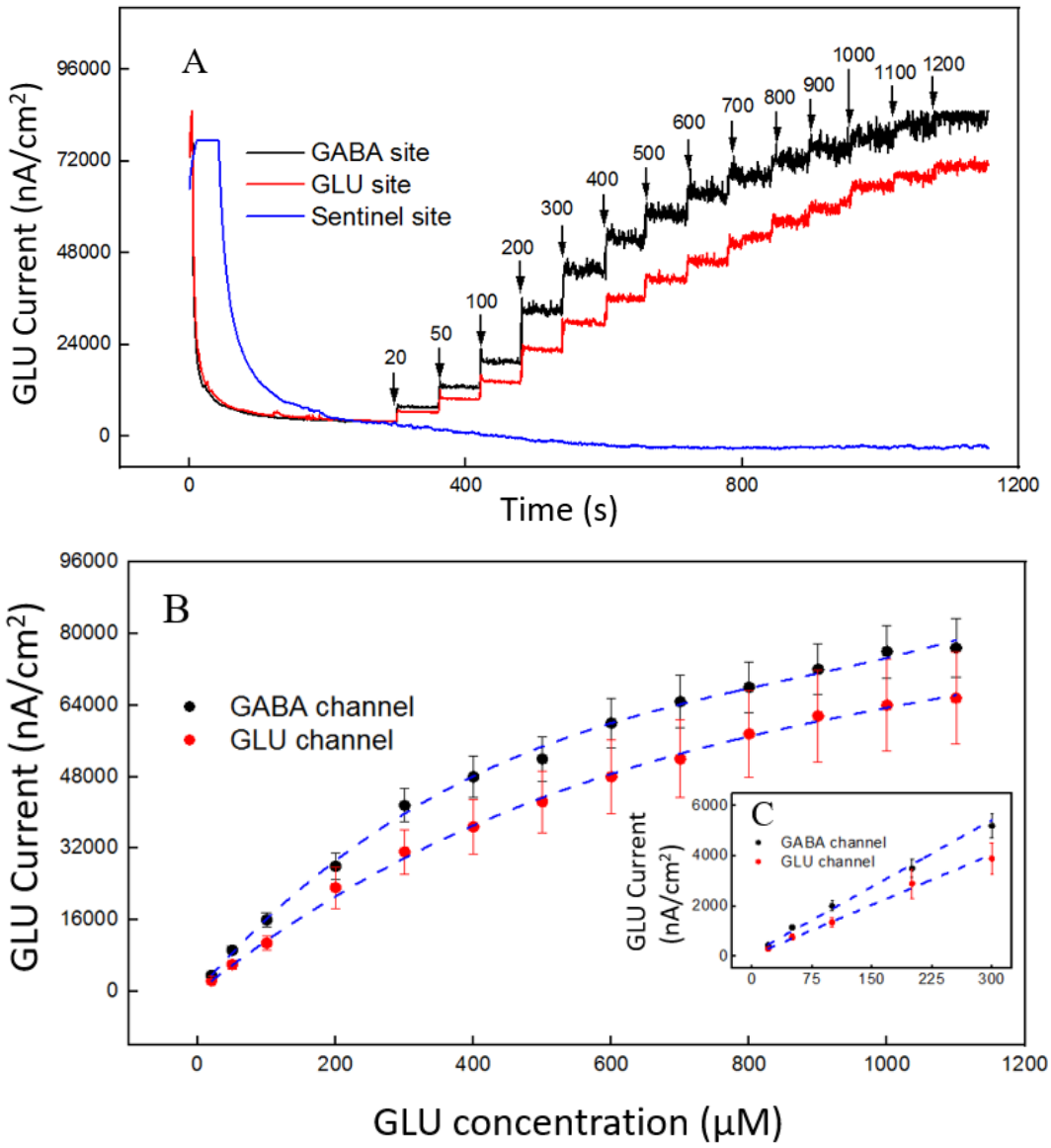

Figure 5-5: A. Shows response at 20-1200 μM GLU. The arrows show the infusion point and the numbers represent GLU concentration in μM. GABA channel (black line), GLU channel (red line) and sentinel channel (blue line). B. Shows response against GLU concentration in GABA channel and GLU channel C. Shows response against GLU concentration in the linear range in GABA channel and GLU channel.

5.5 GABA Calibration in presence of Glutamate

In these experiments we did the GABA calibration in presence of GLU as we have in Chapter-4. For these experiments we calibrate GLU in 10-300 µM range in various GABA concentrations. We did the GLU calibration in 1X PBS+ no GABA, 1X PBS+ 50 µM GABA, 1X PBS+ 100 µM GABA, 1X PBS+ 300 µM GABA, 1X PBS+ 500 µM GABA and 1X PBS+ 1000 µM GABA. The responses are shown in Figure 5-6.

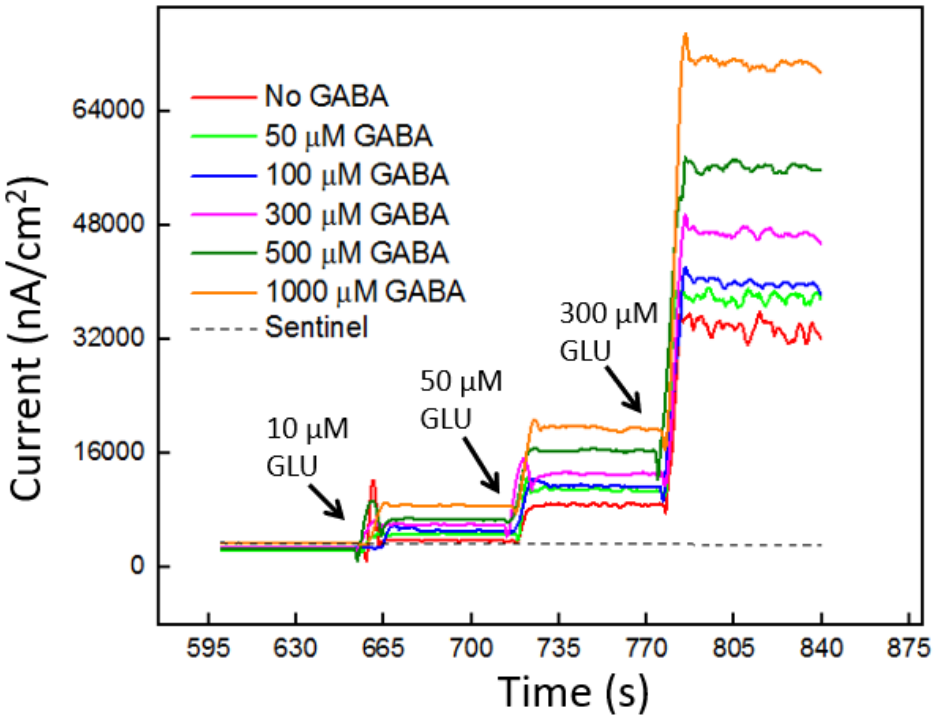

Figure 5-6: Glutamate responses in the GABA channel for different GABA concentration. The GLU response in the sentinel line is shown as black line.

As we can see from the Figure 5-6 ,with increasing GABA concentration the GLU signal increases too. When GABA is present in the solution, the H_2O_2 current response is from both GABA and GLU oxidation and we expect it to be larger than the response when there was no GABA. Therefore, higher GABA concentrations appear to induce a greater response GABA channel and greater I_{GABA}, which is the GABA signal. Therefore,

the GLU sensitivity in GABA channel increases with higher GABA concentration, whereas the GLU sensitivity in the GLU channel remains almost similar (no considerable increase/decrease in the signals). The apparent equal sensitivity can also be taken as proof that the increase in sensitivity in GABA channel is due to GABA concentration s and not random. Table 5-2 shows the sensitivity of the GABA and GLU channels for different GABA concentrations.

Table 5-2: Sensitivity (SS, nA/μMcm^2) different GABA concentrations. Sensitivity at 0μM GABA is shown as SS_0, Sensitivity at 50μM GABA is shown as SS_{50}, and so forth.

Channel	**SS_0**	**SS_{50}**	**SS_{100}**	**SS_{300}**	**SS_{500}**	**SS_{1000}**
GABA	104±12	120±18	128±17	152±21	184±27	224±41
GLU	55±7	64±10	45±8	44±6	43±7	41±9

The LOD in GABA and GLU channels for different GABA concentration. LOD is in the hundreds of nanomolar (nM) range as shown in Table 5-3. It is consistent with results we got in the Chapter-4. We can get I_{GABA} same way we discussed in Chapter-4. More about I_{GABA} and how it can be used to get GLU and GABA concentration is discussed in the next section. Table 5-3 shows the LOD of both these channels. The sentinel channel doesn't show sensitivity towards GLU as it does not have any enzymes.

Table 5-3: Limit of detection (LOD, μM) for different GABA concentrations. LOD at 0μM GABA is shown as LOD_0, Sensitivity at 50μM GABA is shown as LOD_{50}, and so forth.

Channel	LOD_0	LOD_{50}	LOD_{100}	LOD_{300}	LOD_{500}	LOD_{1000}
GABA	0.15±0.01	0.13±0.02	0.12±0.01	0.10±0.02	0.08±0.01	0.07±0.001
GLU	0.26±0.03	0.23±0.05	0.33±0.02	0.34±0.09	0.36±0.11	0.38±0.127

5.6 Quantification of GABA and Glutamate

Determining the GABA and GLU concentration follows similar process we discussed in Chapter-4. We observed the current difference between the GABA and GLU site. We observed increased current densities with increasing GABA concentration. Figure 5-7 shows this trend. If we subtract the current at a certain GABA concentration from the current at a no GABA concentration; we get the I_{GABA}. This is also shown in Figure 5-7.

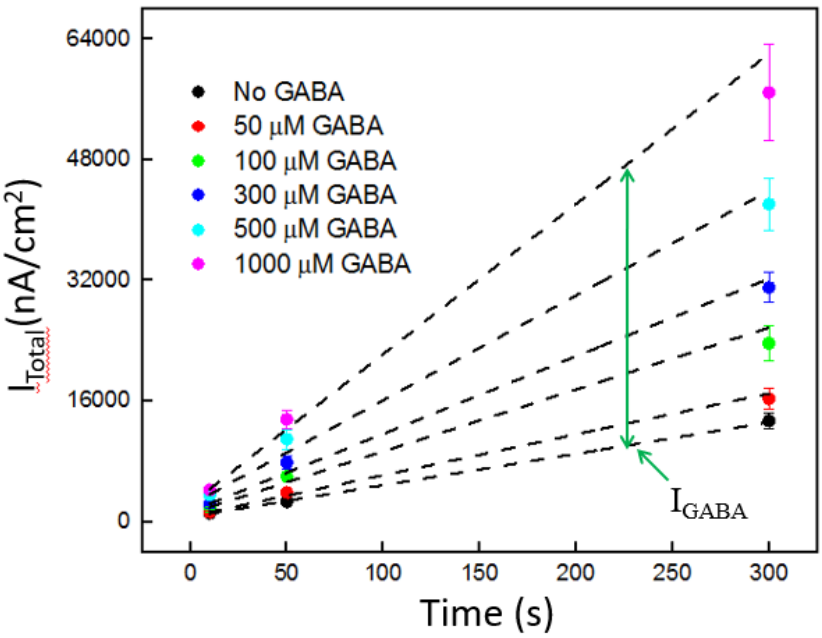

Figure 5-7: Current difference between GABA and GLU channel. Legends: no GABA (black dots), 50 µM GABA (red dots), 100 µM GABA (green dots), 300µM GABA (blue dots), 500 µM GABA (cyan dots) and 1000 µM GABA (magenta dots). Linear fitting parameters: no GABA: slope= 40±5 nA/µMcm^2; R^2=0.999, 50 µM GABA: slope= 51±11 nA/µMcm^2; R^2=0.995, 100 µM GABA: slope= 83±13 nA/µMcm^2; R^2=0.988, 300 µM GABA: slope= 102±13 nA/µMcm^2; R^2=0.993, 500 µM GABA: slope= 138±17 nA/µMcm^2; R^2=0.992 and 1000 µM GABA: slope= 197±26 nA/µMcm^2; R^2=0.992. Error values are shown in mean ± SEM.

We plot GLU response against GLU concentration as shown in Figure 5-8. It is the environmental GLU (GLU_E) as we've seen in earlier chapter. With the values of I_{GABA}, we plot I_{GABA} against the GLU concentration for different GABA concentrations as shown in Figure 5-8. Firstly, we determined the peak current in sentinel wire (e.g. 30 pA). After that, the peak current in GLU wire was calculated (e.g. 470 pA). The difference of these currents is the GLU current (e.g. 470-30=440 pA). Then, from the calibration curve GLU conc. was calculated. (e.g. if sensitivity of GLU wire is 10 pA/µM then GLU concentration in this case is 440/10=44 µM), shown in Figure 5-8.

Next, we determined the peak current in GABA wire (e.g. 2000 pA). Then according to the GLU sensitivity of the GABA wire, we subtracted the current from GABA wire current. (e.g., If the GLU sensitivity of the GABA wire is 15 pA/μM; then we subtract 15*44= 660 from the 2000 pA. 2000-600=1400 pA). The difference between the sentinel and the current above is our I_{GABA} (e.g. 1400-30= 1330 pA). Finally, from the GLU conc. and I_{GABA} we get the GABA conc. with the help of calibration curve shown in Figure 5-8.

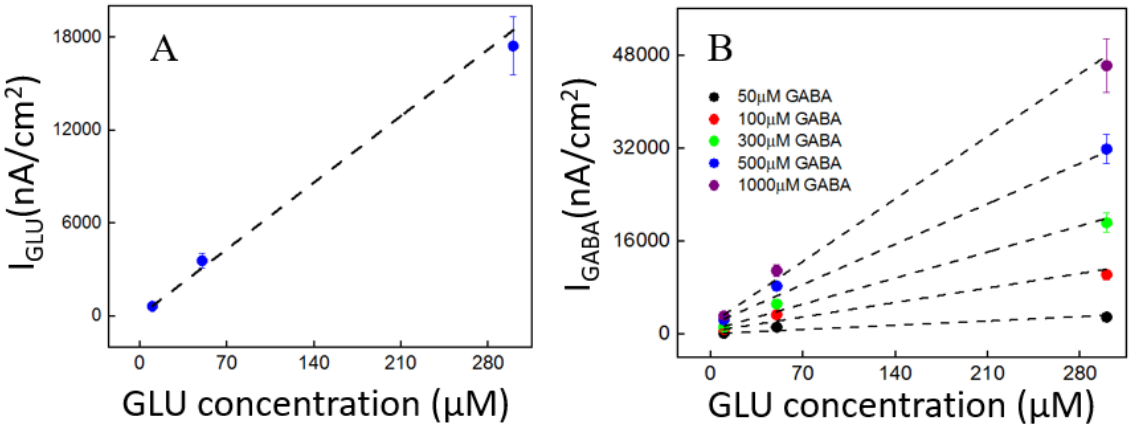

Figure 5-8: Scheme for quantification procedure for GABA and GLU concentration. A. GLU calibration in 1X PBS for GLU wire, we will get out GLU concentration from here. Linear parameters for the line: Slope=61 ± 6.4 nA/μMcm^2; R^2= 0.934 B. shows the difference in current, I_{GABA} vs GLU concentration, we will get our GABA concentration from here. Linear parameters: for 50μM GABA line, slope= 12 ± 3.8 nA/μMcm^2; R^2= 0.939; for 100μM GABA line, slope= 36 ± 12; R^2= 0.966; 300μM GABA line, slope= 64 ± 16 R^2= 0.967; 500μM GABA line, slope= 100± 21; R^2= 0.978 and for 1000μM GABA line, slope= 161± 25; R^2= 0.986. Error values are shown in mean ± SEM.

CHAPTER 6

REAL-TIME GABA AND GLUTAMATE MEASUREMENT

6.1 GABA and Glutamate Measurement in 8-TRK Probe

6.1.1 Probe modification for GABA and GLU Measurement in Rat Brain Slices

Hippocampal slices were prepared from an adult Sprague Dawley rat. The tissue slice is 400μm thick. However, as discussed in chapter-4 the sites (electrodes) in 8-TRK are 2mm apart. To solve this problem, we brought the sites closer. Figure 6-1 shows the new configuration of the GABA and GLU sites. The distance between the electrodes is now 100 μm, which is comparable to tissue thickness (400 μm).

Enzyme coating was done in the GABA and GLU sites in the same process as discussed in Chapter-4. Additionally, to block interferent molecules we also coated a mPD layer. The mPD layer was electrochemically deposited using Cyclic voltammetry between +0.2 V and +0.8 V, 50 mV/s, 20 min in 10 mM mPD solution. A calibration curve was constructed before performing the *ex vivo* recordings in order to convert current from GABA release to GABA concentration at the probe. This calibration curve is constructed based on the procedure detailed in Figure 4-16. The data plotted in Figure 6-1 is constructed in the same way as that of Figure 4-19. This I_{GLU} and I_{GABA} can be used to get GABA and GLU concentration.

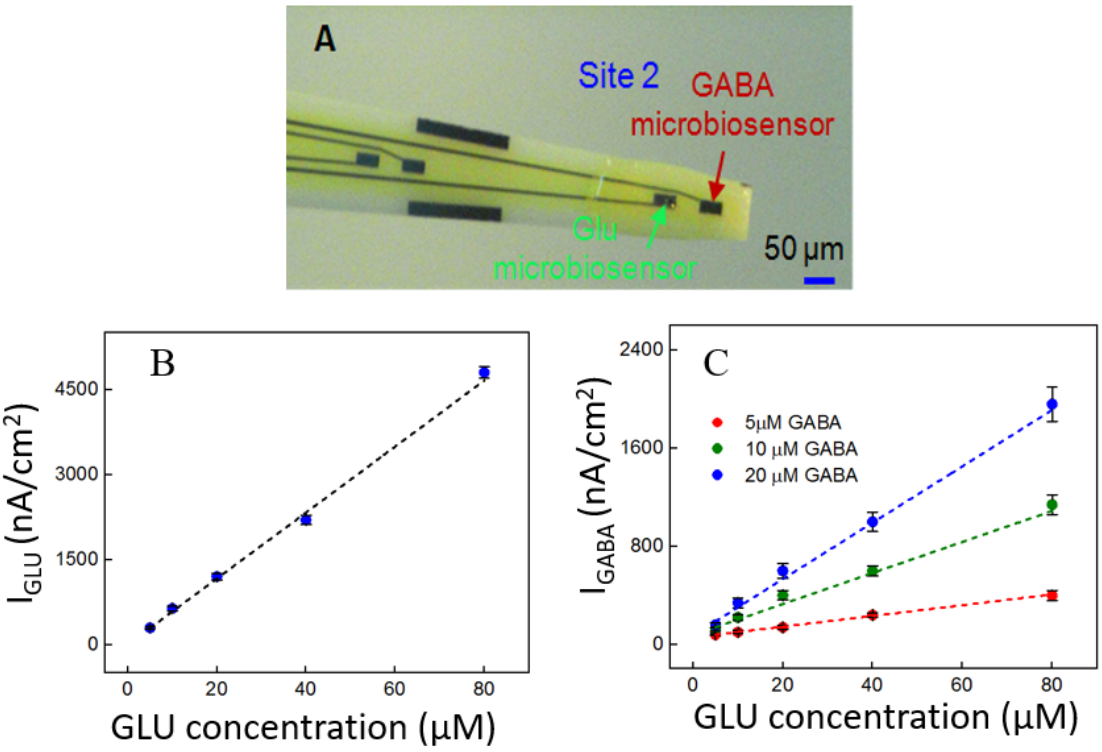

Figure 6-1: A. Shows the new probe placements. The distance between the sites is 100 µm. B. Current signals for varying Glu concentrations (5, 10, 20, 40, and 80 µM, blue dots) and the linear fit (black dashed). Linear fit parameters: Glu sensitivity: 58.2 ± 3 nA/µMcm^2, R^2= 0.99364. C. I_{GABA} for varying Glu concentrations. Legend: 5 µM GABA (red dots), 10 µM GABA (green dots) and 20 µM GABA (blue dots); linear fit for 5 µM GABA (red dashed), linear fit parameters: slope = 4.2 ± 0.12 nA/µMcm^2, R^2= 0.99699, the linear fit for 10 µM GABA (green dashed), linear fit parameters: slope = 12.6 ± 1.8 nA/µMcm^2, R^2= 0.9699 and linear fit for 20 µM GABA (blue dashed), linear fit parameters: slope = 22.8± 4 nA/µMcm^2, R^2= 0.98967 [14].

6.1.2 Real-time measurement of GABA and Glutamate in Rat Slice

Simultaneous and continuous real-time detection of GABA and glutamate (GLU) was accomplished using electrically stimulated release in a hippocampal slice model. We used a range of 100 µA pulse widths to induce release of the neurotransmitters as shown in Table 6-1 to determine the responsiveness of the sensor to varying levels of stimulation which included single pulses ranging from 1s to 25 ms in duration and a pulse train of ten 5 ms pulses. Figure 6-2 shows the signals in both the electrodes in different pulses.

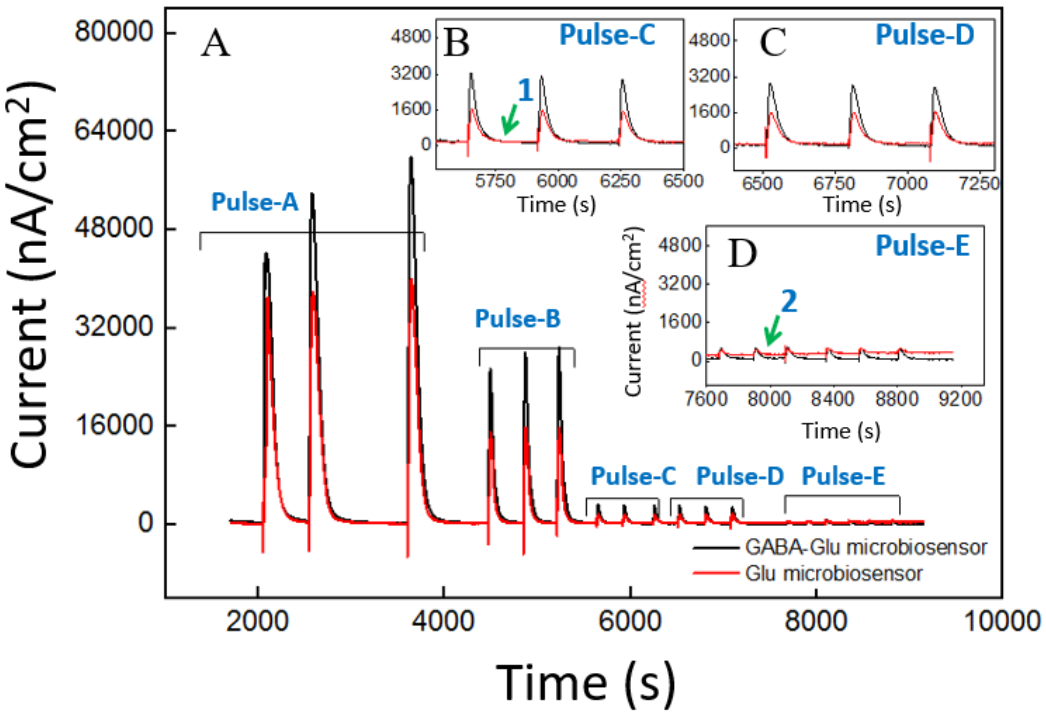

Figure 6-2: *Ex-vivo* recording of stimulated release of Glu and GABA in rat hippocampal slice preparation. A. Current responses to unipolar stimulation (tungsten wires, 100 µA) are shown. Stimulation pulse parameters (Pulse A–E) and conversion of peak current measurements to Glu and GABA concentrations are discussed for points 1 and 2 in subsequent sections Insets B, C, and D show details of the responses to shorter pulse widths [14].

The GABA signal was derived by subtracting the signal from the GOx-coated glutamate microbiosensor from the GABASE-GOx-coated GABA microbiosensor. The GABA signal and GLU signal is represented in Figure 6-3. As expected, the amplitude of GABA and glutamate release scaled with pulse width (Figure 6-3). In some cases, GABA had shorter peak duration, and in all cases the concentration of GABA rose faster than glutamate concentration (Figure 6-3).

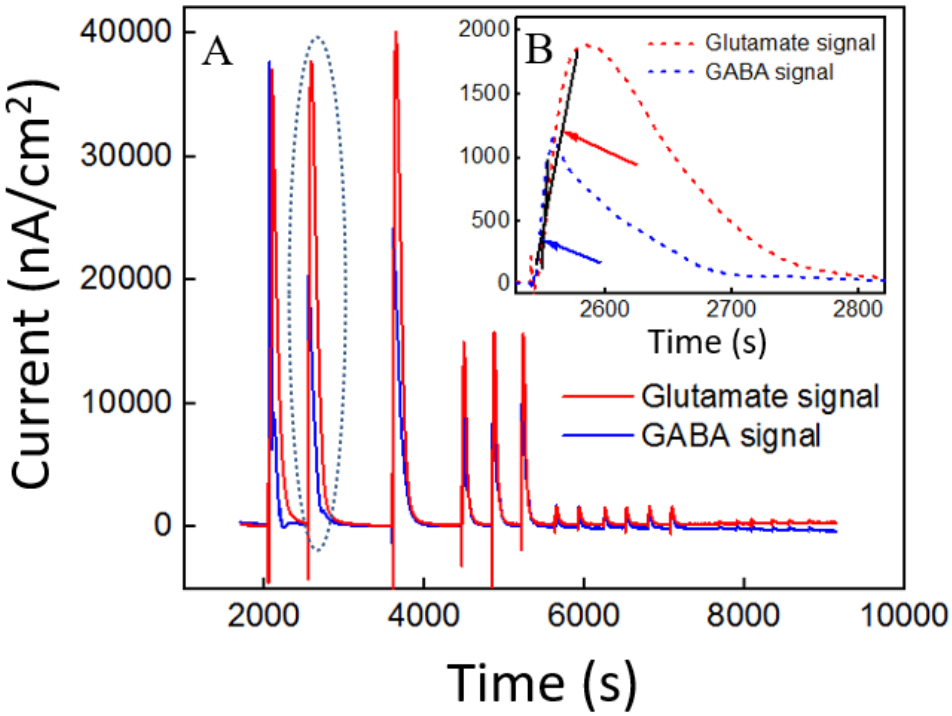

Figure 6-3: *Ex vivo* recording of stimulated release of Glu and GABA in rat hippocampal slice preparation. A. Processed GABA signal with Glu signal from responses to all stimulations in Figure 6-2. The GABA trace (blue trace) is the difference between the signals from the GABA-glutamate and the Glu microbiosensor sites (red trace). B. Inset shows the rise time, $t_{r10\text{-}90}$, for the GABA signal (blue curve) and the Glu signal (red curve) from the boxed region in A. Arrows indicate the slope of line drawn from $t_{r10\text{-}90}$ for GABA (blue arrow points to line) and $t_{r10\text{-}90}$ for Glu (red arrow points to line). The rise times for GABA were faster than for Glu, as the difference in the slopes of the lines illustrate[14].

For example, the mean rise time (±SEM) for a 25-ms stimulation was 6.94±0.9 s for GABA and 3.12±0.35 s for glutamate (n = 6, $p<0.05$). The rise time along with the pulse characteristics is shown in Table 6-1.The general trend we see here is with increasing time of the stimulation gives us higher rise time for both GABA and GLU signals. This is due to higher number of neurons firing in high duration pulses.

Table 6-1: Pulse parameters and rise time of the response [14]

Pulse ID	**Pulse parameters**	**Glutamate t_{r10-90} (s)**	**Glutamate – GABA t_{r10-90} (s)**	**GABA Δt_{r10-90} (s)**
A	1000 ms single pulse	25±2.2	17±1.24	8±1.2
B	250 ms single pulse	19±1.9	14±1.1	5±0.45
C	50 ms single pulse	7±0.85	12±1	5±0.6
D	Ten 5-ms pulses separated by 1 ms	7±0.8	12±1	5±0.75
E	25 ms single pulse	4±0.25	7±0.9	3±0.35

Both GABA and glutamate leak out of neuronal synapses after neurons release these neurotransmitters. Mechanisms exist to quickly scavenge and recycle these neurotransmitters, but some molecules diffuse through the extracellular space [25], [111], [112]. Thus, the there is a slight delay from stimulation to response, as well as a long decay period as GABA and glutamate are eventually cleared. Both of these dynamic processes are evident in the traces shown in Figure 6-3with a rapid, but not immediate increase in neurotransmitter concentration, and a slower decline to baseline representing release and uptake, respectively.

Peak current measurements in is shown in Table 6-2 represent a range of stimulated release of GABA and glutamate. These measurements correspond to curves labeled 1and 2 in Figure 6-2. Peak concentrations ranged from 5 – 35 μM for glutamate and 5 – 13 μM for GABA. The steps of calculating each parameter is shown below the table.

Table 6-2: Conversion of current to glutamate and GABA concentration in *ex vivo* recordings[14]

Points[1]	**Glutamate Signal (pA)[2]**	**Glutamate (μM)[3]**	**Difference in signal (pA)[4]**	**GABA (μM)[5]**
1	74	35	25	13
2	10	5	6	5

[1]Number corresponds to signal trace number in Figure 6-2. [2]From Figure 6-2, the $I_{H_2O_2(E)}$ value, i.e. the local Glu signal is measured. [3]Then the local GLU concentration is known from Figure 6-1. [4]The difference in signal, i.e. I_{GABA} value is the difference between the $I_{H_2O_2}$values obtained from the two microbiosensors in Figure 6-3. [5]Now, knowing the GLU concentration, which is the x-coordinate in Figure 6-1(C) and the I_{GABA} value, which is the y-coordinate in Figure 6-1(C), one can find the GABA concentration for the two points. Thus, these microprobes can measure GABA and glutamate at concentrations that are well below normal levels [28],[103] making them suitable to study impaired release in disease states. Furthermore, numerous cycles of stimulated release with consistent current amplitude for each level of stimulation and without adding any exogenous substrates, such as α-ketoglutarate, support the premise

that endogenous products of the conversion of glutamate provide the substrate for the GABASE reaction. This is an important capability for future *in-vivo* applications.

6.2 GABA and Glutamate Measurement in Microwire Probe

6.2.1 GLU and GABA Release is Dependent on Stimulation Frequency

We used three stimulation frequencies, 10, 50, and 140 Hz, to evoke GLU and GABA release. Each of these stimuli issued 5s trains of 100 µA square pulses with 1ms width. We randomized the types of stimulations to avoid systematic error. Prior to initiating the next stimulation, we allowed current responses to return to baseline to avoid effects from potentiation. Between subsequent stimulation, we used a single 100ms control pulse (100 µA square pulse). Control pulses produced the same GLU response throughout each recording session indicating that brain slices were in good health and that stimulation-induced potentiation has not occurred [96].

Both GABA and GLU current increased with increasing stimulation frequency. Representative traces of responses to randomized stimulation are shown in Figure 6-4. The common pattern we observed here is the lower stimulation pulse (10 Hz) gave smaller signals for both GLU and GABA. With increasing frequency, the signals rose higher. We made sure that the control pulse response similar throughout the recording. When we saw a change in our control pulse, we concluded our tissue is no longer healthy for recording. At this point, we start recording from a different tissue. Figure 6-4 also shows response for different stimulation frequencies. The responses were significantly different in terms of amplitude and rise time/fall time. It is evident with the use of different axis scale (time vs current) for different stimulation frequencies (and control pulse).

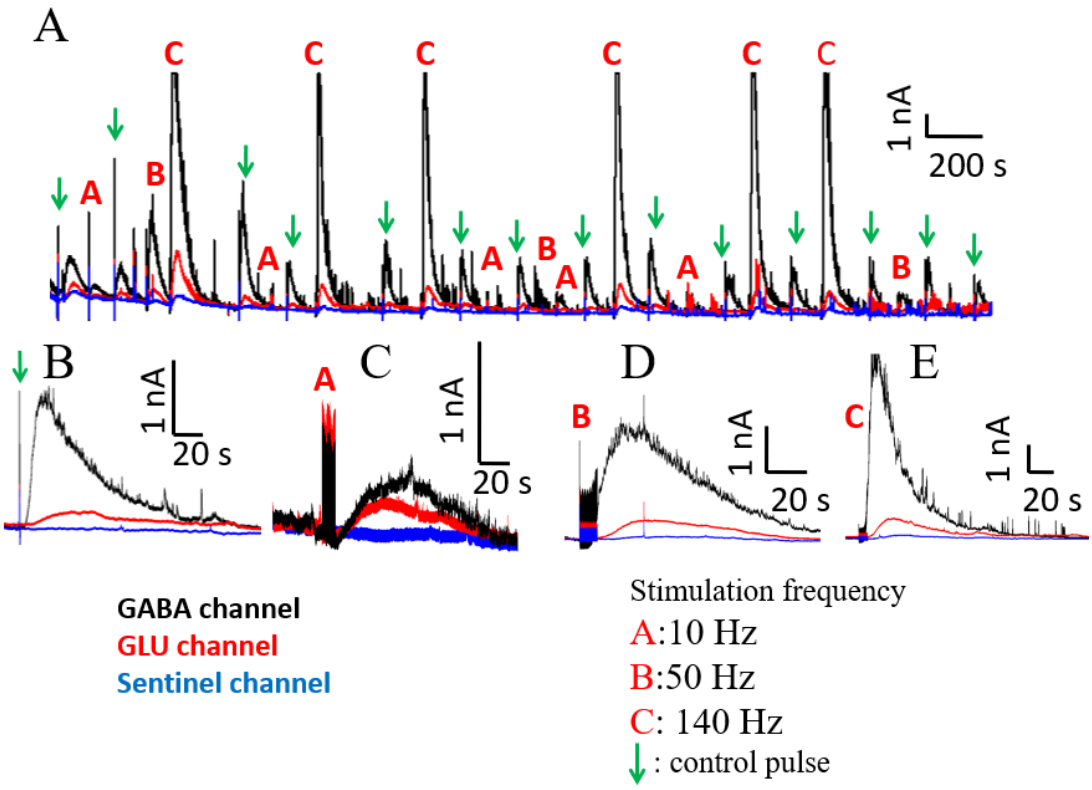

Figure 6-4: Microwire biosensor current in response to three different stimulation frequencies. A. Representative recording of current in response to 100 µA stimulation with 10, 50, or 140 Hz pulse trains, denoted by A, B, C (red font), respectively and to a single 100 ms control pulse indicated by green downward arrows. B-E. Details of selected current responses to 10, 50 and 140 Hz stimulation from Panel A are shown in C, D, and E, respectively. The control pulse is shown in B. In all these cases the black traces indicate the signal in GABA channel, red traces indicate signal in GLU channel and blue traces indicate the signals in sentinel channels. GABA channel is coated with 0.1 unit/µL GABASE+0.1 unit/µLGOx and GLU channel is coated with 0.1 unit/µLGOx. Sentinel channel has no enzymes.

6.2.2 Extracellular Concentration of GLU and GABA

Peak concentration increased as stimulation frequency increased for both GABA and GLU as shown in Figure 6-5. GABA concentration increased in a linear fashion whereas GLU increase was not linear Figure 6-5. GLU concentration increased to a lesser extent between 50 and 140 Hz than between 10 and 50 Hz, perhaps due to inhibition from increased GABA. Furthermore, both GLU and GABA concentrations were higher after a single stimulation (100-ms control pulse) than after 10 Hz stimulation. GLU concentration increased significantly from 50± 5 μM to166 ± 28 μM when the stimulation frequency was increased from 10 to 50 Hz. GLU concentration rose to 264 ± 43 μM (mean ± SEM) when the stimulation frequency was increased to 140 Hz, although the increase in concentration from 50 to 140 Hz pulses represented a non-significant trend ($p = 0.063$). However, the difference in concentration between 10 and140 Hz stimulation was significant.

Similarly, GABA concentration increased from 72±14 μM to 296± 53 μM from 10 Hz to 50 Hz stimulation, and it rose further, to 793 ± 27 μM (mean ± SEM) in response to 140Hz pulses. In addition, mean peak GLU and GABA concentrations were significantly different in response to the control pulse. Furthermore, the difference was highly significant for 50 Hz stimulation and for 140 Hz pulses Figure 6-5.

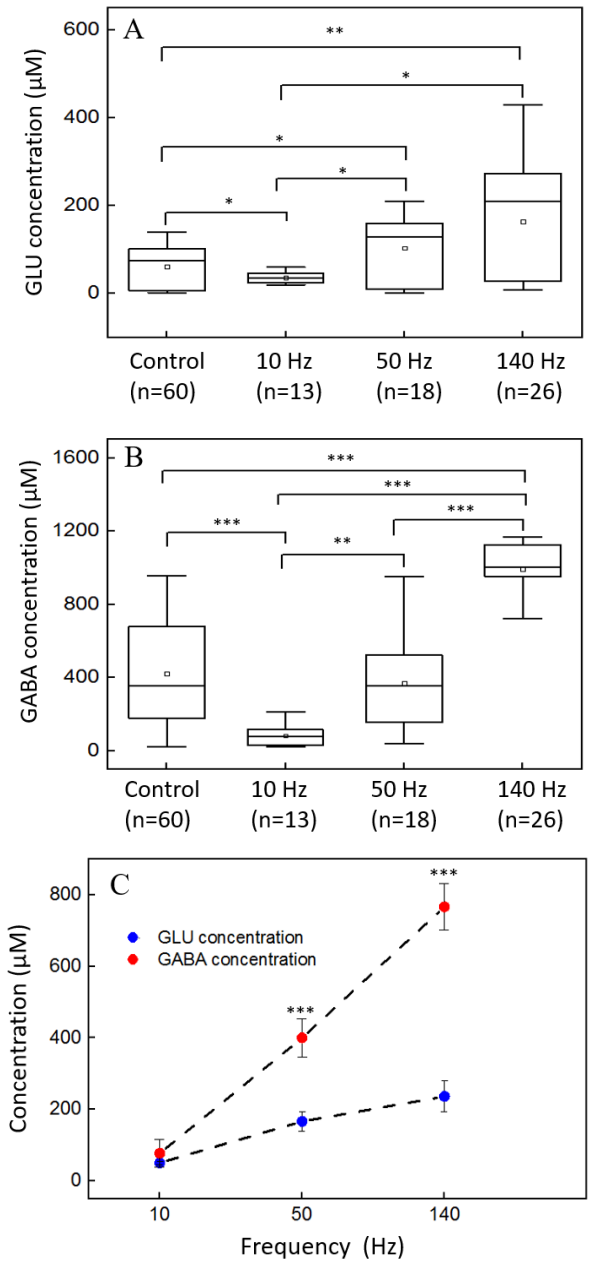

Figure 6-5: Peak GLU and GABA concentration. A. Mean peak GLU concentration for different stimulation. B. Mean peak GABA concentration for different stimulation C. Lines on the scatter plot show that the rate of increase in extracellular GLU (blue) and GABA (red). Results are shown as mean ± SEM (error bars). Statistically significant differences are denoted by asterisks over horizontal brackets in A and B; in C (independent Wilcoxon tests, * $p \leq 0.05$, ** $p < 0.01$, *** $p < 0.001$). (Data provided by T.A. Murray)

6.2.3 Response Characteristics of GLU and GABA peaks

Dynamic features of extracellular GLU and GABA release, evident in the shape of the current peaks, scaled with stimulation frequency. For example, both the rise time (T_R) and the decay time (T_D) of GLU and GABA peaks increased as stimulation frequency increased (Figure 6-6 and Figure 6-7). In general, the duration of the peaks (FDHM, Figure 6-6 and Figure 6-7) scaled with increasing stimulation frequency except for a non-significant difference between GLU peak duration after 50 and 140Hz pulses.

Interestingly, for the single control pulses, mean GLU and GABAT_R values were similar to 50Hz stimulation, whereas mean GLU and GABA T_D and FDHM values were most similar to 10 Hz stimulation. No differences were observed between GLU and GABA for the same parameter and stimulation frequency. Increased stimulation frequency produced higher concentrations of GLU and GABA. This could be due to recruitment of a greater number of glutamatergic neurons and GABAergic neurons, and/or longer firing periods of the same population of cells, in response to higher frequency stimulation. In either scenario, more neurotransmitters are released which would take longer to diffuse toward the biosensors, and require more time for astrocytic uptake. Thus, it is not surprising that T_R, T_D and FDHM increased as the concentration of GLU and GABA increased. The decay time for GLU is shown in Figure 6-6 and for GABA it is shown in Figure 6-7. For the GLU signal there was no significant difference between decay time in 50 Hz and 140 Hz stimulation. The same pattern is not observed in the GABA response, for 50 Hz and 140 Hz there is no significant difference in GABA response decay time (see APPENDIX C for all wilcoxon p-values).

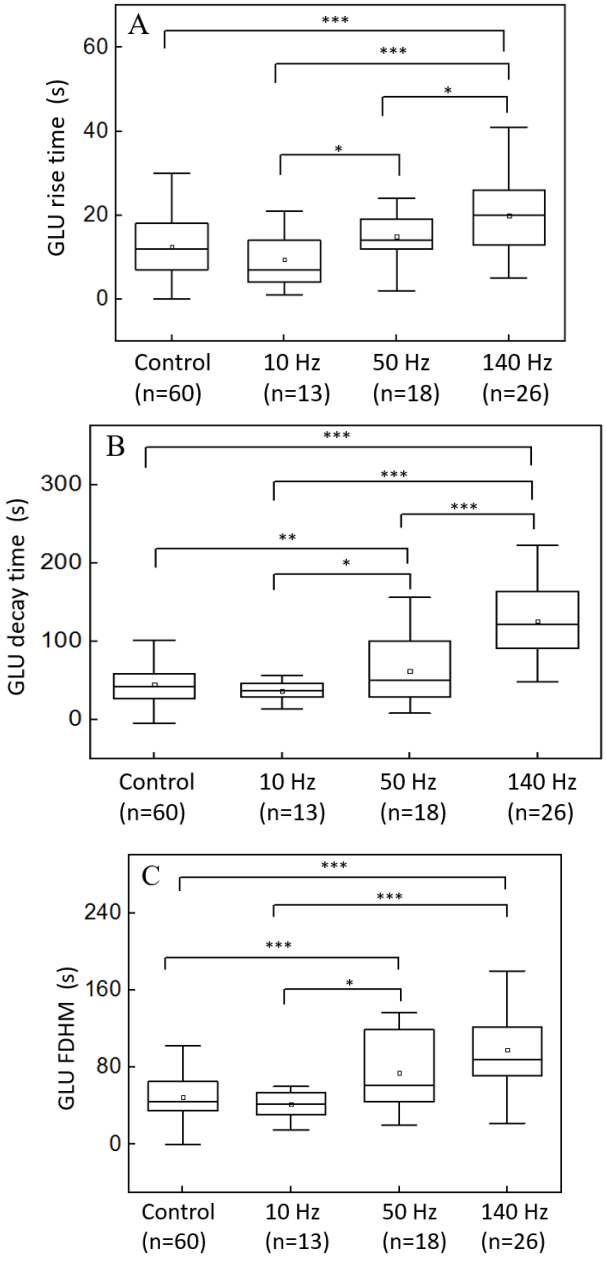

Figure 6-6: GLU peak characteristics. Rise time (*A*, T_R), decay time (*B*, T_D), and duration (*C*, FDHM) of extracellular GLU release increased as stimulation frequency increased. A. Differences in mean rise times between 10, 50 and 140 Hz for GLU. B. Differences in mean decay times between 10, 50 and 140 Hz for GLU C. Differences in mean FDHM times between 10, 50 and 140-Hz for GLU * $p < 0.05$, ** $p < 0.01$, *** $p < 0.001$. (Data provided by T.A. Murray)

T_D and FDHM, in combination, show the decay time for the signal. Taking these results together we can conclude that the decay time is higher than the rise time. It also makes sense because the GLU signal increase is thought be originated in the neuronal firing which is in millisecond range. In contrast the decay is probably due to the uptake of GLU in astrocytes which takes few seconds.

6.2.4 E:I ratio of Excitatory Glutamate and Inhibitory GABA

GLU is the major excitatory (E) neurotransmitter in the brain and GABA is the major inhibitory (I) neurotransmitter. Both are plentiful in CA1. We calculated the ratio of GLU to GABA concentration (E: I ratio) for each stimulation condition (Figure 6-8). Mean E:I ratios for a single control pulse and 10, 50 and 140Hz pulses, were0.64 ± 0.10, 1.27 ± 0.26, 0.54 ± 0.09 and 0.36 ± 0.06 (mean ± SEM), respectively. This trend toward lower E:I ratios as stimulation frequency increased was significant between 10Hz and 50Hz, and 10Hz and 140Hz pulses, and between control and 10Hz stimulations. The reduction in the E/I ratio from 50Hz to 140Hz stimulation was a non-significant trend ($p = 0.09$), see APPENDIX C for all wilcoxon p-values. Durand et al. showed seizure suppression by high frequency optogenetic stimulation in hippocampus of animal models of epilepsy, where the suppression was attributed to the activation of GABA receptors in GABAergic interneurons [113]. This work and others have demonstrated that electrical high frequency stimulation suppress seizures by generating a depolarization block related to the inactivation of sodium channels or driving GABA release during stimulation.

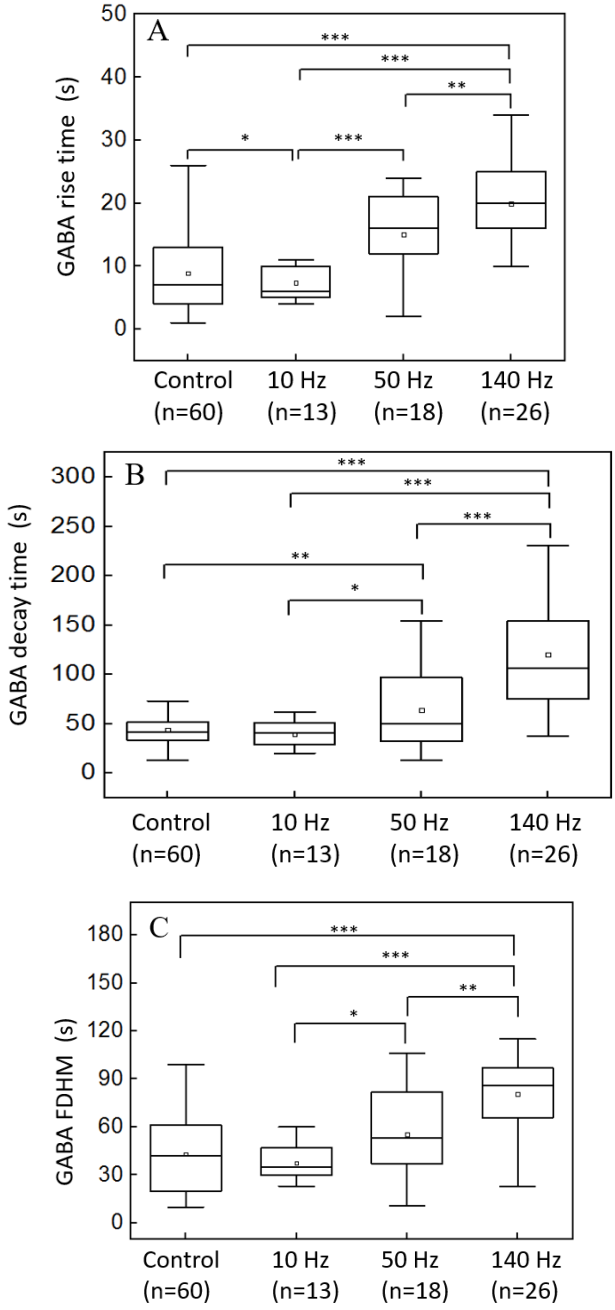

Figure 6-7: GABA peak characteristics. Rise time (A, T_R), decay time (B, T_D), and duration (C, FDHM) of extracellular GABA release increased as stimulation frequency increased. A. Differences in mean rise times between 10, 50 and 140 Hz for GABA. B. Differences in mean decay times between 10, 50 and 140 Hz for GABA C. Differences in mean FDHM times between 10, 50 and 140-Hz for GABA * $p < 0.05$, ** $p < 0.01$, *** $p < 0.001$. (Data provided by T.A. Murray)

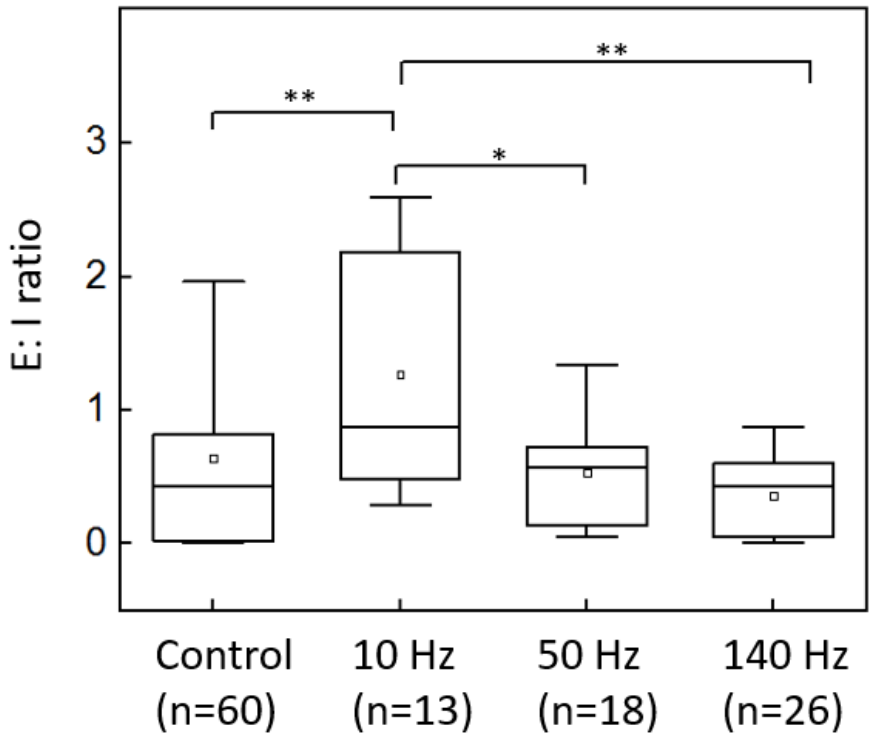

Figure 6-8: The ratio of peak concentrations of GLU (excitatory input, E) and GABA (inhibitory input, I). Significant decreases occurred between 10 and 50 Hz and 10 and 140 Hz stimulation. A non-significant trend toward lower E: I value was observed for higher frequency stimulation between 50 and 140 Hz ($p = 0.09$). Wilcoxon ranked sum test, * $p < 0.05$, ** $p < 0.01$. (Data provided by T.A. Murray)

In addition, it has been estimated that a single GABAergic cell may affect more than a thousand pyramidal cells [114]. Therefore, activation of GABAergic neurons becomes dominant at high frequency stimulation, which led to a recovery of the E/I balance and seizure suppression. In our work, we observed a huge activation of GABAergic neurons at 140 Hz. This excess GABA could have reduced excitatory synaptic transmission by decreasing excitatory postsynaptic potentials and GLU release and even block action potential propagation as suggested in literature [115],[116].

6.2.5 *In vivo* Recordings in Freely Moving Rat

We recorded GABA and GLU in an awake, freely moving rat two weeks (Wk 2) after guide cannula implantation and again during week 10 and week 16 which was eight and fourteen weeks, respectively, following the first recording (Figure 6-9). Freshly calibrated microwire biosensors were inserted into the permanently implanted cannula for each recording session. In between recordings, a filler wire was inserted into the cannula to maintain the patency of its lumen. After acquiring baseline recordings, we employed the lithium-pilocarpine model of epilepsy to induce epileptogenesis. Current traces shown in Figure 6-9. are after subtraction of sentinel current for both biosensor channels and also after subtraction of GLU current from the GABA channel. For better visualization, we did not include the sentinel channel; we also down sampled and used a moving average to better visualize GLU and GABA baselines. GLU and GABA dynamics were markedly different between various behaviors, which included grooming, walking, sleeping, and epileptic seizures. We observed spontaneous seizures at Wk 10 and several sleep/wake cycles at Wk 16. The sleep/awake time we determined from our detailed notes during the recording session. The rat dozed off (laid down, eyes closed) periodically which we named as a sleep cycle. When the rat started moving around the cage or we saw movement with eyes open we named them wake cycle. We did not observe any movement artifacts when the rat walked, groomed, or slept. However, pronounced motion artifacts occurred whenever the rat bumped its head on the side of the cage. The magnitude of this artifact was greater than two times the highest current peaks seen during normal behaviors. One example of how GLU and GABA varies with behavior can be seen in a segment of the Wk 10 recording (Figure 6-9A).Activities

during this recording include walking, resting, grooming, and several different types of seizure behaviors. At the start of this segment, the rat was awake but not moving (horizontal gray bar on the left). During this 70-s time period, several short and steep fluctuations occurred that resemble interictal spikes, commonly observed in electroencephalograms, that suggests a seizure has recently occurred or is about to occur [117], [118]. The full duration of these spikes (time from departure to return to baseline) was 443.3 ± 136.6 ms (mean ± SD, n = 9) and the frequency of these spikes was 0.13 Hz. GABA and GLU concentrations were calculated using calibration curves for each biosensor that were constructed prior to recording. The concentration at these low points was 4 ± 1 μM and 2 ± 0.8 μM for GLU and GABA, respectively and baseline levels were 18 ± 4 μM and 15 ± 5μM, respectively (mean ± SD, n = 9).The period of interictal-like spiking was followed by normal walking with larger and more frequent fluctuations in both neurotransmitters. After this we observed lower amplitude fluctuations on the same baseline as the rat rested. The frequency of these periods was similar (walking, 9.7 Hz; resting, 13.0 Hz). Following these time periods, a rapid increase in fluctuation amplitude (GLU, 6 ± 2 μM; GABA, 10 ± 3 μM), and frequency (28 Hz) preceded and continued through a 21s long period of grooming. A brief, 3s rest period followed. During this time, the GABA baseline began to decrease while the GLU baseline remained unchanged. As the rat began grooming again both GLU and GABA baseline concentrations steadily dropped from 18 μM to 8 μM for GLU and from 17 μM to 5 μM for GABA (Figure 6-9A, middle gray bar shows GABA baseline slope). After a steep decrease in GABA (Figure 6-9A, left downward arrow), baseline GABA slowly increased but remained below baseline by 50%, while baseline GLU remained steady.

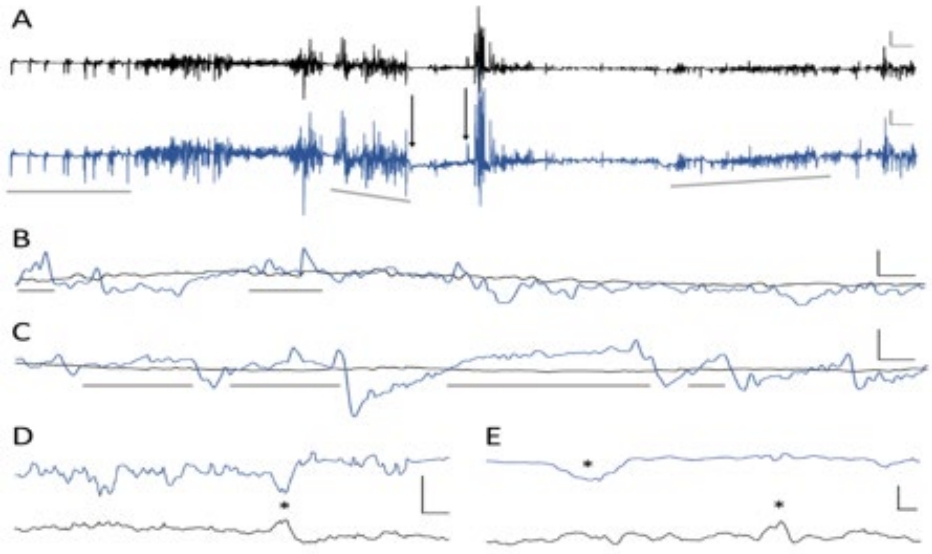

Figure 6-9: *In vivo* GLU (black) and GLU (blue) dynamics change with different types of behavior. A. Vertical scale bar 1 nA and horizontal scale bar 20 s for both GLU and GABA traces. B.C. Representative sleep-wake cycles at week 16. Vertical scale bars 0.5 nA and 1.0 nA for top and bottom plots, respectively, and horizontal scale bars represent 2 min for both. D. Signal after two weeks after cannula implantation Vertical scale bar 0.1 nA and horizontal scale bar 125 ms. E. signal from the same rat as shown in D, 8 weeks after the first recording. Vertical scale bar 0.2 nA and horizontal scale bar 100 ms (Figure provided by P.T. Doughty, K.A. Ponder and T.A. Murray, 2020).

Several behaviors are captured in this 8-min 40-s recording in Figure 6-9A. Ictal-like peaks appear in the first 70 s when the rat is not moving (horizontal gray bar). This is followed by walking and grooming (between left and middle gray bars). Movement ceased between the two downward arrows as the rat abruptly stopped moving (frozen posture). A rapid decrease in GLU and GABA occurred at the onset of freezing (left arrow). GABA gradually increased until the point when the rat clearly exhibited seizure behavior with forelimb clonus, which is a Racine Scale 3 behavior during epileptic seizures in rats. Coinciding with clonus are brief sharp peaks in both neurotransmitters (right arrow). After this, GABA and GLU fluctuated rapidly and after a few seconds the rat began rearing and fell which are Racine Scale 4 and 5 behaviors, respectively.

Maximum current fluctuations in both biosensor channels were observed just before and through rearing. After this, the rat ceased rearing but continued to exhibit mouth and facial movements with some occasional head bobbing for the remainder of this recording segment. These are Racine Scale 1 and 2 behaviors, respectively. During this period, GABA current dropped rapidly (just before inclined gray bar, A) and then steadily rose (slope denoted by inclined gray bar on right, Thirty-three seconds after the sudden drop in GABA, the rat had a seizure that began with forelimb clonus (Figure 6-9A, right downward arrow) with brief simultaneous peaks in both neurotransmitters (GLU increased 50.0 ± 25.0% and GABA 50.0 ± 14/3% over their baseline concentration, respectively). Forelimb clonus is a Racine Scale 3 behavior in rodent models of epilepsy[119]. Within two seconds, large amplitude and rapid changes in GLU and GABA began to occur. A few seconds later, the rat reared and fell over, which are Racine Scale 4 and 5 behaviors, respectively. The large peaks in both neurotransmitters ended as the seizure behavior transitioned to Racine Scale 1 facial movements. The baseline of both neurotransmitters remained below pre-seizure levels with progressively lower fluctuations in concentration of around 1 μM for each neurotransmitter. Baseline GLU concentration remained at 8 ± 4 μM while GABA slowly rose from 2 to 6μM. Almost two min after the seizure began, the GABA signal suddenly decreased again to 2 μM and then began a steady increase over the next two minutes to 11 μM (Figure 6-9A, inclined gray bar to right). Baseline levels of both neurotransmitters remained lower than pre-seizure baseline throughout the seizure.

We compared the mean baseline concentration for each behavior (Figure 6-9 A) and calculated an E:I ratio for each. As expected, seizure activity was dominated by

excitation. The E: I for interictal activity were 1.20 and for Racine Scale 1 – 5 behaviors it was 2.88. Conversely, awake behaviors of walking, resting and grooming were dominated by inhibition (E: I = 0.89). During the pre-seizure period (between arrows, Fig. 8A) and as seizure was waning, during the last two minutes of the recorded traces, the E:I ratio was 1.0. Notably, the mean E: I ratio for the entire period was dominated by excitation (E: I = 1.39).

A very different relationship of GLU and GABA signals was observed during sleep cycles. GABA signals rose before the onset of sleep. Prior to arousal, the GABA current rapidly declined. Six sleep-wake cycles from week 16 are shown in Figure 6-9B, C, with sleep denoted by horizontal gray bars. Mean peak concentration of GABA during sleep increased 31.2±8.6% (mean±SD, n = 6) above the overall mean for the series of sleep-wake cycles and then decreased 31.9±11.7% (mean±SD, n = 6) during awake behaviors. Whereas relatively large changes were observed in GABA, the concentration of GLU remained stable throughout these cycles, although it did rise and fall during other types of behaviors (not shown). The maximum GABA concentration during periods of sleep and the minimum concentration for periods of wakefulness were used to calculate the E: I ratio for each episode. The mean E: I ratios for sleep and wakefulness were 0.67 ± 0.04 and 1.32 ± 0.24, respectively (mean ± SD, n=6 each) indicating that inhibition dominated during sleep and excitation during wakefulness. Interestingly, the mean E: I for all sleep and wake periods were 0.995, which is close to complete balance. GABA current steadily increased prior to each of six episodes of sleep (gray bars) and remained elevated with some fluctuation during sleep. Immediately prior to waking, GABA levels rapidly fell and remained low during activity.

Biosensor current was recorded at 1000 Hz for all sessions. Recordings were generally down-sampled and smoothed to better observe shifts in neurotransmitter levels with behavior. When analyzing raw current data, subsecond fluctuations in GABA and GLU current were observed that were not related to electronic noise (e.g., not 60 Hz oscillation). Two examples are shown in Figure 6-9(Panels D & E); both recordings were acquired during calm walking. As glutamatergic and GABAergic neurons form feedback networks in the hippocampus, it was not surprising to observe some opposing transient changes in current. The first example illustrates this phenomenon with a decrease in GABA and corresponding increase in GLU (asterisk, Figure 6-9 D). This set of peaks had a FDHM of 70 ms. Peak current was determined using calibration curves for each biosensor channel. Mean GABA concentration before and after the peak was 3.8 μM and 5.1 μM, respectively. Concentration rapidly decreased by 0.6 μM then increased by 1.8 μM and remained slightly higher. GLU followed a similar time course, but the signal was inverted compared to GABA. Mean GLU concentrations before and after this peak were15.3μM and 12.1μM, respectively. Peak concentration increased by 1μM and then rapidly declined by 4 μM and remained low during this time segment.

The second example of sub-second fluctuations in GABA and GLU current were recorded eight weeks later in week 10 (Figure 6-9). In contrast to the simultaneous, opposing peaks in Figure 6-9 D, the two peaks in Figure 6-9 E was separated by 600ms. Mean GABA concentration before and after the drop (asterisk) was 19 μM and 22 μM, respectively. GABA rapidly dropped by 8 μM and then increased by 11 μM. Mean GLU concentration before and after the peak (asterisk) was 15 μM and 14 μM, respectively.

GLU increased by 4 μM and decreased by 5 μM. The GABA and GLU peaks had a FDHM of 235 ms and 128 ms, respectively.

6.2.6 Peak Concentration Depends on Stimulation Frequency

While extracellular GABA and GLU peak concentration increased with increasing stimulation frequency, their responses were different. Mean peak GABA concentration increased 26-fold over baseline compared to 15-fold increase for GLU. In addition, we observed a linear increase in hippocampal GABA release with increasing stimulation frequency. In contrast, GLU increased at a lower rate from 50 Hz to 140Hz stimulation versus from 10 Hz to 50Hz. It appears that the glutamatergic neurons in CA1 are less sensitive to 140Hz stimulation. Our results are in agreement with Mantovani et.al., who reported a marked increase in GABA release and little effect on GLU release in human neocortical brain slices after 130 Hz stimulation [120]. Using optogenetics, Chiang et.al.,also found that high frequency stimulation of the hippocampus predominantly drove GABA release [113]. GABA release is primarily achieved through activation of GABA receptors. For example, the GABA release during the high frequency stimulation of human neocortical slices was dependent on $GABA_A$ receptor-mediated chloride influx [120], [121]. However, GABA release was also dependent on voltage-gated sodium channels. This combined effect of Cl^- and Na^+ dependent release of GABA may have contributed to the relatively high concentration of GABA with 140 Hz stimulation.

Other research on the effects of electrical stimulation[122] and optogenetic stimulation [123] have revealed frequency-dependent increases in extracellular GLU in the sub-thalamic nucleus and globus-pallidus, respectively, likely due to increased

neuronal stimulation and/or decreased astrocytic uptake. Similarly, we expected that the glutamate responses in the hippocampus would vary with stimulus frequency. Another study observed a linear increase in thalamic GLU release (up to 400 μM) with stimulation frequency from10 Hz to 300 Hz [124]. The authors identified two sources of GLU release, one from depolarization of glutamatergic afferents to the thalamus, a neuronal source, and release of stored vesicular GLU in astrocytes, a non-neuronal source. They also noted that because astrocytes are non-excitable cells, they are more likely to produce linear response to electrical stimulation. Our data shows a non-linear increase in hippocampal GLU release (up to 264 ± 43 μM) with stimulation frequency (10 – 140 Hz). This increase could be due to increased recruitment and depolarization of glutamatergic neurons [114], and possibly electrically stimulated release of stored GLU from astrocytes [112].

Peak GABA concentrations in our study were much higher than commonly reported concentrations in the hippocampus using microdialysis. Those studies reported basal levels up to 0.5 μM for GABA [125], [126] and, after KCl stimulation, levels increased up to 2.5 μM for GABA [126]. In contrast, at least one microdialysis study reported a nearly 1000% higher concentration after stimulation with KCl [127], which is far lower than our maximum peak concentration. In the present study, we stimulated the Schaffer collaterals, which is likely to elicit synchronous firing in CA1 that recruits a relatively large number of glutamatergic pyramidal cells and GABAergic interneurons [96]. Given the placement of our microwires, a large proportion of our biosensor surfaces were probably in close contact with active synapses of these cells [27], not only during the response to electrical stimulation but also between stimulation as these neurons are

known to fire tonically[128]. Thus, we would expect to detect higher baseline and peak concentrations of GABA after electrical stimulation. Similar to our observations, another research group has shown that synaptically released GABA in cultured rat primary hippocampal cells reach transiently high concentrations (~1.5–3 mM) using electrophysiology and computer modeling [129].Similar to GABA, the baseline and peak GLU concentration that we observed was higher than microdialysis studies. However, our range of concentrations was similar to the range of concentrations found in other studies [27].

6.2.7 E: I Ratio Varies Nonlinearly with Stimulation Frequency

We observed a marked decrease in the E: I ratio in CA1 from 10 Hz to 50Hz stimulation and from 10 Hz to 140Hz pulses. This decrease was nonlinear. There was also a nonsignificant trend suggesting a possible decrease from 50 Hz to 140Hz. For the low frequency, 10Hz stimulation, the E: I ratio was greater than one suggesting that 10Hz pulses elicit an overall excitatory response in CA1. In contrast, the 50 Hz and 140Hz stimulations resulted in E: I ratios of less than one. Even though both GLU and GABA concentrations increased with 50 Hz and 140Hz pulses, the balance shifted to an inhibitory response with markedly higher GABA concentrations, especially after 140Hz stimulation. Increased GABA inhibition likely led to the nonlinear increase in GLU. To avoid GLU excitotoxicity, the absolute concentration of GLU may not be as important as the ratio of excitatory to inhibitory signaling. A human and nonhuman primate study has shown that after a certain time, the E: I balance is restored, even after seizure activities [130].

CHAPTER 7

CONCLUSION AND FUTURE WORK

7.1 Conclusion

In this dissertation we have developed a detailed understanding of GLU-GABA probe based on our novel mechanism. We characterized and validated our probe in both commercial and wire-based platform. We were able to show the effects of process parameters in sensor performance. We were able to demonstrate the application of these sensors in brain tissue slices and freely awake moving rats. The following conclusions can be drawn from our work on sensor development in ceramic based 8-TRK probes.

1. To determine GABA and GLU our sensor does not require addition of external reagents (e.g., α-ketoglutarate). In that sense our sensor is truly is truly self-sufficient and is the first of its' kind.
2. GABA sensitivity is highest when we have 0.1unit/μL GABASE and 0.1unit/μLGOx. The sensitivity value is 141 nA/μMcm^2 which is almost 4 times the value found in literature [14], [15]. However, the GLU sensitivity is highest when we have 0.4unit/μLGOx. The sensitivity value is 335 nA/μMcm^2 which is comparable to previous work done in our lab [90].

3. Both GABA and GLU sensitivity is highest when have one drop of enzyme (optimum enzyme loading). The thickness in that was 0.49±0.03 for GABA electrode and 0.38±0.05 in case of GLU electrode. The thickness increased with higher loading and sensitivity decreased.
4. The enzyme activities and sensor performance are pH dependent. GABA electrode gives highest GABA sensitivity at pH=9 and GLU sensitivity is highest at pH=7. This information helps us to interpolate various pH conditions in our experimental environment.
5. The GABA electrode follows the Michaelis-Menten equation. The saturation concentration depends upon the amount of α-ketoglutarate in the solution. The saturation limit is ~100 μM GABA (sensitivity is lower for low α-ketoglutarate concentration).
6. A layer of meta-polyphenylene diamine acted as our interference rejection layer. It blocks all the common interferent that is found in normal brain environment. Additionally, we demonstrated that this layer can be customized for thickness by varying the scan rate.
7. We were able to validate our sensor in brain slice environment and use our novel procedure for quantification of GABA and GLU.

In our wire-based sensor characterization we took the optimum parameters of sensor design and solved the dimensional issue we faced in the 8-TRK probe. We were also able to validate our custom probe *ex-vivo* and *in-vivo*. The following conclusions can be drawn from wire-based sensor experiments.

1. Our microwire biosensor design is not only advantageous for future, longitudinal *in vivo* recording, its geometry has distinct advantages over shank-style neural recording probes for brain slice and cell culture models. Shank-style probes are designed to record electrical signals from different regions of the brain for *in vivo* studies. In contrast, brain slices are cut thin and placed horizontally in a recording chamber to extend tissue viability and function. Thus, a geometric profile in which all of the microwire biosensor sites contact the slice in the same horizontal plane provides an advantage. Similarly, cultured cells for *in vitro* models grow in a thin layer on a flat cell culture dish. Again, a microwire biosensor in which all probe sites are in a horizontal plane equidistant from the cells is a desirable arrangement. In our previous studies, we experienced difficulties in using shank-style microbiosensor arrays when recording from brain slices and cultured cells. When recording in brain slices, we could only use two of the eight sensor sites on a shank-style probe; the same was true for cell culture recording.
2. The sensitivity of GABA channel is 17 ±1.12 nA/μMcm^2. We note that GABA sensitivity is dependent upon the storage conditions. If the sensors are stored 4°C instead of room temperature, we get almost 10-times more sensitivity.
3. The GLU sensitivity is 95±9.34 nA/μMcm^2 which comparable to sensors in similar geometry[131].

4. The GLU linear range is 0-300 μM and GABA linear range is 0-500 μM, which makes our packaging suitable for high concentration recording.
5. We validated our probe in the tissue environment with varying frequencies. We were able to measure GLU and GABA levels real-time continuously. We were also able to measure E: I ratio for different frequencies. Interestingly, we observed a huge activation of GABAergic neurons at 140 Hz. This excess GABA could have reduced excitatory synaptic transmission by decreasing excitatory postsynaptic potentials and GLU release and even block action potential propagation as suggested by Ruiz et al. We observed progressively smaller peak concentrations of GABA and GLU as stimulation frequency decreased [115]. However, the E/I ratio was not linear, suggesting that GABA and GLU release in response to different frequencies of stimulation is complex. Our system should be useful in studying responses to a wide range of stimulation parameters.
6. We measured GLU and GABA levels in awake-freely moving live rat. We were able to track sub-second concentration fluctuation of both GABA and GLU.

7.2 Future Work

Our works lays out a structured framework for GABA and GLU microelectrode sensor. Based on our research experience obtained in my dissertation, I would like suggest the following future work guidelines:

1. Electrochemical deposition of the enzyme in the electrode surface. This has been demonstrated before in literature[132]–[134]. Our preliminary data is shown in Figure 7-1 In this experiment 10 V_{p-p} is used for 15 minutes.

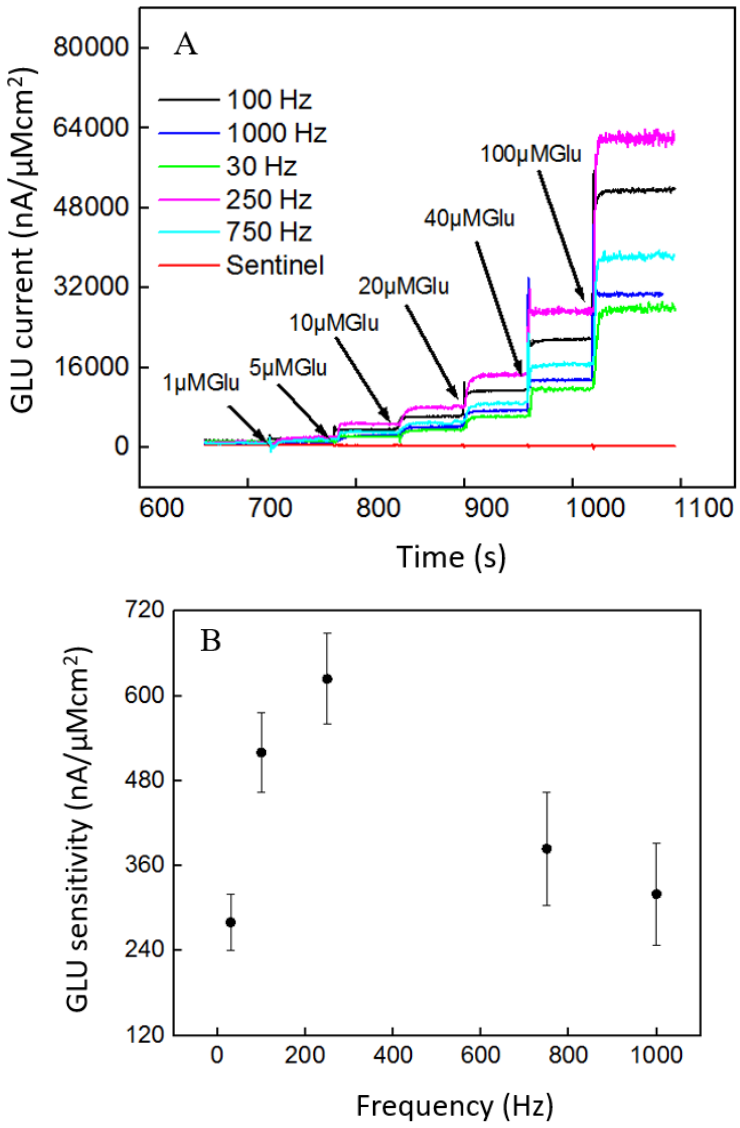

Figure 7-1: A.GLU calibration 1-100 μM for different frequency. The sentinel used here is coated with BSA at 1000 Hz (red line). The sensitivity at 30 Hz is 282±38 nA/μMcm^2, the sensitivity at 100 Hz is 522±68 nA/μMcm^2, the sensitivity at 250 Hz is 624±72 nA/μMcm^2, the sensitivity at 750 Hz is 384±56 nA/μMcm^{2}and the sensitivity at 1000 Hz is 320±43 nA/μMcm^2.

2. Addition of microfluidic channel for *in-situ* calibration. In our experiments we use the calibration values before the *ex-vivo/in-vivo* experiments to calculate the peaks (concentration). However, if the electrode fouls during the course of the experiments we have no way to account for that. A micro-fluidic channel along the channels (shank) will enable us to inject constant amount of our analyte and check for sensitivity instantaneously.
3. Addition of one wire for ascorbic acid measurement. We can keep better track of our interferent (distinguish between H_2O_2 and ascorbic acid) if we coat one wire with ascorbate oxidase and interferent layer. This fourth wire can help measure H_2O_2 and other ROS, whereas other channels are used to measure GABA, GLU and ascorbic acid (sentinel wire).

APPENDIX A

LINEAR RANGE AND MICHAELIS-MENTEN EQUATION

A.1 Saturation Kinetics and Michaelis-Menten Equation

For most of the chemical reactions, the reaction rate is proportional to the concentration of the reactant. So, these chemical reactions follow straight-line formula. However, enzyme-catalyzed reactions do not follow this paradigm. Typically if we plot the initial velocity of an enzyme as function of substrate concentration we get a rectangular hyperbola [135] as shown in Figure A-1.

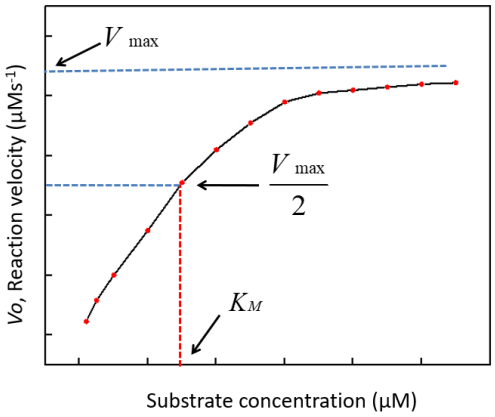

Figure A-1: The rate, or velocity, of an enzyme-catalyzed reaction as a function of substrate concentration

The contemporary Michaelis-Menten equation relates these parameters: V_{max} and K_M. The K_M is the substrate concentration at half-maximal velocity, which corresponds to $V_{max}/2$. The equation is as follows:

$$v = \frac{v_{max}[s]}{K_M + [s]} \qquad \textbf{Eq. A-1}$$

Here *v* represents the reaction velocity, v_{max} is the maximal velocity, K_M the substrate concentration at half-maximal velocity, and*[S]* is the substrate concentration. We can conclude from here that, in normal conditions and specific amounts of enzyme, an enzyme exhibits a maximum velocity (V_{max}), which is approached as a limiting value as the substrate concentration increases. The half of V_{max} and the corresponding concentration, K_M defines the linear range of enzymatic oxidation. This linear range is very important in our sensor development. Throughout our studies we have shown the linear range for our sensors (both 8-TRK and wire based).

A.2 Linear Approximation and Enzyme Inhibitory Mechanism

We rewrite Eq. A-1 to get the linear equation for the reaction velocity, *v.* This linear approximation is termed as Lineweaver-Burk equation. The equation is as follows:

$$\frac{1}{v} = \frac{K_M}{v_{max}[s]} + \frac{1}{v_{max}} \qquad \textbf{Eq. A-2}$$

This equation can be compared with the equation for a straight line: y=mx+b, where m is the slope and b is the y-intercept. In the Lineweaver-Burk equation, K_M/V_{max} is the slope (or m) and $1/V_{max}$ is the y-intercept (or b). For enzymes that obey Michaelis-Menten kinetics, when the reciprocal of the substrate concentration (1/S) is plotted versus the reciprocal of the velocity (1/v), results similar to those displayed in Figure A-2 is

obtained. Lineweaver-Burk equation can be used to explain multi-substrate and multi-enzyme reaction kinetics.

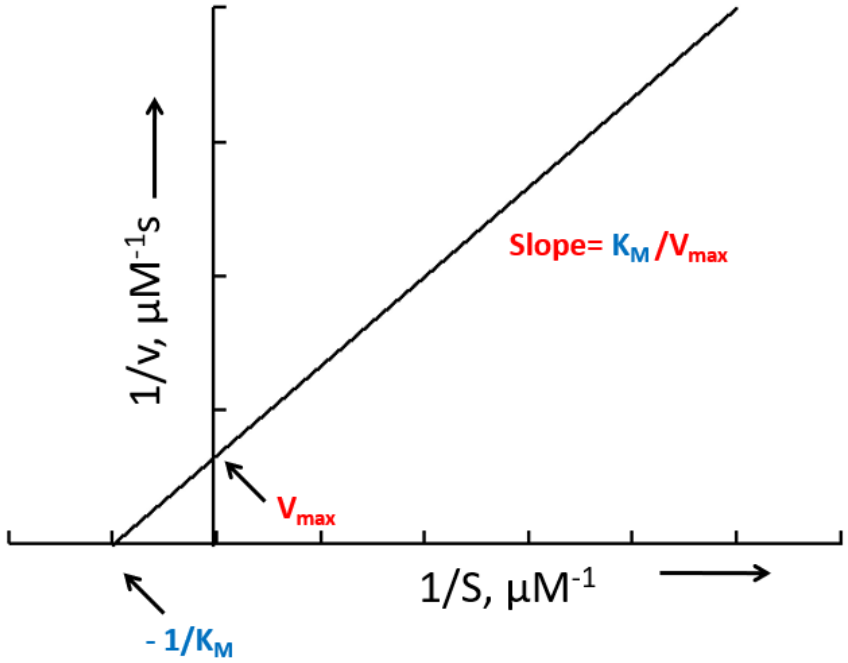

Figure A-2: Lineweaver-Burk equation for enzyme dependent oxidation

For enzymes with subsequent reaction, the v_{max} value and the slope value can shift upward or downward based on the type of reaction. This has been also used to explain multi-substrate reaction[136]. We also note that, the slope in this case is the reciprocal of the sensitivity. The increased slope value gives us lower sensitivity.

In the traditional approach, reversible enzyme inhibitors bind nearly instantaneously to the active sites of enzymes to exert their inhibitory effect[135]. There are three different types inhibitory mechanisms available [135]. In the competitive mechanism, inhibition occurs because enzymes bind to the same substrate as inhibitor; therefore, the slopes increases which results in the loss of sensitivity [135]. In uncompetitive mechanism, inhibitor binds to the enzyme-substrate complex and slopes

remains constant. In this mechanism no significant change in sensitivity is observed [135]. In non-competitive mechanism, the inhibitors bind to both free enzymes and enzyme-substrate complex. In this case, both the slope and x-intercept can change in both directions depending on reaction conditions. Therefore, we expect change in both sensitivity and linear range. The predominant mechanism in our experiments is assumed to be the competitive inhibition mechanism. In our case, when GABASE concentration increases, the sensitivity decreases. The same is true for GOx enzymes. We can hypothesize, that this decrease can be attributed to the inhibitory mechanism.

APPENDIX B

GABA AND GLUTAMATE SENTIVITY COMPARISON

Table B-1 shows the GABA and GLU for different enzyme concentration described in 4.3.

Table B-1: Sensitivity of GABA and GLU enzyme in varying enzyme concentrations. GABAse+GOx is the enzyme concentration. SS_{GABA} and $SS_{GABA-GLU}$ is GABA and GLU sensitivity of GABA electrode. SS_{GLU} is GLU sensitivity of GLU electrode

GABAse+GOx	**SS_{GABA}**	**$SS_{GABA-GLU}$**	**SS_{GLU}**
0.05+0.1	68±7	112±11	102±10
0.05+0.2	56±5	147±14	127±11
0.05+0.3	54±5	183±9	163±13
0.05+0.4	51±4	213±15	198±18
0.05+0.6	51±4	90±6	85±8
0.05+0.8	49±3	81±7	74±6
0.1+0.1	82±11	201±20	167±15
0.1+0.2	65±9	258±22	199±17
0.1+0.3	54±7	312±29	266±18

Table B-1 (cont.): Sensitivity of GABA and GLU enzyme in varying enzyme concentrations. GABAse+GOx is the enzyme concentration. SS_{GABA} and $SS_{GABA-GLU}$ is GABA and GLU sensitivity of GABA electrode. SS_{GLU} is GLU sensitivity of GLU electrode.

GABAse+GOx	**SS_{GABA}**	**$SS_{GABA-GLU}$**	**SS_{GLU}**
0.1+0.4	44±8	397±32	335±29
0.1+0.6	36±7	228±12	200±11
0.1+0.8	32±14	210±11	180±8
0.2+0.1	72±10	151±15	138±18
0.2+0.2	63±7	195±19	187±17
0.2+0.3	62±8	245±23	221±19
0.2+0.4	59±7	299±27	268±24
0.2+0.6	61±6	132±13	119±11
0.2+0.8	59±4	113±9	101±9
0.3+0.1	53±5	98±9	87±5
0.3+0.2	45±4	130±12	121±13
0.3+0.3	44±4	151±14	145±16
0.3+0.4	43±3	181±15	168±20
0.3+0.6	42±4	87±9	76±9
0.3+0.8	43±3	75±5	68±7
0.4+0.1	39±4	148±11	129±18
0.4+0.2	31±3	187±15	173±17
0.4+0.3	29±3	235±18	213±19

Table B-1 (cont.): Sensitivity of GABA and GLU enzyme in varying enzyme concentrations. GABAse+GOx is the enzyme concentration. SS_{GABA} and $SS_{GABA-GLU}$ is GABA and GLU sensitivity of GABA electrode. SS_{GLU} is GLU sensitivity of GLU electrode.

GABAse+GOx	**SS_{GABA}**	**$SS_{GABA-GLU}$**	**SS_{GLU}**
0.4+0.4	30±4	286±23	256±24
0.4+0.6	28±5	127±11	106±11
0.4+0.8	30±7	107±10	95±9
0.8+0.1	17±4	89±8	82±5
0.8+0.2	14±3	123±10	114±11
0.8+0.3	13±3	145±13	133±18
0.8+0.4	14±2	167±18	153±19
0.8+0.6	13±1	79±8	68±6
0.8+0.8	14±3	71±5	58±7

APPENDIX C

WILCOXON RANK SUM FOR DIFFERENT PARAMETERS

C.1 GLU and GABA Concentration

Table C-1: Wilcoxon rank for GLU concentrations A, B, C and control (Ctrl) pulse

	A	**B**	**C**	**Ctrl**
A	0	0.0392	0.0546	0.0809
B	0.0392	0	0.0626	0.0469
C	0.0546	0.0546	0	0.0045
Ctrl	0.0809	0.0469	0.0045	0

Table C-2: Wilcoxon rank for GABA concentrations A, B, C and control (Ctrl) pulse

	A	**B**	**C**	**Ctrl**
A	0	0.014	3.2×10^{-5}	0.441
B	0.014	0	0.09	9.1×10^{-5}
C	3.2×10^{-5}	0.09	0	2.9×10^{-12}
Ctrl	0.441	9.1×10^{-5}	2.9×10^{-12}	0

C.2 Wilcoxon Rank for GLU Peak Characteristics

Table C-3 shows the wilcoxon rank for GLU rise time (T_{10-90}) for A, B, C and control (ctrl) pulse.

Table C-3: Wilcoxon rank for GLU rise time (T_{10-90}) for A, B, C and control (Ctrl) pulse.

	A	**B**	**C**	**Ctrl**
A	0	0.014	4.89×10^{-5}	0.08
B	0.014	0	0.030	0.17
C	4.89×10^{-5}	0.030	0	2.03×10^{-5}
Ctrl	0.08	0.17	2.03×10^{-5}	0

Table C-4 shows wilcoxon rank for GLU decay time (T_{90-10}) for A, B, C and control (Ctrl) pulse.

Table C-4: Wilcoxon rank for GLU decay time (T_{90-10}) for A, B, C and control (Ctrl) pulse.

	A	**B**	**C**	**Ctrl**
A	0	0.047	1.02×10^{-5}	0.40
B	0.047	0	9.8×10^{-4}	0.003
C	1.02×10^{-5}	9.8×10^{-4}	0	4.97×10^{-20}
Ctrl	0.40	0.003	4.97×10^{-20}	0

Table C-5 shows Wilcoxon rank for GLU FDHM (T_{50-50}) for A, B, C and control (Ctrl) pulse.

Table C-5: Wilcoxon rank for GLU full duration half maximum (T_{50-50}) for A, B, C and control (Ctrl) pulse.

	A	**B**	**C**	**Ctrl**
A	0	0.0016	5.12×10^{-7}	1.09×10^{-6}
B	0.0016	0	1.15×10^{-7}	0.5103
C	5.12×10^{-7}	1.15×10^{-7}	0	1.01×10^{-7}
Ctrl	1.09×10^{-6}	0.5103	1.01×10^{-7}	0

C.3 Wilcoxon Rank for GABA Peak Characteristics

Table C-6 shows the wilcoxon rank for GABA rise time for A, B, C and control (Ctrl) pulse.

Table C-6: Wilcoxon rank for GABA rise time (T_{10-90}) for A, B, C and control (Ctrl) pulse.

	A	**B**	**C**	**Ctrl**
A	0	2.03×10^{-4}	3.03×10^{-9}	0.01
B	2.03×10^{-4}	0	0.01	0.02
C	3.03×10^{-9}	0.01	0	5.01×10^{-9}
Ctrl	0.01	0.02	5.01×10^{-9}	0

Table C-7 shows wilcoxon rank for GABA decay time (T_{90-10}) for A, B, C and control (Ctrl) pulse.

Table C-7: Wilcoxon rank for GABA decay time (T_{90-10}) for A, B, C and control (Ctrl) pulse.

	A	**B**	**C**	**Ctrl**
A	0	0.047	$1.2x10^{-5}$	0.31
B	0.047	0	$1.09 x10^{-3}$	0.003
C	$1.2x10^{-5}$	$1.09 x10^{-3}$	0	$4.09 x10^{-15}$
Ctrl	0.31	0.003	$4.09 x10^{-15}$	0

Table C-8 shows wilcoxon rank for GABA FDHM (T_{50-50}) for A, B, C and control (Ctrl) pulse.

Table C-8: Wilcoxon rank for GABA full duration half maximum (T_{50-50}) for A, B, C and control (Ctrl) pulse.

	A	**B**	**C**	**Ctrl**
A	0	0.048	$9 x10^{-8}$	0.30
B	0.048	0	0.003	0.06
C	$9 x10^{-8}$	0.003	0	$1.2 x10^{-10}$
Ctrl	0.30	0.06	$1.2 x10^{-10}$	0

C.4 Wilcoxon Rank for E: I Ratio

Table C-9 shows the wilcoxon rank for E: I ratio for A, B, C and control (Ctrl) pulse (Figure 6-8).

Table C-9: Wilcoxon rank for E: I ratio for A, B, C and control (Ctrl) pulse.

	A	**B**	**C**	**Ctrl**
A	0	0.0482	0.002	0.0122
B	0.0482	0	0.0916	0.5098
C	0.002	0.0916	0	0.6377
Ctrl	0.0122	0.5098	0.6377	0

BIBLIOGRAPHY

[1] C. L. Gooch, E. Pracht, and A. R. Borenstein, "The burden of neurological disease in the United States: A summary report and call to action," *Ann. Neurol.*, vol. 81, no. 4, pp. 479–484, Apr. 2017.

[2] P. S. Cahill, Q. D. Walker, J. M. Finnegan, G. E. Mickelson, E. R. Travis, and R. M. Wightman, "Microelectrodes for the Measurement of Catecholamines in Biological Systems," *Anal. Chem*., vol. 68, no. 18, pp. 3180–3186, Sep. 1996.

[3] J. J. Burmeister, K. Moxon, and G. A. Gerhardt, "Ceramic-based multisite microelectrodes for electrochemical recordings," *Anal. Chem.*, vol. 72, no. 1, pp. 187–192, Jan. 2000.

[4] G. Jobst et al., "Thin-Film Microbiosensors for Glucose−Lactate Monitoring," *Anal. Chem*., vol. 68, no. 18, pp. 3173–3179, Jan. 1996.

[5] R. M. Robinson, D. L., and Wightman, "Rapid dopamine release in freely moving rats," in Electrochemical Methods for Neuroscience, A. C. M. and L. M. Borland, Ed. Boca Raton,FL: *CRC Press/Taylor & Francis*, 2007, pp. 17–34.

[6] D. L. Robinson, A. Hermans, A. T. Seipel, and R. M. Wightman, "Monitoring Rapid Chemical Communication in the Brain," *Chem. Rev*., vol. 108, no. 7, pp. 2554–2584, Jul. 2008.

[7] S. G. Sandberg and P. A. Garris, Neurochemistry of Addiction: Monitoring Essential Neurotransmitters of Addiction. *CRC Press/Taylor & Francis*, 2010.

[8] I. Willuhn, M. J. Wanat, J. J. Clark, and P. E. M. Phillips, "Dopamine Signaling in the Nucleus Accumbens of Animals Self-Administering Drugs of Abuse," *Springer*, Berlin, Heidelberg, 2010, pp. 29–71.

[9] C. fu Chen and K. L. Drew, "Droplet-based microdialysis-Concept, theory, and design considerations," *J. Chromatogr*. A, vol. 1209, no. 1–2, pp. 29–36, Oct. 2008.

[10] D. L. Robinson, B. J. Venton, M. L. A. V. Heien, and R. M. Wightman, "Detecting subsecond dopamine release with fast-scan cyclic voltammetry in vivo," *Clinical Chemistry*, 2003, vol. 49, no. 10, pp. 1763–1773.

[11] O. Niwa, R. Kurita, T. Horiuchi, and K. Torimitsu, "Small-volume on-line sensor for continuous measurement of gamma-aminobutyric acid.," *Anal. Chem*., vol. 70, no. 1, pp. 89–93, 1998.

[12] J. J. Burmeister, V. A. Davis, J. E. Quintero, F. Pomerleau, P. Huettl, and G. A. Gerhardt, "Glutaraldehyde cross-linked glutamate oxidase coated microelectrode arrays: Selectivity and resting levels of glutamate in the CNS," *ACS Chem. Neurosci.*, vol. 4, no. 5, pp. 721–728, 2013.

[13] N. Sekioka, D. Kato, R. Kurita, S. Hirono, and O. Niwa, "Improved detection limit for an electrochemical γ-aminobutyric acid sensor based on stable NADPH detection using an electron cyclotron resonance sputtered carbon film electrode," *Sensors Actuators, B Chem*., vol. 129, no. 1, pp. 442–449, 2008.

[14] I. Hossain et al., "A Novel Microbiosensor Microarray for Continuous ex Vivo Monitoring of Gamma-Aminobutyric Acid in Real-Time," *Front. Neurosci*., vol. 12, no. August, pp. 1–13, 2018.

[15] J. J. Burmeister, D. A. Price, F. Pomerleau, P. Huettl, J. E. Quintero, and G. A. Gerhardt, "Challenges of simultaneous measurements of brain extracellular GABA and glutamate in vivo using enzyme-coated microelectrode arrays," *J. Neurosci. Methods*, vol. 329, Jan. 2020.

[16] R. Bhat et al., "Inhibitory role for GABA in autoimmune inflammation," Proc. Natl. Acad. Sci. U. S. A., vol. 107, no. 6, pp. 2580–2585, Feb. 2010.

[17] S. Smith and T. Sharp, "Measurement of GABA in rat brain microdialysates using o-phthaldialdehyde-sulphite derivatization and high-performance liquid chromatography with electrochemical detection," *J. Chromatogr. B Biomed.* Sci. Appl., vol. 652, no. 2, pp. 228–233, 1994.

[18] W. L. Caudill, G. P. Houck, and R. M. Wightman, "Determination of gamma-aminobutyric acid by liquid chromatography with electrochemical detection.," *J. Chromatogr.*, vol. 227, no. 2, pp. 331–9, Feb. 1982.

[19] M. Auteri, M. Zizzo, and R. Serio, "The GABAergic System and the Gastrointestinal Physiopathology," *Curr. Pharm. Des*., vol. 21, no. 34, pp. 4996–5016, Sep. 2015.

[20] J. Tian, Y. Lu, H. Zhang, C. H. Chau, H. N. Dang, and D. L. Kaufman, "γ-Aminobutyric Acid Inhibits T Cell Autoimmunity and the Development of Inflammatory Responses in a Mouse Type 1 Diabetes Model," *J. Immunol*., vol. 173, no. 8, pp. 5298–5304, Oct. 2004.

[21] C. G. Ting Wong, T. Bottiglieri, and O. C. Snead, "GABA, γ-hydroxybutyric acid, and neurological disease," *Ann. Neurol.*, vol. 54, no. S6, pp. S3–S12, 2003.

[22] S. Takamori, "VGLUTs: 'Exciting' times for glutamatergic research?," *Neurosci. Res.*, vol. 55, no. 4. pp. 343–351, Aug-2006.

[23] C. J. Swanson, M. Bures, M. P. Johnson, A. M. Linden, J. A. Monn, and D. D. Schoepp, "Metabotropic glutamate receptors as novel targets for anxiety and stress disorders," *Nat. Rev. Drug Disco.*, vol. 4, no. 2. pp. 131–144, Feb-2005.

[24] J. W. Olney, "Neurotoxicity of excitatory amino acids", in *Kainic acid as a Tool in Neurobiology*, P. L. McGreer, E.G., Olney, J.W., and McGreer, Ed. New York: *Raven Press*, 1978, pp. 95–112.

[25] N. C. Danbolt, "Glutamate uptake," *Prog. in Neurobiol.*, vol. 65, no. 1. pp. 1–105, Sep-2001.

[26] A. Badalyan, M. Dierich, K. Stiba, V. Schwuchow, S. Leimkühler, and U. Wollenberger, "Electrical wiring of the aldehyde oxidoreductase PaoABC with a polymer containing osmium redox centers: Biosensors for benzaldehyde and GABA," *Biosensors*, vol. 4, no. 4, pp. 403–421, 2014.

[27] A. Scimemi and M. Beato, "Determining the Neurotransmitter Concentration Profile at Active Synapses," *Mol. Neurobiol.* ,vol. 40, pp. 289–306, 2009.

[28] G. Grabauskas, "Time course of GABA in the synaptic clefts of inhibitory synapses in the rostral nucleus of the solitary tract," *Neurosci. Lett*., vol. 373, no. 1, pp. 10–15, Dec. 2004.

[29] Y. Ke, B. M. Cohen, J. Y. Bang, M. Yang, and P. F. Renshaw, "Assessment of GABA concentration in human brain using two-dimensional proton magnetic resonance spectroscopy.," *Psychiatry Res*., vol. 100, no. 3, pp. 169–78, Dec. 2000.

[30] D. L. Robinson and R. M. Wightman, Rapid Dopamine Release in Freely Moving Rats. *CRC Press/Taylor & Francis*, 2007.

[31] P. D. Suzdak and J. A. Jansen, "A Review of the Preclinical Pharmacology of Tiagabine: A Potent and Selective Anticonvulsant GABA Uptake Inhibitor," *Epilepsia*, vol. 36, no. 6, pp. 612–626, 1995.

[32] A. Weltin, J. Kieninger, and G. A. Urban, “Microfabricated, amperometric, enzyme-based biosensors for in vivo applications,” *Anal. Bioanal. Chem*., vol. 408, no. 17, pp. 4503–4521, 2016.

[33] U. Ungerstedt, Measurement of neurotransmitter release by intracranial dialysis. In: Measurement of Neurotransmitter Release In Vivo. New York: *Wiley*, 1984.

[34] R. T. Kennedy, C. J. Watson, W. E. Haskins, D. H. Powell, and R. E. Strecker, “In vivo neurochemical monitoring by microdialysis and capillary separations.,” *Curr. Opin. Chem. Biol*., vol. 6, no. 5, pp. 659–65, Oct. 2002.

[35] J. Kehr and U. Ungerstedt, “Fast HPLC estimation of gamma-aminobutyric acid in microdialysis perfusates: effect of nipecotic and 3-mercaptopropionic acids.,” *J. Neurochem.*, vol. 51, no. 4, pp. 1308–10, Oct. 1988.

[36] H. L. Rowley, K. F. Martin, and C. A. Marsden, “Determination of in vivo amino acid neurotransmitters by high-performance liquid chromatography with o-phthalaldehyde-sulphite derivatisation,” *J. Neurosci. Methods*, vol. 57, no. 1, pp. 93–99, Mar. 1995.

[37] A. A. Monge-Acuña and J. Fornaguera-Trías, “A high performance liquid chromatography method with electrochemical detection of gamma-aminobutyric acid, glutamate and glutamine in rat brain homogenates,” *J. Neurosci. Methods*, vol. 183, no. 2, pp. 176–181, 2009.

[38] N. J. Reinhoud, H. J. Brouwer, L. M. Van Heerwaarden, and G. A. H. Korte-Bouws, “Analysis of glutamate, GABA, noradrenaline, dopamine, serotonin, and metabolites using microbore UHPLC with electrochemical detection,” *ACS Chem. Neurosci.,* vol. 4, no. 5, pp. 888–894, 2013.

[39] G. A. Kinney, L. S. Overstreet, and N. T. Slater, “Prolonged physiological entrapment of glutamate in the synaptic cleft of cerebellar unipolar brush cells,” *J. Neurophysiol*., vol. 78, no. 3, pp. 1320–1333, 1997.

[40] J. Shen et al., “Determination of the rate of the glutamate/glutamine cycle in the human brain by in vivo 13C NMR,” *Proc. Natl. Acad. Sci. U. S. A*., vol. 96, no. 14, pp. 8235–8240, Jul. 1999.

[41] R. A. de Graaf, D. L. Rothman, and K. L. Behar, “State of the art direct 13C and indirect 1H-[13C] NMR spectroscopy in vivo. A practical guide,” *NMR Biomed*., vol. 24, no. 8, pp. 958–972, Oct. 2011.

[42] K. Alakurtti, J. J. Johansson, T. Tuokkola, K. Någren, and J. O. Rinne, “Rostrocaudal gradients of dopamine D2/3 receptor binding in striatal subregions measured with [^{11}C]raclopride and high-resolution positron emission tomography,” *Neuroimage*, vol. 82, pp. 252–259, Nov. 2013.

[43] M. Kågedal et al., “A positron emission tomography study in healthy volunteers to estimate mGluR5 receptor occupancy of AZD2066 - Estimating occupancy in the absence of a reference region,” *Neuroimage*, vol. 82, pp. 160–169, Nov. 2013.

[44] J. Ceccarini et al., “Optimized in vivo detection of dopamine release using18F-fallypride PET,” *J. Nucl. Med.*, vol. 53, no. 10, pp. 1565–1572, Oct. 2012.

[45] S. M. Borisov and O. S. Wolfbeis, “Optical biosensors,” *Chemical Reviews*, vol. 108, no. 2. pp. 423–461, Feb-2008.

[46] X. D. Wang and O. S. Wolfbeis, “Fiber-optic chemical sensors and biosensors (2008-2012),” *Analytical Chemistry*, vol. 85, no. 2. pp. 487–508, 15-Jan-2013.

[47] S. Okumoto, L. L. Looger, K. D. Micheva, R. J. Reimer, S. J. Smith, and W. B. Frommer, “Detection of glutamate release from neurons by genetically encoded surface-displayed FRET nanosensors,” *Proc. Natl. Acad. Sci. U. S. A.*, vol. 102, no. 24, pp. 8740–8745, Jun. 2005.

[48] S. A. Hires, Y. Zhu, and R. Y. Tsien, “Optical measurement of synaptic glutamate spillover and reuptake by linker optimized glutamate-sensitive fluorescent reporters,” *Proc. Natl. Acad. Sci. U. S. A.*, vol. 105, no. 11, pp. 4411–4416, Mar. 2008.

[49] J. S. Marvin et al., “An optimized fluorescent probe for visualizing glutamate neurotransmission,” *Nat. Methods*, vol. 10, no. 2, pp. 162–170, Feb. 2013.

[50] M. L. Sethi, “Enzyme inhibition X: colorimetric method for determining gabase activity and its comparison with a spectrophotometric method.,” *J. Pharm. Biomed. Anal.*, vol. 11, no. 7, pp. 613–7, Jul. 1993.

[51] R. M. Wightman, L. J. May, and A. C. Michael, “Detection of dopamine dynamics in the brain,” *Analytical Chemistry*, vol. 60, no. 13. pp. 769–779, 1988.

[52] M. L. A. V Heien et al., “Real-time measurement of dopamine fluctuations after cocaine in the brain of behaving rats,” *Proc. Natl. Acad. Sci. U. S. A.*, vol. 102, no. 29, pp. 10023–10028, Jul. 2005.

[53] P. Chen, B. Xu, N. Tokranova, X. Feng, J. Castracane, and K. D. Gillis, “Amperometric Detection of Quantal Catecholamine Secretion from Individual Cells on Micromachined Silicon Chips,” *Anal. Chem.*, vol. 75, no. 3, pp. 518–524, Feb. 2003.

[54] Y. Dong, M. L. Heien, M. M. Maxson, and A. G. Ewing, “Amperometric measurements of catecholamine release from single vesicles in MN9D cells,” *J. Neurochem.*, vol. 107, no. 6, pp. 1589–1595, Dec. 2008.

[55] P. E. M. Phillips and R. M. Wightman, “Critical guidelines for validation of the selectivity of in-vivo chemical microsensors,” *Trends Anal. Chem.*, vol. 22, no. 8, pp. 509–514, 2003.

[56] R. D. O’Neill, “Microvoltammetric techniques and sensors for monitoring neurochemical dynamics in Vivo: A review,” *Analyst*, vol. 119, no. 5, pp. 767–779, 1994.

[57] S. Y. Chang et al., “Wireless fast-scan cyclic voltammetry to monitor adenosine in patients with essential tremor during deep brain stimulation,” *Mayo Clin. Proc*., vol. 87, no. 8, pp. 760–765, 2012.

[58] C. Tan, G. Dutta, H. Yin, S. Siddiqui, and P. U. Arumugam, “Detection of neurochemicals with enhanced sensitivity and selectivity via hybrid multiwall carbon nanotube-ultrananocrystalline diamond microelectrodes,” *Sensors Actuators, B Chem.*, vol. 258, no. November 2017, pp. 193–203, 2018.

[59] J. Park, P. Takmakov, and R. M. Wightman, “In vivo comparison of norepinephrine and dopamine release in rat brain by simultaneous measurements with fast-scan cyclic voltammetry,” *J. Neurochem*., vol. 119, no. 5, pp. 932–944, 2011.

[60] B. J. Venton, D. J. Michael, and R. M. Wightman, “Correlation of local changes in extracellular oxygen and pH that accompany dopaminergic terminal activity in the rat caudate-putamen,” *J. Neurochem*., vol. 84, no. 2, pp. 373–381, Jan. 2003.

[61] M. A. Bunin and R. M. Wightman, “Quantitative evaluation of 5-hydroxytryptamine (serotonin) neuronal release and uptake: An investigation of extrasynaptic transmission,” *J. Neurosci*., vol. 18, no. 13, pp. 4854–4860, Jul. 1998.

[62] R. M. Wightman and J. B. Zimmerman, “Control of dopamine extracellular concentration in rat striatum by impulse flow and uptake,” *Brain Research Reviews*, vol. 15, no. 2. pp. 135–144, 1990.

[63] Z. A. McElligott et al., “Noradrenergic synaptic function in the bed nucleus of the stria terminalis varies in animal models of anxiety and addiction,” *Neuropsychopharmacology*, vol. 38, no. 9, pp. 1665–1673, Aug. 2013.

[64] A.J. Bard and L.F. Faulkner, Electrochemical methods: fundamentals and applications, 2nd ed. New York, NY: *Wiley*, 2001.

[65] W. Kissinger, P. and Heineman, Laboratory techniques in electroanalytical chemistry. *Marcel Dekker, Inc*. New York, 1996.

[66] M. D. Gibson, “Neural Biosensor Probes for Simultaneous Electrophysiological and Neurochemical Measurements with High Spatial and Temporal Resolution,” University of Michigan, Ann arbor, MI, 2011.

[67] V. H. Cifuentes Castro et al., “An update of the classical and novel methods used for measuring fast neurotransmitters during normal and brain altered function.,” *Curr. Neuropharmacol.*, vol. 12, no. 6, pp. 490–508, Dec. 2014.

[68] K. M. Mitchell, “Acetylcholine and Choline Amperometric Enzyme Sensors Characterized in Vitro and in Vivo,” *Anal. Chem.*, vol. 76, no. 4, pp. 1098–1106, Feb. 2004.

[69] S. A. Rothwell, S. J. Killoran, and R. D. O’Neill, “Enzyme immobilization strategies and electropolymerization conditions to control sensitivity and selectivity parameters of a polymer-enzyme composite glucose biosensor,” *Sensors*, vol. 10, no. 7, pp. 6439–6462, 2010.

[70] N. Vasylieva, S. Marinesco, D. Barbier, and A. Sabac, “Silicon/SU8 multi-electrode micro-needle for in vivo neurochemical monitoring,” *Biosens. Bioelectron.*, vol. 72, pp. 148–155, Oct. 2015.

[71] O. Frey et al., “Enzyme-based choline and l-glutamate biosensor electrodes on silicon microprobe arrays,” *Biosens. Bioelectron.*, vol. 26, no. 2, pp. 477–484, Oct. 2010.

[72] J. Wang, “Electrochemical Glucose Biosensors,” *Chem. Rev.*, vol. 108, no. 2, pp. 814–825, Feb. 2008.

[73] N. V. Kulagina, L. Shankar, and A. C. Michael, “Monitoring Glutamate and Ascorbate in the Extracellular Space of Brain Tissue with Electrochemical Microsensors,” *Anal. Chem.*, vol. 71, no. 22, pp. 5093–5100, Nov. 1999.

[74] W. H. Oldenziel, G. Dijkstra, T. I. F. H. Cremers, and B. H. C. Westerink, “In vivo monitoring of extracellular glutamate in the brain with a microsensor,” *Brain Res.*, vol. 1118, no. 1, pp. 34–42, Nov. 2006.

[75] K. N. Hascup, “Functional properties of l- glutamate regulation in anesthetized and freely moving mice,” University of Kentucky, Lexinton, KY, 2007.

[76] C. E. Mattinson, J. J. Burmeister, J. E. Quintero, F. Pomerleau, P. Huettl, and G. A. Gerhardt, “Tonic and phasic release of glutamate and acetylcholine neurotransmission in sub-regions of the rat prefrontal cortex using enzyme-based microelectrode arrays,” *J. Neurosci. Methods*, vol. 202, no. 2, pp. 199–208, Nov. 2011.

[77] E. R. Hascup, F. Pomerleau, P. Huettl, G. A. Gerhardt, and K. N. Hascup, "Second-by-second measures of L-glutamate in the prefrontal cortex and striatum of freely moving mice," *J. Pharmacol. Exp. Ther*., vol. 324, no. 2, pp. 725–731, Feb. 2008.

[78] K. N. Hascup et al., Second-by-Second Measures of L-Glutamate and Other Neurotransmitters Using Enzyme-Based Microelectrode Arrays. *CRC Press/Taylor & Francis*, 2007.

[79] M. G. Garguilo and A. C. Michael, "Quantitation of Choline in the Extracellular Fluid of Brain Tissue with Amperometric Microsensors," *Anal. Chem*., vol. 66, no. 17, pp. 2621–2629, 1994.

[80] F. Mazzei, F. Botrè, G. Lorenti, and F. Porcelli, "Peroxidase based amperometric biosensors for the determination of γ-aminobutyric acid," *Anal. Chim. Acta*, vol. 328, no. 1, pp. 41–46, Jul. 1996.

[81] U. W. Artavazd Badalyan, Silke Leimkühler, Konstanze Stiba, "Biosensor for measuring GABA," European patent EP2505658, vol. 1, no. 19, pp. 1–18, 2007.

[82] P. M. Talauliker et al., "Ceramic-based microelectrode arrays: Recording surface characteristics and topographical analysis," *J. Neurosci. Methods*, vol. 198, no. 2, pp. 222–229, Jun. 2011.

[83] A. Weltin, J. Kieninger, B. Enderle, A. K. Gellner, B. Fritsch, and G. A. Urban, "Polymer-based, flexible glutamate and lactate microsensors for in vivo applications," Biosens. Bioelectron., vol. 61, pp. 192–199, Nov. 2014.

[84] A. Weltin, B. Enderle, J. Kieninger, and G. A. Urban, "Multiparametric, flexible microsensor platform for metabolic monitoring in vivo," *IEEE Sens. J.,* vol. 14, no. 10, pp. 3345–3351, 2014.

[85] Y. Hu, Y. Zhang, and G. S. Wilson, "A needle-type enzyme-based lactate sensor for in vivo monitoring," *Anal. Chim. Acta*, vol. 281, no. 3, pp. 503–511, Sep. 1993.

[86] Y. Hu, K. M. Mitchell, F. N. Albahadily, E. K. Michaelis, and G. S. Wilson, "Direct measurement of glutamate release in the brain using a dual enzyme-based electrochemical sensor," *Brain Res*., vol. 659, no. 1–2, pp. 117–125, Oct. 1994.

[87] C. P. McMahon et al., "Oxygen tolerance of an implantable polymer/enzyme composite glutamate biosensor displaying polycation-enhanced substrate sensitivity," *Biosens. Bioelectron*., vol. 22, no. 7, pp. 1466–1473, Feb. 2007.

[88] C. P. McMahon and R. D. O'Neill, "Polymer−Enzyme Composite Biosensor with High Glutamate Sensitivity and Low Oxygen Dependence," *Anal. Chem*., vol. 77, no. 4, pp. 1196–1199, Feb. 2005.

[89] R. D. O'Neill, S. C. Chang, J. P. Lowry, and C. J. McNeil, "Comparisons of platinum, gold, palladium and glassy carbon as electrode materials in the design of biosensors for glutamate," *Biosens. Bioelectron*., 2004, vol. 19, no. 11, pp. 1521–1528.

[90] C. Tan, P. T. Doughty, K. Magee, T. A. Murray, and S. Siddiqui, "Effect of Process Parameters on Electrochemical Performance of a Glutamate Microbiosensor Effect of Process Parameters on Electrochemical Performance of a Glutamate Microbiosensor," *J. of the Electrochem. Soc*. 167. 027528. doi:10.1149/1945-7111/ab6b0b, 2020.

[91] R. J. Geise, J. M. Adams, N. J. Barone, and A. M. Yacynych, "Electropolymerized films to prevent interferences and electrode fouling in biosensors," *Biosens. Bioelectron*., vol. 6, no. 2, pp. 151–160, 1991.

[92] N. Wahono, S. Qin, P. Oomen, T. I. F. Cremers, M. G. de Vries, and B. H. C. Westerink, "Evaluation of permselective membranes for optimization of intracerebral amperometric glutamate biosensors," *Biosens. Bioelectron*., vol. 33, no. 1, pp. 260–266, Mar. 2012.

[93] J. J. Burmeister, T. D. Coates, and G. A. Gerhardt, "Multisite microelectrode arrays for measurements of multiple neurochemicals," *Annual International Conference of the IEEE Engineering in Medicine and Biology - Proceedings*, 2004, vol. 26 VII, pp. 5348–5351.

[94] J. L. Scoggin et al., "An enzyme-based electrochemical biosensor probe with sensitivity to detect astrocytic versus glioma uptake of glutamate in real time in vitro," *Biosens. Bioelectron*., vol. 126, pp. 751–757, Feb. 2019.

[95] S. Ben-Amor et al., "Enhanced detection of hydrogen peroxide with platinized microelectrode arrays for analyses of mitochondria activities," *Electrochim. Acta*, vol. 126, pp. 171–178, Apr. 2014.

[96] C. Song et al., "Role of α7-nicotinic acetylcholine receptors in tetanic stimulation-induced γ oscillations in rat hippocampal slices," *Neuropharmacology*, vol. 48, no. 6, pp. 869–880, 2005.

[97] L. R. Wilson, S. Panda, A. C. Schmidt, and L. A. Sombers, "Selective and Mechanically Robust Sensors for Electrochemical Measurements of Real-Time Hydrogen Peroxide Dynamics in Vivo," *Anal. Chem*., vol. 90, no. 1, pp. 888–895, 2018.

[98] P. T. Doughty, "Real-time neurotransmitter monitoring of neuronal networks," Ph.D. dissertation, Louisiana Tech University, Ruston, LA 2019. [Online]. Available: https://digitalcommons.latech.edu/dissertations/834.

[99] L. Tretter and V. Adam-Vizi, “Alpha-ketoglutarate dehydrogenase: a target and generator of oxidative stress.,” *Philos. Trans. R. Soc. Lond. B. Biol. Sci.*, vol. 360, no. 1464, pp. 2335–45, Dec. 2005.

[100] L. H. Long and B. Halliwell, “Artefacts in cell culture: α-Ketoglutarate can scavenge hydrogen peroxide generated by ascorbate and epigallocatechin gallate in cell culture media,” *Biochem. Biophys. Res. Commun.*, vol. 406, no. 1, pp. 20–24, Mar. 2011.

[101] K. A. Nath, E. O. Ngo, R. P. Hebbel, A. J. Croatt, B. Zhou, and L. M. Nutter, “alpha-Ketoacids scavenge H_2O_2 in vitro and in vivo and reduce menadione-induced DNA injury and cytotoxicity.,” *Am. J. Physiol.*, vol. 268, no. 1 Pt 1, pp. C227-36, Jan. 1995.

[102] C. Tan, “Development of amperometric microbiosensors for neurochemical detection,” Ph.D. disseration,Louisiana Tech University, Ruston, LA 2019. [Online]. Available: https://digitalcommons.latech.edu/dissertations/835.

[103] K. Moussawi, A. Riegel, S. Nair, and P. W. Kalivas, “Extracellular glutamate: functional compartments operate in different concentration ranges.,” *Front. Syst. Neurosci.*, vol. 5, p. 94, 2011.

[104] K. Kanamori and B. D. Ross, “Chronic electrographic seizure reduces glutamine and elevates glutamate in the extracellular fluid of rat brain,” *Brain Res.,* vol. 1371, pp. 180–191, Jan. 2011.

[105] H. L. Rowley, K. F. Martin, and C. A. Marsden, “Decreased GABA release following tonic-clonic seizures is associated with an increase in extracellular glutamate in rat hippocampus in vivo.,” *Neuroscience*, vol. 68, no. 2, pp. 415–22, Sep. 1995.

[106] L. Medina-Ceja, K. Pardo-Peña, A. Morales-Villagrán, J. Ortega-Ibarra, and S. López-Pérez, “Increase in the extracellular glutamate level during seizures and electrical stimulation determined using a high temporal resolution technique.,” *BMC Neurosci.*, vol. 16, p. 11, Mar. 2015.

[107] J. Arima et al., “Structural characterization of l-glutamate oxidase from Streptomyces sp. X-119-6,” *FEBS J.*, vol. 276, no. 14, pp. 3894–3903, Jul. 2009.

[108] T. Tseng, C.-F. Chang, and W.-C. Chan, “Fabrication of Implantable, Enzyme-Immobilized Glutamate Sensors for the Monitoring of Glutamate Concentration Changes in Vitro and in Vivo,” *Molecules*, vol. 19, no. 12, pp. 7341–7355, Jun. 2014.

[109] R. Khan, W. Gorski, and C. D. Garcia, “Nanomolar Detection of Glutamate at a Biosensor Based on Screen-Printed Electrodes Modified with Carbon Nanotubes.,” *Electroanalysis*, vol. 23, no. 10, pp. 2357–2363, Oct. 2011.

[110] L. Hertz, “The Glutamate–Glutamine (GABA) Cycle: Importance of Late Postnatal Development and Potential Reciprocal Interactions between Biosynthesis and Degradation,” *Front. Endocrinol. (Lausanne).*, vol. 4, p. 59, May 2013.

[111] M. B. Robinson and J. G. Jackson, “Astroglial glutamate transporters coordinate excitatory signaling and brain energetics,” *Neurochemistry International*, vol. 98. Elsevier Ltd, pp. 56–71, 01-Sep-2016.

[112] K. Boddum et al., “Astrocytic GABA transporter activity modulates excitatory neurotransmission,” *Nat. Commun.*, vol. 7, Nov. 2016.

[113] C. C. Chiang, T. P. Ladas, L. E. Gonzalez-Reyes, and D. M. Durand, “Seizure suppression by high frequency Optogenetic stimulation using in vitro and in vivo animal models of epilepsy,” *Brain Stimul.*, vol. 7, no. 6, pp. 890–899, Nov. 2014.

[114] A. Sik, M. Penttonen, A. Ylinen, and G. Buzsaki, “Hippocampal CA1 interneurons: An in vivo intracellular labeling study,” *J. Neurosci.*, vol. 15, no. 10, pp. 6651–6665, 1995.

[115] A. Ruiz, R. Fabian-Fine, R. Scott, M. C. Walker, D. A. Rusakov, and D. M. Kullmann, “GABAA receptors at hippocampal mossy fibers.,” *Neuron*, vol. 39, no. 6, pp. 961–73, Sep. 2003.

[116] S. J. Zhang and M. B. Jackson, “GABAA receptor activation and the excitability of nerve terminals in the rat posterior pituitary.,” *J. Physiol.*, vol. 483, no. 3, pp. 583–595, Mar. 1995.

[117] M. Lévesque, R. Herrington, L. Leclerc, M. A. Rogawski, and M. Avoli, “Allopregnanolone decreases interictal spiking and fast ripples in an animal model of mesial temporal lobe epilepsy,” *Neuropharmacology*, vol. 121, pp. 12–19, Jul. 2017.

[118] K. J. Staley, A. White, and F. E. Dudek, “Interictal spikes: Harbingers or causes of epilepsy?,” *Neuroscience Letters*, vol. 497, no. 3. pp. 247–250, 27-Jun-2011.

[119] R. J. Racine, “Modification of seizure activity by electrical stimulation: II. Motor seizure,” *Electroencephalogr. Clin. Neurophysiol.*, vol. 32, no. 3, pp. 281–294, 1972.

[120] M. Mantovani et al., “Neuronal electrical high frequency stimulation enhances GABA outflow from human neocortical slices,” *Neurochem. Intl.*vol. 49, pp. 347–350, 2006.

[121] C.-F. Chuang , “High-Frequency Stimulation of the Subthalamic Nucleus Activates Motor Cortex Pyramidal Tract Neurons by a Process Involving Local Glutamate, GABA and Dopamine Receptors in Hemi-Parkinsonian Rats,” *Chin. J. Physiol.*, vol. 61, no. 2, pp. 92–105, Apr. 2018.

[122] K. H. Lee et al., “High-frequency stimulation of the subthalamic nucleus increases glutamate in the subthalamic nucleus of rats as demonstrated by in vivo enzyme-linked glutamate sensor,” *Brain Res.*, vol. 1162, pp. 121–129, Aug. 2007.

[123] T. Viereckel, Å. Konradsson-Geuken, and Å. Wallén-Mackenzie, “Validated multi-step approach for in vivo recording and analysis of optogenetically evoked glutamate in the mouse globus pallidus,” *J. Neurochem.*, vol. 145, no. 2, pp. 125–138, Apr. 2018.

[124] F. Agnesi, C. D. Blaha, J. Lin, and K. H. Lee, “Local glutamate release in the rat ventral lateral thalamus evoked by high-frequency stimulation,” *J. Neural Eng*., vol. 7, no. 2, 2010.

[125] G. Nyitrai, K. Kekesi, and G. Juhasz, “Extracellular Level of GABA and Glu: In Vivo Microdialysis-HPLC Measurements,” *Curr. Top. Med. Chem*., vol. 6, no. 10, pp. 935–940, May 2006.

[126] F. Peña and R. Tapia, “Relationships Among Seizures, Extracellular Amino Acid Changes, and Neurodegeneration Induced by 4-Aminopyridine in Rat Hippocampus: A Microdialysis and Electroencephalographic Study,” *J. Neurochem*., vol. 72, no. 5, pp. 2006–2014, Jun. 2008.

[127] F. Kersanté et al., “A functional role for both γ-aminobutyric acid (GABA) transporter-1 and GABA transporter-3 in the modulation of extracellular GABA and GABAergic tonic conductances in the rat hippocampus,” *J. Physiol*., vol. 591, no. 10, pp. 2429–2441, May 2013.

[128] R. D. Traub, M. A. Whittington, S. B. Colling, G. Buzsáki, and J. G. R. Jefferys, “Analysis of gamma rhythms in the rat hippocampus in vitro and in vivo,” *J. Physiol.*, vol. 493, no. 2, pp. 471–484, Jun. 1996.

[129] J. W. Mozrzymas, E. D. Zarmowska, M. Pytel, and K. Mercik, “Modulation of GABAA receptors by hydrogen ions reveals synaptic GABA transient and a crucial role of the desensitization process,” *J. Neurosci*., vol. 23, no. 22, pp. 7981–7992, Sep. 2003.

[130] N. Dehghani et al., “Dynamic balance of excitation and inhibition in human and monkey neocortex,” *Sci. Rep.*, vol. 6, pp. 1–12, 2016.

[131] M. Ganesana, E. Trikantzopoulos, Y. Maniar, S. T. Lee, and B. J. Venton, "Development of a novel micro biosensor for in vivo monitoring of glutamate release in the brain," *Biosens. Bioelectron*., vol. 130, no. October 2018, pp. 103–109, 2019.

[132] M. Ammam and J. Fransaer, "Glucose microbiosensor based on glucose oxidase immobilized by AC-EPD: Characteristics and performance in human serum and in blood of critically ill rabbits," *Sensors Actuators, B Chem.*, vol. 145, no. 1, pp. 46–53, 2010.

[133] M. Ammam and J. Fransaer, "Highly sensitive and selective glutamate microbiosensor based on cast polyurethane/AC-electrophoresis deposited multiwalled carbon nanotubes and then glutamate oxidase/electrosynthesized polypyrrole/Pt electrode," *Biosens. Bioelectron*., vol. 25, no. 7, pp. 1597–1602, Mar. 2010.

[134] M. Ammam and J. Fransaer, "AC-electrophoretic deposition of metalloenzymes: Catalase as a case study for the sensitive and selective detection of H_2O_2," *Sensors and Actuators, B: Chem.*, vol. 160, no. 1. pp. 1063–1069, 2011.

[135] R. Roskoski, "Michaelis-Menten Kinetics", The comprehensive pharmacology refence, doi: 0.1016/B978-0-12-801238-3.05143-6 , 2015.

[136] P.F. Cook and W.W. Cleland, Enzyme kinetics and mechanism. New York: *Garland Science,* 2007.